Passive vibration control by using Nonlinear Energy Sink absorbers. Theoretical study and experimental investigations

Giuseppe Pennisi

THÈSE

En vue de l'obtention du

DOCTORAT DE L'UNIVERSITÉ DE TOULOUSE

Délivré par :

Institut Supérieur de l'Aéronautique et de l'Espace (ISAE)

Présentée et soutenue par :
Giuseppe PENNISI

le jeudi 17 novembre 2016

Titre :

Passive vibration control by using Nonlinear Energy Sink absorbers.
Theoretical study and experimental investigations

Contrôle passif de vibrations à l'aide d'absorbeurs.
Étude théorique et investigations expérimentales

École doctorale et discipline ou spécialité :

ED MEGeP : Génie mécanique, mécanique des matériaux

Unité de recherche :

Institut Clément Ader

Directeur(s) de Thèse :

M. Guilhem MICHON (directeur de thèse)
M. Cyrille STEPHAN (co-directeur de thèse)

Jury :

Pr. Xavier BOUTILLON, École Polytechnique - Président
Pr. Claude-Henri LAMARQUE, ENTPE - Rapporteur
Pr. Brian MANN, Duke University - Examinateur
Pr. Guilhem MICHON, ISAE - Directeur de Thèse
Dr. Cyrille STEPHAN, ONERA DADS - Co-directeur de Thèse
Pr. Olivier THOMAS, ENSAM - Rapporteur

A mio nonno, Prof. Giuseppe Pennisi.

Abstract

Passive vibration control methods using linear dampers have been largely studied and investigated, and they have nowadays a broad range of applications. However, linear dampers are efficient when tuned to the specific frequency to control but present substantial limitations when applied to primary systems with uncertainties on the modal parameters or to systems having a natural frequency that may vary with external forcing.

In this thesis the vibration mitigation in mechanical systems by means of a Nonlinear Energy Sink absorber is studied. The phenomenon governing the physics of this kind of device is referred to as Targeted Energy Transfer and it consists in an irreversible energy transfer from the primary system to the NES where the energy is then dissipated. This energy transfer may occur over a broad range of frequencies with no need for the NES to be tuned to a specific one.

The dynamics of a first type of NES called Vibro-Impact Nonlinear Energy Sink (VI-NES) is experimentally investigated via a harmonically forced single-degree-of-freedom linear oscillator to which a VI-NES is attached. A Targeted Energy Transfer from the LO towards the VI-NES is experimentally observed and a significant reduction of the primary system's resonance peak is obtained. The system is analytically studied by means of the Multiple Scales method and the nonlinear behavior experimentally observed is theoretically explained.

The second type of NES presented is the Magnetic-Strung NES with energy harvesting. This study adds the energy harvesting aspect to the research on nonlinear vibration absorbers. The system consists in a harmonically forced single-degree-of-freedom linear oscillator to which the MS-NES is applied. The type of nonlinearity used can be shaped thanks to a magnetic force aptly introduced, allowing the NES to have several possible configurations. The resulting system is an electro-mechanical system in which the vibration energy of the primary system is absorbed by the NES and subsequently partially dissipated by the viscous damping and partially converted into electrical power. The numerical and experimental studies analyze the performances of the MS-NES both as an energy absorber and as an energy harvester.

Finally, ideas and perspectives arising from this study are discussed and future work directions are provided.

Résumé

Les méthodes de contrôle de vibrations passives basées sur des absorbeurs linéaires ont été largement étudiées et ils ont aujourd'hui une vaste gamme d'applications. Cependant, les absorbeurs linéaires n'étant efficaces que lorsqu'ils sont accordés à la fréquence que l'on veut contrôler, ils présentent des limites considérables quand ils sont appliqués à des systèmes possédant des incertitudes sur les paramètres modaux ou ayant une fréquence propre dépendante de la force extérieure.

Dans cette thèse la réduction des vibrations dans les systèmes mécaniques à l'aide d'un absorbeur Nonlinear Energy Sink est étudiée. Le phénomène qui gouverne la physique de ce dispositif est appelé pompage énergétique (Targeted Energy Transfer) et il consiste en un transfert irréversible d'énergie du système principal vers le NES, où l'énergie est dissipée. Ce transfert d'énergie peut se produire pour une large gamme de fréquences et sans besoin que le NES ne soit accordé à une fréquence spécifique.

La dynamique d'un premier type de NES appelé Vibro-Impact Nonlinear Energy Sink (VI-NES) est investiguée expérimentalement grâce à un oscillateur linéaire (OL) à un degré de liberté forcé harmoniquement auquel le VI-NES est attaché. Le pompage énergétique du OL vers le VI-NES est observé expérimentalement, ce qui a permis d'obtenir une importante réduction du pic de résonance du système principal. Le système est étudié analytiquement à l'aide de la méthode Multi-Echelles et le comportement non-linéaire observé est expliqué théoriquement.

Le deuxième type de NES présenté est le Magnetic-Strung NES avec récupération d'énergie. Cette étude ajoute l'aspect lié à la récupération d'énergie au domaine de recherche des absorbeurs non-linéaires. Le système consiste en un oscillateur linéaire (OL) à un degré de liberté forcé harmoniquement auquel le MS-NES est appliqué. Le force non-linéaire de rappel peut être modulée grâce à une force magnétique introduite judicieusement, ce qui permet au NES d'avoir plusieurs configurations possibles. Le système résultant est un système électromécanique où l'énergie vibratoire du système principal est absorbée par le NES et est ensuite dissipée en partie par l'amortissement visqueux et convertie en partie en puissance électrique. Les études numérique et expérimentale analysent les performances du MS-NES en tant qu'absorbeur d'énergie et en tant que récupérateur d'énergie.

Finalement, les idées et les perspectives issues de cette étude sont traitées et les directions pour les travaux futurs sont fournies.

Acknowledgements

I have been fortunate enough to conduct my PhD research in three different locations, which means that over the last three years I have had the opportunity to live and work in three different cities and to meet so many people whom I should thank for one reason or another.

Tout d'abord je voudrais remercier mon directeur de thèse Dr. Guilhem Michon et mon encadrant ONERA Dr. Cyrille Stéphan. Je voudrais les remercier pour la confiance qu'ils m'ont faite dès le début de la thèse et pour avoir sû être toujours présents tout en me laissant la liberté de faire mes choix et de conduire ma recherche de manière autonome.

Merci à toute l'équipe ONERA-DADS et à son chef Pascal Naudin qui m'ont accueilli pendant une grosse partie de ces trois dernières années. Une mention spéciale pour l'équipe GVT, Pascal et Stéphan. Merci aux doctorants ONERA, Tito, Presidente, Timothé, Quentin, pour toutes les conversations autour des cafés bus les après-midi. Merci à Nadine pour l'organisation de tous mes déplacements.

Merci aux gens qui m'ont accueilli à Toulouse pendant les périodes passée à l'ICA, avec un remerciement particulier pour Jean Benoît pour le support pendant les essais. Merci aux doctorants ICA et à Juan et Joao. Et bien sûr merci à Marie-Odile pour avoir géré les aspects logistiques liés à mes déplacements et congrès.

I would like to thank Dr. Brian Mann for giving me the opportunity to work in his group during the time I spent at Duke, for making me feel at ease in a new environment, and for flying to France to attend my defense. Thanks to Nicholas for his precious help during experiments. Thanks to the people of the University Commons, the Right Side of the Road, and of the International House.

Infine ringrazio la mia famiglia, punto fermo in questo girovagare, per il continuo e incondizionato supporto e incoraggiamento. Grazie per avermi permesso di fare ciò che ho voluto e avermi aiutato a farlo diventare realtà. Ovviamente un pensiero particolare va a mio Nonno, Prof. Giuseppe Pennisi, al quale questo lavoro è dedicato, per essere stato il mio primo tifoso.

Ringrazio i miei amici più stretti, il gruppo dei cani, il Porco, il Crotalo, Palermo, Azara, T, Marx, Marx Jr., Scheggia, il Cappellaio, Manolo, i cui cammini si intrecciano in giro per il mondo senza però riuscire a perdersi. Un grande grazie speciale al Chindemaccio e Jota, per essere arrivati fin qui insieme a me e essere consapevoli di continuare insieme, qualunque sia la prossima fermata.

Grazie a April per avere condiviso gran parte delle gioie e dei dolori di questo lavoro, rimettendomi in carreggiata nei momenti più difficili. Lei forse sarebbe dovuta essere nel paragrafo americano, ma chiaramente occupa un posto molto speciale in tutta questa storia.

Contents

Chapter 1

Introduction

Abstract

In this chapter the context of the work is presented. The fundamentals of linear structural dynamics are reminded along with the technique of vibration mitigation using Tuned Mass Damper (TMD) linear absorbers. The limitations of this kind of devices are shown and then the interest in using nonlinear dynamics to improve the performances. An exhaustive literature review is presented about the concept of Targeted Energy Transfer (TET) and Nonlinear Energy Sink (NES) with a particular attention to the experimental studies. The chapter ends with presenting the motivation of this work and the outline of the dissertation.

1.1 Linear Structural Dynamics

The forces that are usually involved in classical structural dynamics problems can be classified as: inertial, dissipative, restoring and any type of external force. All these forces being in equilibrium with each other, the balance equation can be symbolically written as:

$$F_I + F_D + F_R = F_E \tag{1.1}$$

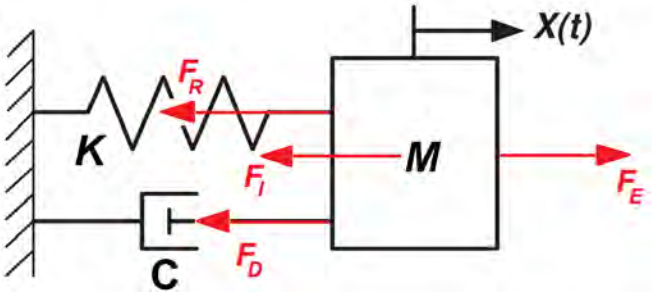

Figure 1.1: Schematic of the forces involved in a classical structural dynamics problem.

Where F_I, F_D, F_R and F_E are respectively the inertial, dissipative, restoring and external forces. In linear structural dynamics all these forces can be expressed as linearly proportional to the displacement x and its derivatives $\dot{x}$ and $\ddot{x}$ through the structural parameters mass M, damping C and stiffness K:

$$F_I = M\ddot{\mathbf{x}} \quad F_D = C\dot{\mathbf{x}} \quad F_R = K\mathbf{x} \tag{1.2}$$

Finally the classical structural dynamics equation is obtained:

$$M\ddot{\mathbf{x}} + C\dot{\mathbf{x}} + K\mathbf{x} = F_E \tag{1.3}$$

For a single degree of freedom system harmonically forced Eq.(1.3) becomes:

$$\ddot{x} + 2\xi\omega_0\dot{x} + \omega_0^2 x = F_e \quad F_e = F_0/M\sin(\Omega t) \tag{1.4}$$

Where $\omega_0 = \sqrt{K/M}$ is the natural frequency and $\xi = \frac{C}{2\sqrt{KM}}$ is the damping ratio.

Eq.(1.4) represents the governing equation for a single degree of freedom mechanical system harmonically forced by a sinusoidal force with frequency Ω. Once the transient solution vanished, the steady-state response of the

system is a sinus with the same frequency as the exciting force and shifted in phase by $\phi = \arctan\left(\frac{2\omega\omega_0\xi}{\omega^2-\omega_0^2}\right)$:

$$x(t) = \frac{F_0}{M\omega\sqrt{(2\omega_0\xi)^2 + \frac{1}{\omega_0^2}(\omega_0^2-\omega^2)^2}}\sin(\Omega t - \phi) \tag{1.5}$$

In the same way the response of a linear system can be expressed in the frequency domain as:

$$\frac{X}{F_0} = \frac{(1/k)}{(1-(\frac{\Omega}{\omega_n})^2 + i2\xi\frac{\Omega}{\omega_n})} = H(i\Omega) \tag{1.6}$$

Where $H(i\omega)$ is the transfer function of the mechanical system.

The fact that the response has the same frequency as the external force is just an example of the many convenient properties linear systems have which are applied in many fields as in structural dynamics.

Among all the properties of linear systems, the superposition principle is probably the most important one and it is useful to remind it here as in sharp contrast with the nature of nonlinear systems. In physics and systems theory, the superposition principle, also known as superposition property, states that, for all linear systems, the net response at a given place and time caused by two or more stimuli is the sum of the responses which would have been caused by each stimulus individually. In structural dynamics this principle is widely employed through the modal decomposition theory: the motion of a n-dof structure can be described by the linear combination of n normal modes. Moreover when only one single mode is excited, no energy transfer between different modes is possible and the excited mode will be the only active mode.

It will be shown later on this chapter how nonlinear systems may exhibit a completely different behavior if compared to linear ones and how those principles which were well established and settled may not be valid anymore. New interesting phenomena may arise even with a weak source of nonlinearity.

1.1.1 Vibration mitigation of mechanical structures

The control of vibrations in structural dynamics is still an important area of research as it enables resistance improvement as well as noise reduction and comfort enhancement. Engineering structures undergo multiple sources of vibrations throughout their life and the methods of mitigation can be classified in:

- active control methods have been widely developed throughout the last fifteen years. The principle is to reduce undesirable vibrations by generating an out-of-phase input. Active control usually gives a good vibration reduction performance but an important shortcoming to take into account is that they need an external energy supply.

- semi-active control methods using electro- and magneto-rheological fluids were proposed [DSSC96, CK00]. The particularity of these fluids lies in their varying viscosity with respect to the electric or magnetic field in which they are plunged. Since no energy is transferred to the controlled system, these techniques are robust and reliable while offering a vibration reduction level similar to active techniques. However, the modeling of the fluid behaviors as well as the development of the controller represent major challenges that still complicate the use of the systems for real-life structures.

- passive control methods reduce vibrations by adding to the structure a dissipative material [Nak98] or a dynamical vibration absorber (DVA) [Fra11, DH85]. This technique is very interesting and represents an important alternative to the previous methods as it does not require an external energy supply.

This thesis dissertation focuses on passive control of vibrations using nonlinear absorbers. Before getting into the core of the subject we present first a description of linear vibration reduction methods using Tuned Mass Dampers (TMD). The advantages as well as the limitations of this device will be illustrated and then the interest in considering a nonlinear absorber to overcome these limits will be explained. Then, a brief introduction to the basic principles of nonlinear structural dynamics will precede the discussion about the nonlinear vibration absorbers studied in this work.

1.2 Linear vibration absorber: Tuned Mass Damper

The Tuned Mass Damper (TMD) is probably the most popular device for passive vibration mitigation of mechanical structures. It has a broad range of applications thanks to its linear behavior and the solid theoretical and mathematical basis which it relies on. It is commonly used for civil (e.g., Millenium bridge, Taipei 101 and Burj-el-Arab buildings) and electromechanical engineering structures (e.g., cars and high-tension lines). Despite the well-established theory and the linear characteristics, the design of such

an absorber may be a challenging problem when it is coupled to more complex structures.

The first studies on the TMD date back to the patent concerning the work carried out by Frahm [Fra11] in 1911. He considered a linear attachment composed of a mass and a spring coupled to a harmonically forced conservative linear oscillator (LO) as depicted in Fig.1.2.

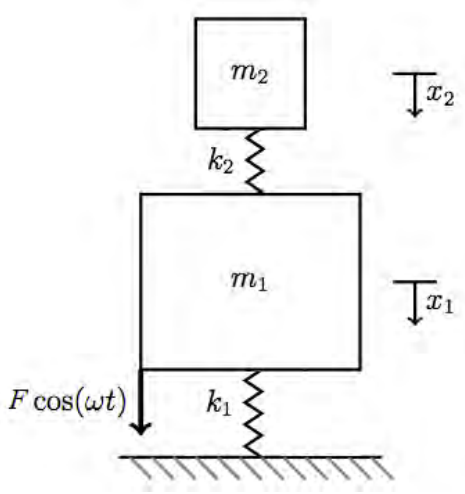

Figure 1.2: Tuned Mass Damper without viscous damping coupled to a linear oscillator.

The system displayed in Fig1.2 is governed by the equations of motion:

$$\begin{aligned} m_1\ddot{x}_1 + k_1x_1 + k_2(x_1 - x_2) &= F\cos(\omega t) \\ m_2\ddot{x}_2 + k_2(x_2 - x_1) &= 0 \end{aligned} \tag{1.7}$$

Assuming a response $x_1 = X_1\cos(\omega t)$, the LO displacement can be expressed as:

$$X_1 = \frac{(k_2 - \omega^2 m_2)F}{(k_1 + k_2 - \omega^2 m_1)(k_2 - \omega^2 m_2) - k_2^2} \tag{1.8}$$

When the LO is excited at its natural frequency $\omega = \omega_1$, the tuning condition to minimize its displacement is:

$$\omega_a = \sqrt{\frac{k_2}{m_2}} = \sqrt{\frac{k_1}{m_1}} = \omega_1 \tag{1.9}$$

Where ω_a is the natural frequency of the absorber. Then Eq.(1.9) says that the absorber has to be tuned on the same natural frequency as the linear

oscillator. The resulting coupled 2 dof-system presents two resonance peaks in the neighborhood of the previous resonance ω_a as displayed in Fig.1.3. This case may create problems for slightly varying natural frequencies.

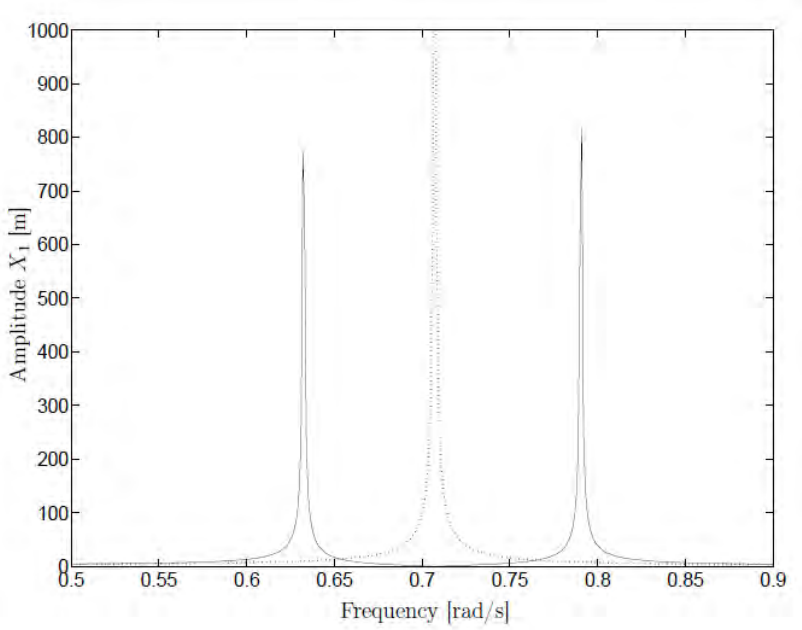

Figure 1.3: FRF of the LO without absorber (dotted line) and with the undamped TMD absorber (solid line).

Ormondroyd and Den Hartog [ODH28] showed that a damped TMD (Fig.1.4) is able to overcome this limit. The coupled system presents a lower attenuation at the resonance frequency but no neighborhood peaks anymore. In Fig.1.5 the FRF of a LO coupled to a damped TMD and its dependence on the damping c_2 is shown. After that first proposition of damped TMD, many studies have focused their attention on the optimization process and several techniques and methods have been developed.

The first optimization technique presented in [ODH28] was the H_∞ optimization, consisting in minimizing the maximum amplitude magnification factor of the primary system $\frac{x_1}{x_{st}}$, with x_{st} being the static displacement $x_{st} = \frac{F}{k_1}$. Today one of the most common technique is the Den Hartog method [DH85] called fixed-point theory. As illustrated in Fig.1.5, irrespective of the value of the damping c_2, two invariant points exist for the FRFs. The optimal tuning parameter $\frac{\omega_a}{\omega_1}$ is then obtained by imposing the same

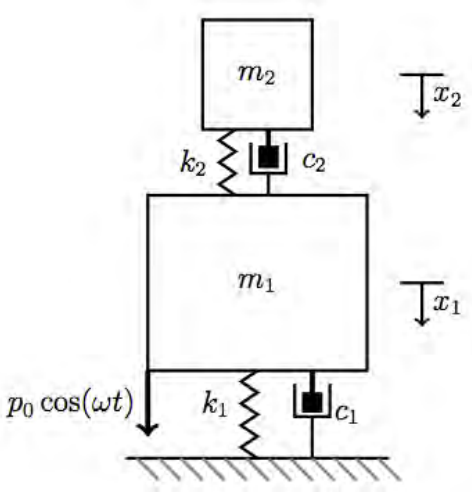

Figure 1.4: Tuned Mass Damper with viscous damping coupled to a linear oscillator.

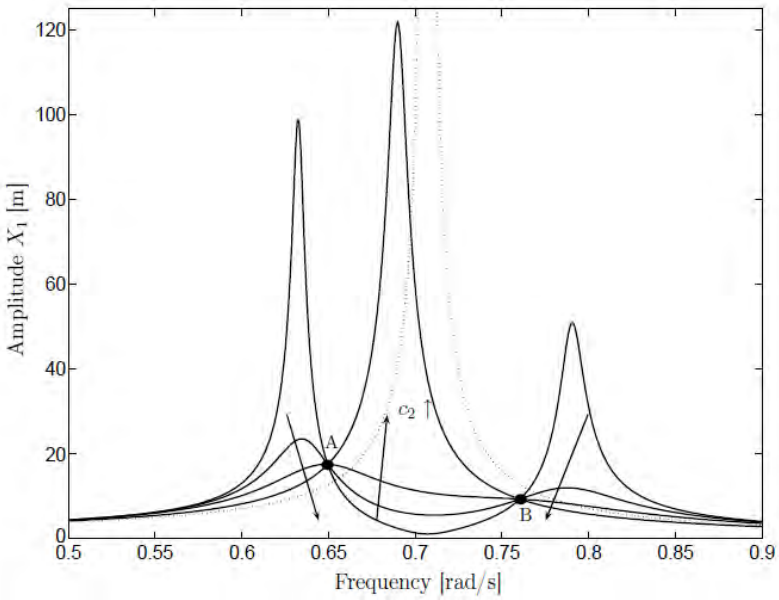

Figure 1.5: FRF of the LO without absorber (dotted line) and with the damped TMD absorber (solid line). The response depends on the absorber damping c_2.

ordinate for the two points. In [Bro46] a method to derive the optimal damping by imposing the fixed points to be the points of maximum amplitude is proposed. In [NM97] an exact formulation of the solution of the problem is presented.

The methods mentioned so far apply to problems where the LO is conservative, i.e. undamped. When the LO is damped the fixed-points theory cannot be used as no invariant points exist. We list here just some relevant studies dealing with the problem of a damped LO. In [Pen98] Chebyshevs min-max criterion is applied, in [Tho80, Tho81] control theory is used. Finally, perturbation methods techniques are presented in [ANB02, FA93] and nonlinear programming in [JC88, JC89].

1.2.1 Tuned Mass Damper performance

We discuss here the performance of a Tuned Mass Damper coupled to a single degree of freedom primary structure. Both the absorber and the primary system are weakly damped. The equations of motion can be written as:

$$\begin{gathered} m_1\ddot{x}_1 + c_1\dot{x}_1 + c_2(\dot{x}_1 - \dot{x}_2) + k_1x_1 + k_2(x_1 - x_2) = F\cos(\omega t) \\ m_2\ddot{x}_2 + +c_2(\dot{x}_2 - \dot{x}_1) + k_2(x_2 - x_1) = 0 \end{gathered} \tag{1.10}$$

We consider here that the TMD is tuned using the basic relation given by Eq.(1.9), so that its natural frequency matches the natural frequency of the primary system. Using a similar approach as explained in [VGa09], the ratio between the energy dissipated by the TMD and the input energy is defined:

$$E_{TMD}(t) = \frac{c_2\int_0^t(\dot{x}_1(\tau) - \dot{x}_2(\tau))^2 d\tau}{\frac{1}{2}m_1\dot{x}_1(0)^2}; \quad E_{TMD,t>>1} = E_{TMD}(t >> 1) \tag{1.11}$$

The input energy corresponds to an impulse in the initial velocity of the primary system $X = \dot{x}_1(t = 0)$.

Fig.1.6 [VGa09] displays the percentage of energy dissipated as a function of the natural frequency of the primary system and of the initial impulse $X = \dot{x}_1(0)$. The first observation is that that energy dissipated is not dependent on the initial impulse. This is a characteristic caused by the linearity of the system: if an input X gives rise to an output Y, an input a times X will give rise to an output a times Y. The percentage dissipated is then invariant regardless of the initial impulse X.

The second observation is that the energy dissipated has a strongly dependence on the natural frequency of the primary system, i.e. on the tuning

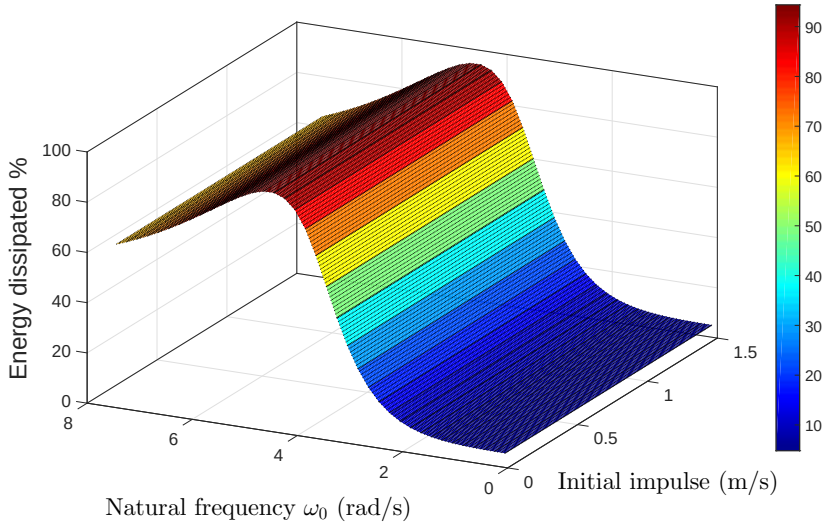

Figure 1.6: Percentage of energy dissipated by the TMD as a function of the natural frequency of the absorber and of the initial impulse $\dot{x}_1(0)$.

condition. It has a maximum at the optimal tuning condition when it is able to dissipate up to 95% of the input energy, but its performance quickly gets worse if the tuning frequency slightly varies. This may creates robustness problems for primary systems with uncertainties on the modal parameters or for systems having a natural frequency that may vary with external forcing, like for example nonlinear systems given their frequency-energy dependence. Moreover the fact the TMD has to be tuned to one specific frequency makes it difficult, or even impossible, to damp several modes of a multiple-degree-of-freedom system with the same device.

1.3 Nonlinear Energy Sink

In the search of improving the performances of the TMD and overcoming its limitations, a research field focusing on nonlinear vibration absorbers has become more and more relevant over the last decades. The first studies focusing on using nonlinearities in vibration mitigation date back to the 50s [Rob52, Pip53, Arn55] and it was in 1982 that a first practical nonlinear absorber using a softening stiffness was presented [HN82]. The source of nonlinearity involved in Nonlinear Vibration Absorbers may in principle be of any kind. As an example, centrifugal pendulum vibration absorbers

used in rotating systems were first studied in [DH38] and lately improved in [Mad80, Den92, SSH06].

Nonlinear absorbers captured the attention of researchers especially because of their ability to "adapt" themselves to the primary system they are attached to without being tuned to a specific frequency. As they do not have a preferential resonant frequency, they are able to interact with the primary system over a broad range of frequency and then to be effective on all the modes within that range.

The nonlinear Targeted Energy Transfer (TET or energy pumping) was observed by Gendelman [Gen01] who studied a 2-DOF system composed of a linear oscillator nonlinearly coupled to an oscillator with zero linear stiffness. Not having a linear stiffness is a crucial point in order to not have a preferential frequency of oscillation. In [Gen12] it was shown that when the energy of the LO is above a certain threshold, a localized periodic motion of the nonlinear oscillator is excited so that the energy is transferred from the LO and finally dissipated. A nonlinear absorber showing this kind of behavior is called Nonlinear Energy Sink (NES).

Further investigations were performed in [VGMM01a, VGMM01b] and TET was defined as the one-way (irreversible on average) channeling of vibrational energy from the directly excited linear primary structure to the attached NES. The mechanism leading to the TET was found to be a transient resonant capture (TRC) thanks to which the NES and LO get into a 1:1 resonance. A threshold criterion for the TET to be enabled was formulated in [Vak01]. It was shown that a dependence of the NES efficiency on the energy present in the system exists: the NES appears to be active beyond a certain threshold of primary system energy. This is a very important difference compared to linear absorbers since as seen in the previous section their performance does not depend on the input energy (impulse X). The concept of Nonlinear Normal Modes was used in [GMVB03, Vak04, MR05] to describe the 1:1 resonance motion involved in the TET mechanism. It was shown that the phenomenon can be described as a degeneration of the underlying Hamiltonian system and that the damping plays a key role in it. A tool utilizing an energy-frequency plot and the wavelet transform spectra to analyze the energy exchange during TET was present in [KVM$^+$05]. The effect of uncertain parameters and more analytic results on energy pumping were shown in [GL06, GAT$^+$07, GL05b].

Experimental works have investigated this phenomenon and are presented in [MBV05, GAT$^+$07, KKM$^+$07]. They have provided evidence that the dynamics which governs the energy transfer phenomenon is a 1:1 resonance capture between the primary system and the NES. As mentioned

earlier, the intrinsic nonlinear nature of the NES allows a 1:1 resonance to occur over a broad range of frequency. TET under external forcing has been investigated theoretically [SG08a] and experimentally [GMSB14a] showing that in addition to the steady state constant amplitude response regime, another type of response can arise referred to as Strongly Modulated Response (SMR). NESs have also been studied when applied to passive control of instabilities. In [GB10] the NES was used to control the limit cycles of a Van der Pol oscillator. In [LVB$^+$07, LKM$^+$07, LVB$^+$08, GVBM10, HMBV10] it was used to suppress aeroelastic instabilities. The complexification-averaging method was used and three mechanisms have been observed: the complete suppression of the instability, the stabilization and the modulation of the response. The aerolelastic instabilities in civil engineering were also studied in [VML11, PLP11].

Most of the works mentioned so far have dealt with a nonlinearity represented by a cubic stiffness. The principle consists in using the geometric nonlinearity of an elastic element to attain a restoring force proportional to the cube of the displacement. Nevertheless the nature of the nonlinearity to be used may theoretically be of any kind. Later studies have explored other ideas such as non-polynomial functions [Gen08], multiple states of equilibrium [GL05a], non-smooth functions [GVMB05b, LGSE11, SLD12] and Vibro-Impacts [GVMB05a, KVG08, LNV$^+$09, NLIM$^+$08]. Many of the first works on Vibro-Impacts were based on numerical simulations. Recently, similarly to what was used for smooth nonlinearities, an analytical approach adopting the Multiple Scales method has been proposed in [Gen12] for impulsive forces and extended to the case of a harmonic forcing in [GA15]. In [GMSB14b] an experimental observation of the different regimes of response has been achieved for a VI-NES applied to a harmonically forced linear oscillator.

1.3.1 An example of Nonlinear Energy Sink attached to a single degree of freedom primary system

Here we present an example of a 2-DOF system composed of a linear 1-DOF primary system to which a 1-DOF nonlinear oscillator is attached. This kind of system is displayed schematically in Fig.1.7 and can be described mathematically by the following equations:

$$\begin{aligned} m_1\ddot{x}_1 + c_1\dot{x}_1 + c_2(\dot{x}_1 - \dot{x}_2) + k_1x_1 + k_2(x_1 - x_2)^3 = F\cos(\omega t) \\ m_2\ddot{x}_2 + c_2(\dot{x}_2 - \dot{x}_1) + k_2(x_2 - x_1)^3 = 0 \end{aligned} \tag{1.12}$$

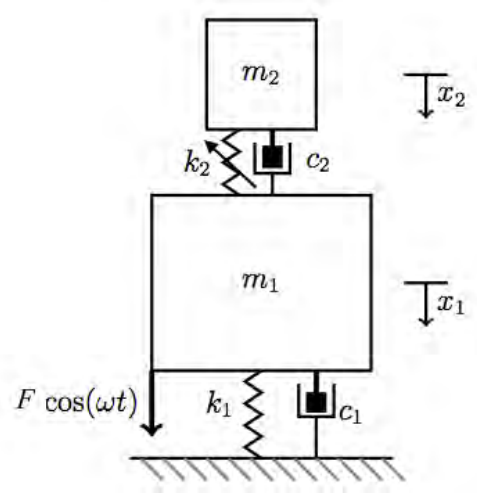

Figure 1.7: A Nonlinear Energy Sink coupled to a 1-DOF linear oscillator.

The system illustrated in Fig.1.7 and governed by Eqs.(1.12) is a classic example of NES, often referred to as *cubic stiffness NES*. In this system the nonlinearity is in the restoring force between the two masses: the force is proportional to the cube of the relative displacement $F_{nl} = k_2(x_2 - x_1)^3$. It is important to emphasize that a system like this may present an interesting and complicated behavior even when the nonlinearity is weak. This 2-DOF system has been extensively studied in the literature and the results of some recent works [LKV$^+$05,KMK$^+$08,MKK$^+$05] can be used to compare its efficacy as a vibration absorber to the performance of the Tuned Mass Damper.

Adopting a similar approach as in Sec.1.2.1, the energy dissipated by the NES following an impulsive external forcing on the primary system can be defined as:

$$E_{NES}(t) = \frac{c_2 \int_0^t (\dot{x}_1(\tau) - \dot{x}_2(\tau))^2 d\tau}{\frac{1}{2} m_1 \dot{x}_1(0)^2}; \quad E_{NES,t>>1} = E_{NES}(t >> 1) \quad (1.13)$$

This quantity is displayed in Fig.1.8 as a function of the natural frequency of the primary system and of the initial impulse $X = \dot{x}_1(0)$. The scenario is now completely different than what we had in Fig.1.6 for the TMD. Two important considerations have to be done:

- The energy dissipated has a strong dependence on the initial impulse X and a threshold exists for the NES to be efficient. In other words

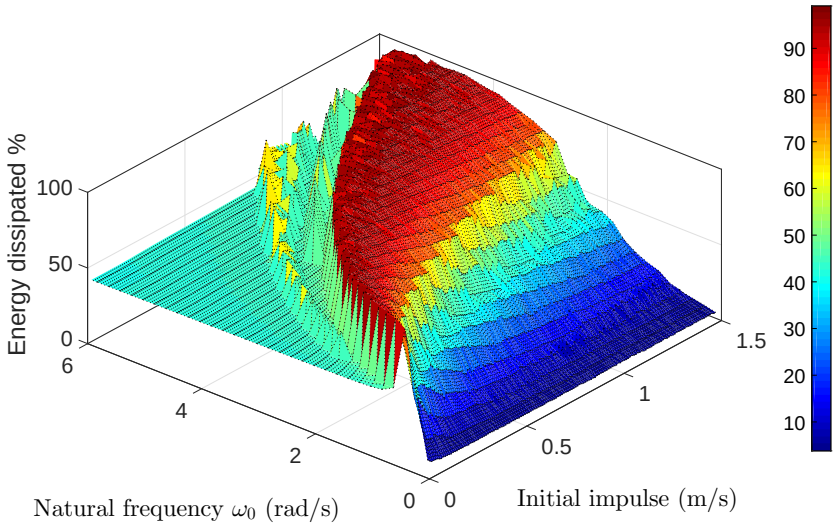

Figure 1.8: Percentage of energy dissipated by the NES as a function of the natural frequency of the absorber and of the initial impulse $\dot{x}_1(0)$.

the NES is able to dissipate the energy of the primary system if this energy is higher than a certain threshold. This minimum amount of energy is required for the energy transfer (TET) to occur.

- The NES is capable of dissipating the energy of the primary system over a broad range of primary system's natural frequency. This characteristic of nonlinear absorbers is due to the fact that the NES does not own a natural frequency and then it can adapt itself to the primary system's oscillations. This is a very important feature especially when there exists some uncertainty about the natural frequency of the system to control.

1.3.2 Underlying Hamiltonian system

As mentioned earlier in this chapter, the mechanism which governs the dynamics of the NES, and its ability to absorb the energy of the primary system it is attached to, is the so-called Targeted Energy Transfer or Energy pumping. This phenomenon can be explained and described by analyzing the corresponding system in the absence of viscous damping, i.e. by considering the underlying conservative Hamiltonian system.

In [VGMM01b] a linear oscillator (LO) coupled to a NES is studied.

It has been shown that the solutions (orbits) of the Hamiltonian systems involving a 1:1 resonance between the LO and the NES are those responsible for the TET. These solutions can be calculated analytically by means of the Complexification-Averaging method presented in [Man01].

The 1:1 solutions exist for any level of energy in the system but they cannot be established if the system is at rest in its initial conditions. There exist then some connecting orbits called impulsive orbits that allow the system to reach the 1:1 resonance. However the impulsive orbits can be excited only if the level of energy is higher than a certain threshold; which explains the sharp discontinuity in the energy dissipated by the NES visible in Fig.1.8. The NES goes from a state of inactivity to a state of activity through a non-smooth transition as soon as the energy threshold condition is satisfied. This is a substantial difference compared to the dynamics of linear absorbers. In [VGMM01a] the mechanism of resonance capture between the NES and the LO is analytically analyzed. In [LKV$^+$05] the periodic orbits of a similar system are studied. It is shown that in addition to the fundamental orbits 1:1, other sub-harmonic orbits exist where the LO and the NES oscillate at different frequencies. The solutions are presented in a frequency-energy plot (FEP) introduced in [VMGB03]. Also the impulsive orbits for the same type of NES were calculated in [KMK$^+$08]. An example of frequency-energy plot is illustrated in Fig.1.9 where we report the diagram presented in [KKM$^+$07]. In this plot, the main branches $S11+$ and $S11-$ represent the solutions where the LO and the NES oscillate at the same frequency. The $+$ and $-$ signs are used to indicate the in-phase and out-of-phase oscillations respectively. The horizontal lines (tongues) represent the sub-harmonic solutions as for example an oscillation 1:3 indicating the NES is vibrating at a frequency three times higher than the LO's. Finally the black dots represent the impulsive orbits.

It is important to notice that for a low level of energy, the $S11\pm$ solutions are the normal modes of the linearized system. In fact, the nonlinearities start to have a tangible role only at a certain level of energy flowing in the system. As an extension of the linear normal modes concept, the families of solutions $S11\pm$ are referred to as Nonlinear Normal Modes (NNMs). We will explain more in detail this concept in the next chapter. However it should be noticed that a NNM, unlike a linear normal mode, has a variable natural frequency which depends on the level of energy of the system. These NNMS can be computed by a method based on continuation technique [PVR$^+$08].

Hence, we can conclude that the Hamiltonian approach gives a significant piece of information as it provides a comprehensive view of all the possible solutions. However, because of the strong dependence of the NNMs on the

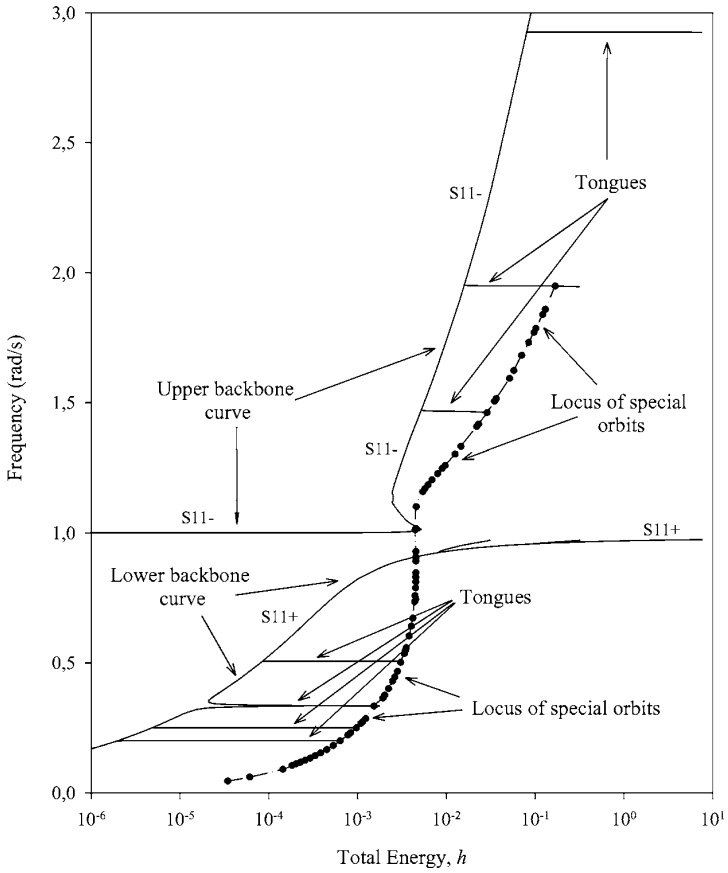

Figure 1.9: Frequency-Energy plot of a linear oscillator coupled to a NES. Image from [KKM+07].

level of energy, the damping plays a crucial role when it comes to studying the dynamics of the system along the NNMs branches as it allows the system to move through different energy levels.

1.3.3 Example of a 1:1 resonance capture in a damped NES attached to a 1 dof linear oscillator

The presence of the damping permits the NES to dissipate the energy of the system. As the energy decreases, the nonlinear normal modes evolve and their frequencies vary. It has been shown that the behavior of the weakly damped system is governed by the dynamics of the underlying Hamiltonian

system: the periodic solutions/orbits, i.e. NNMs, are the same.

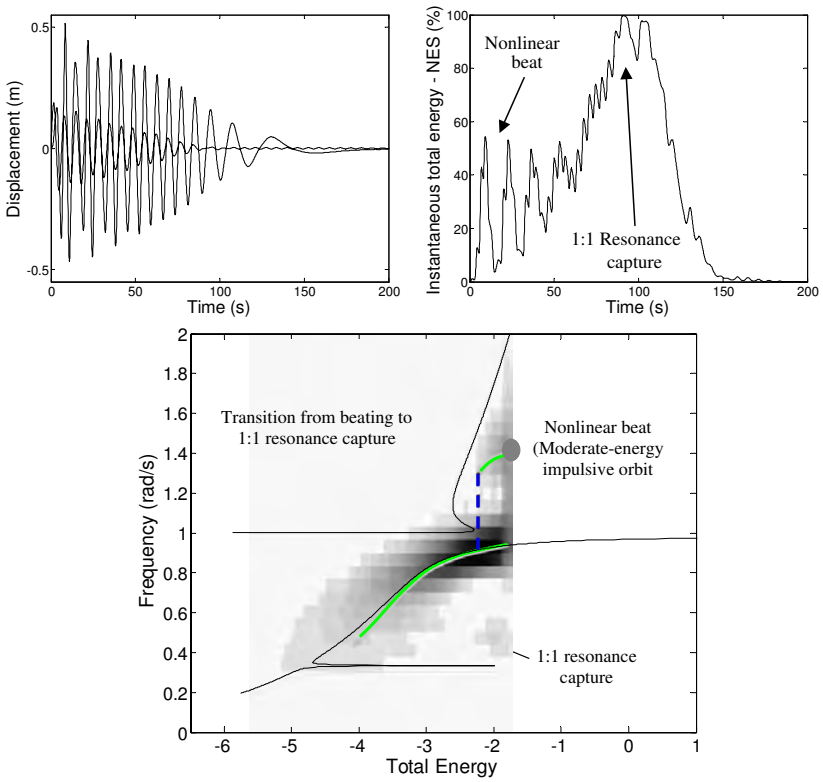

Figure 1.10: Example of numercal simulation of 1:1 resonancne capture. In the bottom figure the projection of the dynamics of the system on the FEP is shown. Images from [KMK$^+$08].

A numerical example taken from [KMK$^+$08] is presented in Fig.1.10. The LO initially at rest is subjected to an impulsive force. The transient response corresponds to the activation of the connective impulse orbits which lead to the 1:1 resonance capture. Once the 1:1 regime is established the energy of the LO is transferred to the NES and dissipated by the viscous damping. An analytic method to study the system taking into account the viscous damping is presented in [Gen04]. The approach is based on the multiple scales method and it consists in breaking down the problem in several sub-problems, each of them at a different time scale. Typically the dynamics of a NES attached to a 1-dof LO appears to have a fast time scale describing the oscillations of the NES at the same frequency as the LO's, and a slower

time scale describing the evolution of the amplitude of the fast oscillations.

Thanks to the multiple scales method, the Slow Invariant Manifold (SIM) of the problem can be obtained. The SIM provides a comprehensive view of all the possible solutions of the problem, stable and unstable. The multiple scales method and the concept of Slow Invariant Manifold are used later on in this dissertation for the analysis of the Vibro-Impact Nonlinear Energy Sink.

1.3.4 Further studies on Targeted Energy Transfer and NES applications

The Targeted Energy Transfer phenomenon was studied in [JMBV03] in the case of a NES attached to a LO subjected to a harmonically excitation. The authors calculated the fixed points of the system by using the complexification-averaging method. For the same system the fixed points were also obtained using the harmonic balance in [MN07].

Besides the steady and quasiperiodic solutions, a NES-LO system may exhibit other types of response that cannot be explained by the study of the fixed points. As mentioned earlier in this chapter, such a system may show a strongly modulated response in which the amplitude of the modulation is comparable to the amplitude of the oscillations. This type of response was firstly explained in [GGL06] and it has represented the object of several further studies [GS07,SG08b]. The strongly modulated response (SMR) has been correlated to the topology of the Slow Invariant Manifold and then to the NES damping and to the mass ratio LO/NES [GSF08], both primarily important parameters. In [SG10a] it was analytically shown that the SMR disappears when the ratio between the mass of the NES and mass of primary system reaches values close to unity. The same authors studied the energy pumping in a system subjected to periodic and random forcing in [SG10b].

Furthermore, Targeted Energy Transfer was studied in acoustics [BCHM10, BCCM12,MBC$^+$11], where an equivalent system to a mechanic LO-NES was obtained. The energy pumping was also observed for NESs applied to continuous structures. In [GV07] the behavior of a linear beam with an attached nonlinear absorber is numerically investigated. The same system is analytically treated in [VG10]. The case of a NES applied to a compressed rod was studied in [GVK07, PGT$^+$07] by means of the Frequency-Energy Plot. On the same system a configuration multi-NES is presented in [TPK$^+$07]. An example of TET occurring for a bi-dimensional primary system is illustrated in [GV09] where multi-NES are used to passively control vibrations of a thin plate.

1.3.5 Review of experimental studies on Targeted Energy Transfer

We report here more in detail a bibliographic review of some of the experimental works on Targeted Energy Transfer that can be found in the literature. A big part of this dissertation has an experimental nature and these studies have been used as basis and inspiration to the work presented in this thesis.

An experimental realization of a NES attached to a 1 dof primary system is presented in [MBV05]. The type of nonlinearity is a cubic stiffness and is obtained by using the elastic force of wires (piano wires) working transversely. In order to have a purely cubic force the wires must not be axially preloaded. This appeared to be a delicate aspect to realize in experiments and it will be taken in consideration later on in this dissertation when the Magnetic-Strung NES is presented. The prototype and the schematic of the NES studied in [MBV05] is illustrated in Fig.1.11.

The same system but with a grounded NES is studied in [KMK$^+$07] and illustrated in Fig.1.12. The TET is experimentally observed as well as the activation threshold for the NES activation. The instantaneous frequency is measured by means of the wavelet technique and the results projected on the theoretical frequency-energy plot. The experimental apparatus used in [BCHM10] is shown in Fig.1.13 where the NES is made out of a flexible membrane.

In [KMK$^+$08] the TET on a 2 dof primary system is investigated. The experimental system is similar to that used in [MBV05] and the multi-modal energy pumping is observed and validated.

Experimental studies related to civil engineering have also been carried out. In [GLP07] a reduced model of a multi-dof building subjected to a harmonical forcing is analyzed. In [NLIM$^+$08] a similar system is studied under the effect of a seismic excitation. In this case a Vibro-Impact NES was utilized (Fig.1.14).

A significant contribution to the study of a Nonlinear Energy Sink attached to a harmonically forced primary system has been made by the Ph.D. thesis work of Etienne Gourc at the ISAE/INSA Toulouse [Gou13]. A cubic stiffness (Fig.1.15) and a Vibro-Impact NES (Fig.1.16) were studied both analytically and experimentally. This work has been considered as a starting point for the study of this Ph.D dissertation.

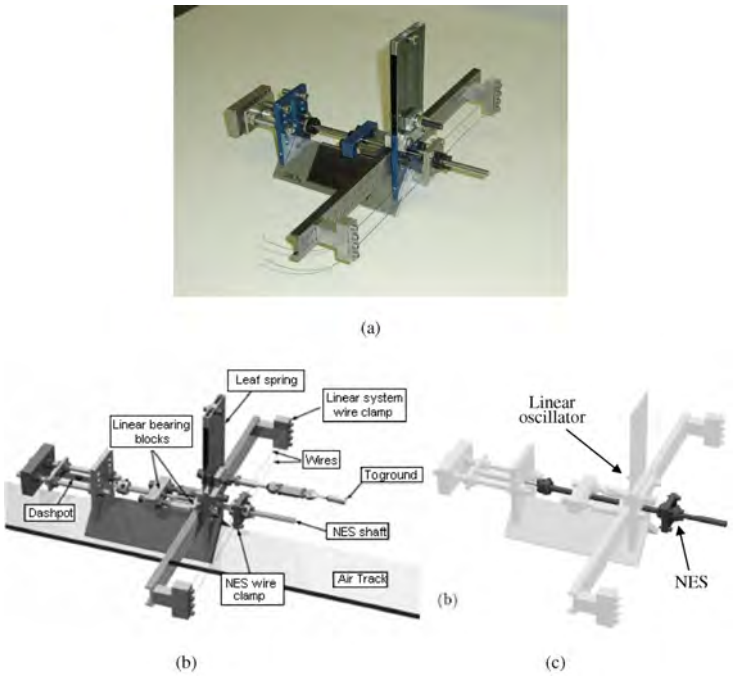

Figure 1.11: Experimental realization and schematic of the NES system studied in [MBV05].

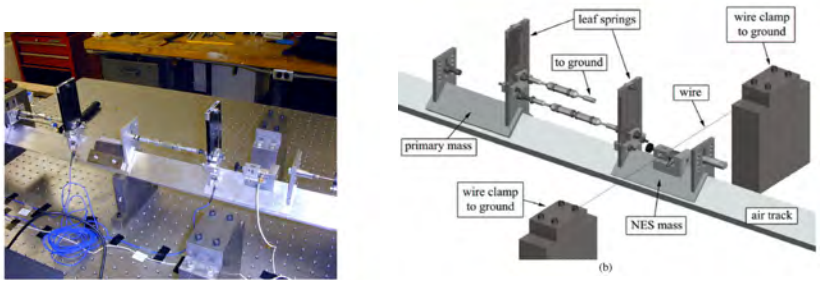

Figure 1.12: Experimental realization and schematic of the grounded NES system studied in [KMK+07].

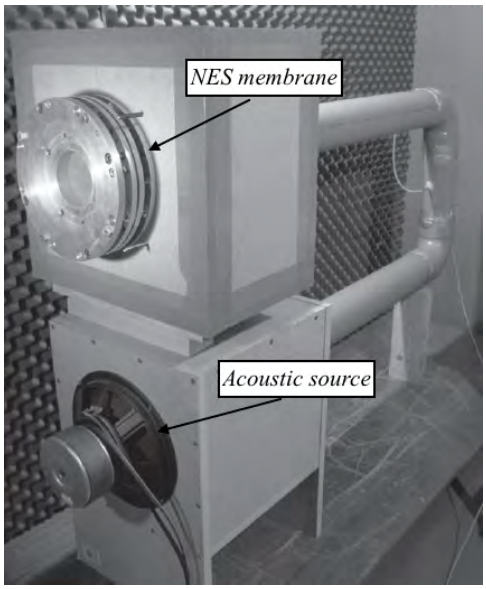

Figure 1.13: Experimental realization of the acoustic NES system studied in [BCHM10].

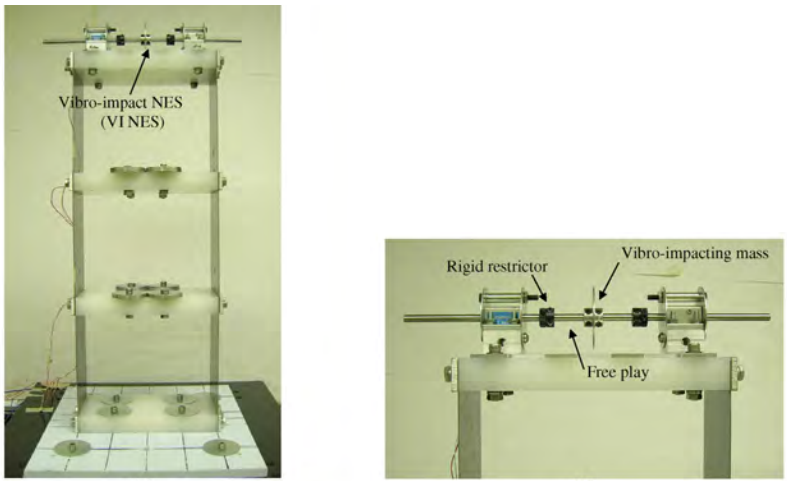

Figure 1.14: Experimental realization and schematic of Vibro-Impact NES system studied in [NLIM$^+$08].

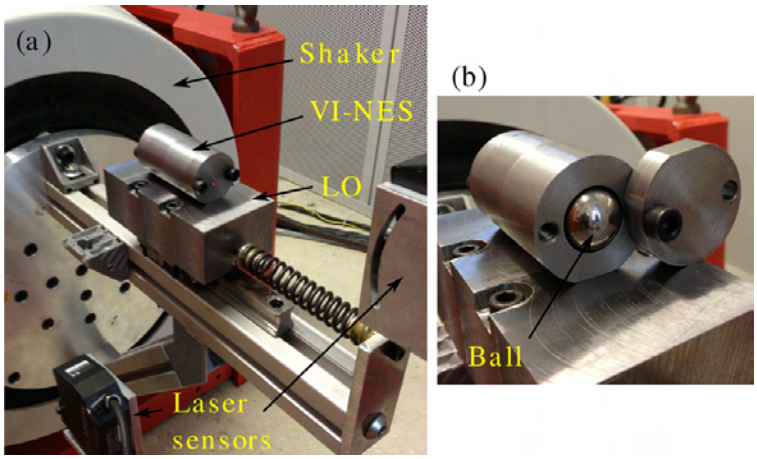

Figure 1.15: Experimental realization of the Vibro-Impact NES system studied in [GMSB14b].

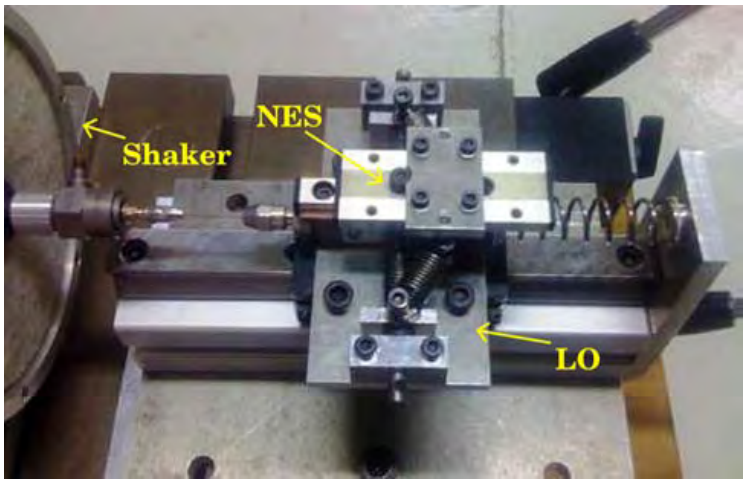

Figure 1.16: Experimental realization of the cubic stiffness NES system studied in [GMSB14a].

1.4 Energy harvesting from vibrations

One of the objectives of this thesis is also to investigate the capability of using a nonlinear vibration absorber not only to dissipate the vibration energy but also to recover it. This aspect is studied later on in this dissertation when the Magentic-Strung NES is presented. In order to achieve this goal a bibliographic study on energy harvesting has been conducted and it is here briefly reported.

Energy harvesting from environment [BTW06] has recently known a growing interest and many works have been motivated by advancements in microelectronics industry which have enabled a reduction in the power consumed by MEMS devices [GJTBW04,RWR03]. Solar, chemical and thermal methods have been extensively investigated and recognized as potential sources of energy. In addition, vibration is another important source and scavenging energy from it has become a promising area of inquiry. First works focused on inertial generators with linear behavior [WY95]. A primary limitation of linear inertial generators is their narrow-band efficacy: their performance significantly decrease for any variation in the excitation frequency. Tuning the device's resonance and widening the bandwidth by adding many oscillators are some methods that have been studied in [SBK08] and [LW06] to overcome this limitation.

However, as for vibration absorbers, nonlinear dynamics seems to offer a suitable alternative to improve performances in energy harvesting. One of the first experimental investigations of an energy harvester specifically designed to exhibit a nonlinear response was described in [MS09] where magnetic levitation was used to extend the device bandwidth. A similar study based on piezoelectric energy conversion is presented in [SMM09]. A piezoelectric nonlinear energy harvester is presented in [YZZ15] where high power output and wide working bandwidth are reached. The same authors have also investigated a new magnetoelectric generator in [ZZ12]. Many systems demonstrate the advantages of monostable Duffing oscillators for increased bandwidth. The bistable Duffing oscillator has also been investigated for energy harvesting in [SMM10] and [MO10].

1.5 Motivation of this doctoral dissertation and outline of the thesis

The literature review presented in this chapter has shown that the Targeted Energy Transfer has been the subject of several theoretical studies and some

experimental investigations. However, in order to fully exploit its potential advantages, the Nonlinear Energy Sink as a vibration absorber still presents some points that should be examined and better understood. For instance, when it comes to vibration mitigation in a practical/industrial application, the complexity of a NES realization often makes engineers lean towards the use of the well-known Tuned Mass Damper. Certainly, whether using a nonlinear or a linear absorber it depends on the single application case and on the criteria to meet [GDK$^+$16]. Nevertheless, we think the potential of the NES deserves additional research in order to attain to a broader knowledge of this device and its operating mechanisms.

Dealing with Nonlinear Structural Dynamics often means that the principles and concepts taken as granted in classical dynamics may not be valid anymore. Especially during experimental studies, this requires an additional effort to understand new and unexpected behaviors that may arise.

In this study we tried to explain the physics of the phenomena we observed by using the tools the mathematics provides. A bridge between mathematical modeling and engineering sense is sought through all the phases of the work presented in this dissertation.

The study of Targeted Energy Transfer (TET) in strongly nonlinear and non-conservative oscillators poses some distinct technical challenges, and dictates the use of concepts, formulations, analytical methodologies and computational techniques from different fields of applied mathematics and engineering, such as dynamical systems and bifurcation theory, numerical signal processing, and experimental dynamics. Therefore, before we initiate our study of the nonlinear dynamics of TET, it is appropriate to first provide some background information related to certain key concepts and methodologies that will be applied in the work that follows.

In the next chapter some fundamental concepts of nonlinear dynamics, used further in the dissertation, are introduced. The classic Duffing oscillator is used as an example to introduce the concept of frequency-energy dependency and bifurcation. The notion of nonlinear normal modes is also introduced by providing some definitions available in the literature and an example on a 2-dof system.

In the third chapter we enter the core of this dissertation by presenting the first NES studied in this work: the Vibro-Impact Nonlinear Energy Sink (VI-NES). An initial study on this kind of system was started by Gourc in [Gou13] and interesting results proved this device as promising especially because of its simplicity in the practical realization. The VI-NES is applied to a single-degree-of-freedom linear oscillator harmonically forced. Depending on external force amplitude and frequency, either a Strongly Modulated

Response (SMR) or a constant amplitude response (CAR) is observed. In both cases an irreversible transfer of energy occurs from the LO towards the VI-NES. The problem is analytically studied by using the multiple scales method. The Slow Invariant Manifold (SIM) and the fixed points of the problem are calculated. Finally a good correlation between experimental and analytical results is shown.

The fourth chapter illustrates the theoretical design and experimental realization of the second type of Nonlinear Energy Sink studied in this work. The goal was to broad our research to the field of energy harvesting and combine it with the nonlinear absorbers' domain. The study was conducted during a visiting period at the Duke University's Mechanical Engineering Department. This collaboration provided significant insights thanks to their expertise in the area of nonlinear dynamics and energy harvesting. The NES analyzed is a cubic NES coupled to an electro-magnetic energy harvester. The mass of the Magnetic-Strung NES is a magnet which is linked to the primary system by means of two strings working transversally. The restoring elastic force of the strings is modulated thanks to the magnetic force applied by two magnets suitably located on the primary mass. The NES' efficiency as an absorber is studied on a harmonically forced 1 degree-of-freedom primary system. The Target Energy Transfer (TET) from the primary system towards the NES is experimentally observed as well as different response regimes like the Strongly Modulated Response. Moreover, the energy harvesting from the vibrating energy of the NES is investigated: the NES mass, made up of a magnet, oscillates into a coil and subsequently creates an electric current. Thus, the vibrating energy of the primary mass is in this way absorbed by the NES and finally converted into electric energy.

The thesis concludes with an analysis of the research conducted and its future perspectives.

Chapter 2

Fundamentals of Nonlinear Dynamics

Abstract

In this chapter some fundamentals of nonlinear structural dynamics are presented. The classical example of the Duffing oscillator is used to introduce the concept of frequency-energy dependency and bifurcation. The notion of nonlinear normal modes is also introduced and their main features presented by providing some examples taken from the literature.

2.1 Duffing oscillator

The differential equation describing many nonlinear oscillators can be written in the form:

$$\frac{d^2x}{dt^2} + f\left(x, \frac{dx}{dt}\right) = 0 \tag{2.1}$$

A convenient way to treat Eq.(2.1) is to rewrite it as a system of two first order ordinary differential equations:

$$\frac{dx}{dt} = y, \quad \frac{dy}{dt} = -f(x, y) \tag{2.2}$$

Which may be generalized as:

$$\frac{dx}{dt} = F(x, y), \quad \frac{dy}{dt} = G(x, y) \tag{2.3}$$

A point which satisfies $F(x, y) = 0$ and $G(x, y) = 0$ is called an equilibrium point. The solution of Eq.(2.3) may be represented by a curve in the $x - y$ phase plane passing through the point of initial conditions (x_0, y_0). Each time a motion passes through a given point (x, y), its direction is always the same. This means a given motion cannot intersect itself. A periodic motion corresponds to a closed curve in the phase plane.

The differential equation:

$$\ddot{x} + \delta\dot{x} + \beta x + \alpha x^3 = \gamma\cos(\omega t) \tag{2.4}$$

is known as the Duffing oscillator's equation and is a classical example of nonlinear system which exhibits interesting nonlinear phenomena. We present here a short analysis of this system to introduce some concepts of nonlinear dynamics which will be used further in this dissertation.

It is a model of a structural system which includes a nonlinear restoring force. It may be used as an approximation for the simple pendulum illustrated in Fig.2.1 and governed by the equation of motion:

$$\frac{d^2\theta}{dt^2} + \frac{g}{L}\sin\theta = 0 \tag{2.5}$$

Expanding $\sin\theta = \theta - \frac{\theta^3}{6} + O(\theta^5)$ we obtain an undamped and unforced Duffing's equation:

$$\frac{d^2\theta}{dt^2} + \frac{g}{L}\left(\theta - \frac{\theta^3}{6}\right) = 0 \tag{2.6}$$

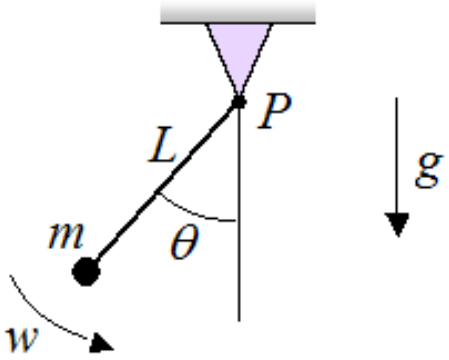

Figure 2.1: Simple pendulum.

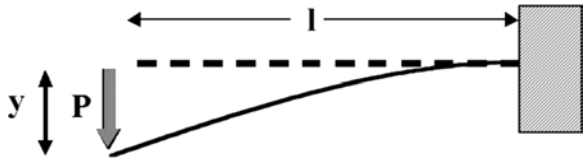

Figure 2.2: Beam with large displacement.

Another example the Duffing equation can model is the structural beam with a transversal load illustrated in Fig.2.2.

If we drop the hypothesis of small displacement, the behavior of the beam is not linear anymore and the equation of motion can be written by adding a nonlinear restoring force:

$$\ddot{x} + 2\xi\omega_n\dot{x} + \omega_n^2 x + \alpha x^3 = F\sin(\Omega t) \tag{2.7}$$

Where ω_n is the natural frequency and ξ the damping ratio.

In the case of an undamped and unforced system the equation of motion becomes:

$$\ddot{x} + \omega_n^2 x + \alpha x^3 = 0 \tag{2.8}$$

Which describes the free oscillations of the system.

2.1.1 Phase space and stability analysis

For $\beta > 0$ the Duffing oscillator can be interpreted as an oscillator with a spring whose restoring force is $F_{el} = \beta x + \alpha x^3$. When $\alpha > 0$ the spring is called hardening, when $\alpha < 0$ it is called softening.

In the case of an undamped and unforced oscillator, if we rewrite the Dumping's equation as a first order system:

$$\frac{dx}{dt} = y, \quad \frac{dy}{dt} = -\beta x - \alpha x^3 \tag{2.9}$$

We can describe the motion of the system in the $x - y$ space, i.e. the trajectory in the phase plane. The integral curve can be expressed as:

$$\frac{dy}{dx} = \frac{\frac{dy}{dt}}{\frac{dx}{dt}} = \frac{-\beta x - \alpha x^3}{y} \tag{2.10}$$

Eq.(2.10) can be integrated to give:

$$E(t) = \frac{y^2}{2} + \beta\frac{x^2}{2} + \alpha\frac{x^4}{4} = constant \tag{2.11}$$

Eq.(2.11) corresponds to the physical principle of conservation of energy and the Duffing oscillator is a Hamiltonian system. For $\alpha > 0$ it is observed that $E(t)$ is a single well potential for $\beta > 0$ and it is a double well potential for $\beta < 0$. The trajectory (y, x) moves on the surface of $E(t)$ keeping $E(t)$ constant. When $\delta > 0$, the system is damped:

$$\frac{dE(t)}{dt} = -\delta\dot{x}^2 \leq 0 \tag{2.12}$$

The trajectory moves on the surface $E(t)$ so that $E(t)$ decreases until one point of equilibrium is reached. For $\alpha > 0$, $\beta > 0$ and $\delta > 0$ the only equilibrium is $(x, y) = (0, 0)$. $E(t)$ is a Lyapunov function[1] and $(x, y) = (0, 0)$ is globally asymptotically stable.

When $\alpha > 0$ and $\beta < 0$ there are three equilibria. This situation is illustrated in Fig.2.3 and Fig.2.4 for the undamped case and in Fig.2.6 for the damped one. Two equilibria are at the bottom of $E(t)$, one is at a peak.

The equilibria of the unforced Duffing oscillator can be obtained by substituting $\ddot{x} = \dot{x} = 0$ to Eq.(2.4):

$$x(\beta + \alpha x^2) = 0 \tag{2.13}$$

The point $x = 0$ is always an equilibrium. Moreover, when $\alpha\beta < 0$, two additional equilibrium points appear. The stability of these points can be

[1] A Lyapunov function is a scalar function $V(y)$ defined on a region D that is continuous, positive definite, $V(y) > 0$ for all $y \neq 0$, and has continuous first-order partial derivatives at every point of D.

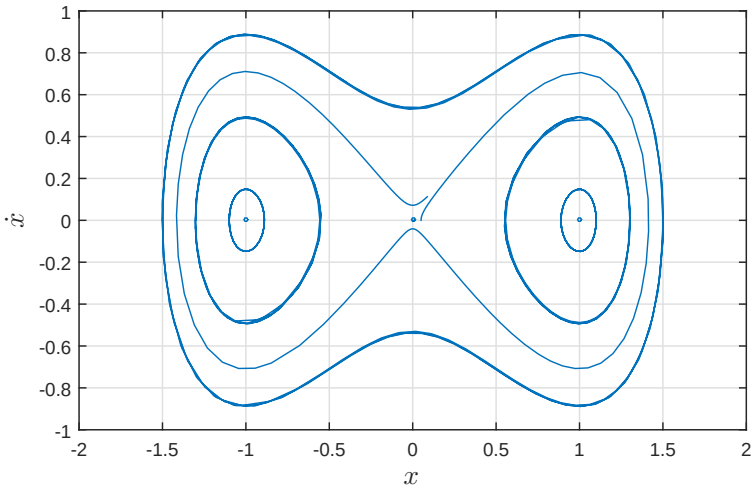

Figure 2.3: Undamped Duffing oscillator's phase space.

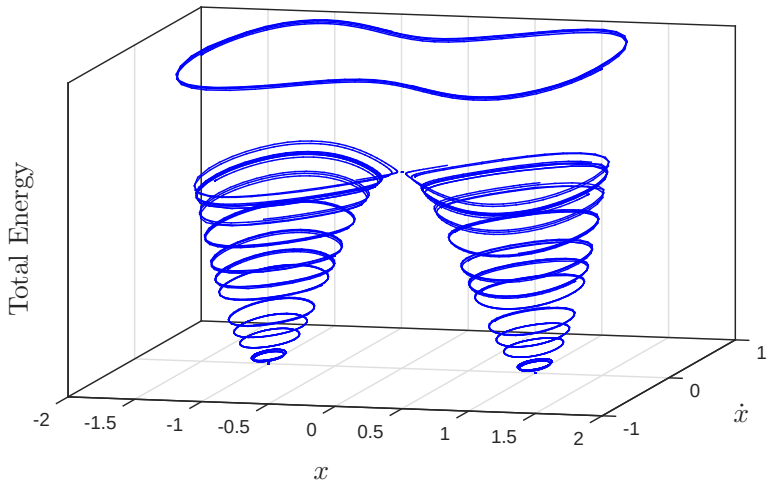

Figure 2.4: Undamped Duffing oscillator's orbits at different levels of total energy.

studied by analyzing the Jacobian matrix of the Eq.(2.4) written as a first order system:

$$\frac{d}{dt}\begin{pmatrix} x \\ \dot{x} \end{pmatrix} = \begin{pmatrix} \dot{x} \\ -\delta\dot{x} - \beta x - \alpha x^3 \end{pmatrix} \tag{2.14}$$

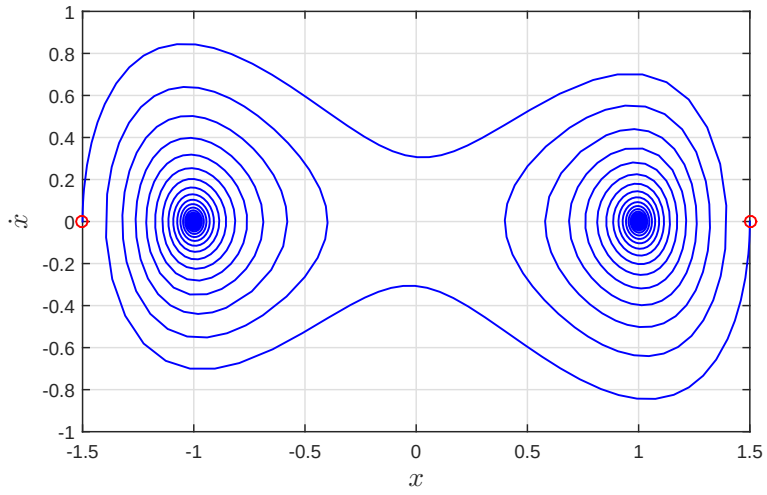

Figure 2.5: Damped Duffing oscillator's phase space for two different initial conditions (red dots).

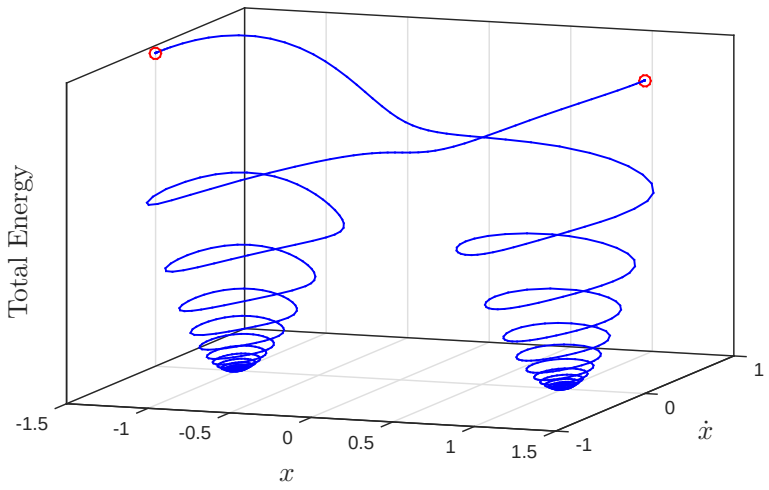

Figure 2.6: Evolution of two damped Duffing oscillator's orbits as the total energy decreases. The red dots represent the initial conditions.

The Jacobian matrix $J(x)$ is:

$$J(x) = \begin{pmatrix} 0 & 1 \\ -\beta - 3\alpha x^2 & -\delta \end{pmatrix} \tag{2.15}$$

Then, the eigenvalues of $J(X)$ for the equilibrium $x = 0$:

$$\lambda = \frac{-\delta \pm \sqrt{\delta^2 - 4\beta}}{2} \tag{2.16}$$

The equilibrium is stable for $\beta \geq 0$ and unstable for $\beta \leq 0$. On the other hand, the eigenvalues of the equilibria $x = \pm\sqrt{-\beta/\alpha}$ are:

$$\lambda = \frac{-\delta \pm \sqrt{\delta^2 + 8\beta}}{2} \tag{2.17}$$

They are stable for $\alpha > 0$ and $\beta < 0$ and unstable for $\alpha < 0$ and $\beta > 0$.

2.1.2 A perturbation method to obtain the backbone curve

If we numerically integrated Eq.(2.4), we would see that the frequency of the periodic motions depended on which closed curve in the phase plane we were on. This effect is typical of nonlinear vibrations and is referred to as the dependence of frequency on amplitude. Analytical methods exist to derive the relationship between frequency and amplitude in Duffing's equations. These methods are called perturbation methods and a detailed review about them can be found in [Nay04].

We present here a simple perturbation method called Lindstedt-Poincaré 's method which we use to obtain the frequency-amplitude relationship in the undamped Duffing oscillator.

We rewrite the Duffing's equation as:

$$\frac{d^2x}{dt^2} + x + \epsilon\alpha x^3 = 0 \tag{2.18}$$

where ϵ is a positive small parameter.

We introduce a stretched time:

$$\tau = \omega t, \qquad \omega = 1 + k_1\epsilon + k_2\epsilon^2 + \dots \tag{2.19}$$

where the coefficients k_i are to be found. Substituting Eq.(2.19) into Eq.(2.18):

$$\omega^2\frac{d^2x}{d\tau^2} + x + \epsilon\alpha x^3 = 0 \tag{2.20}$$

Then we expand x in a power series in ϵ:

$$x(\tau) = x_0(\tau) + \epsilon x_1(\tau) + \epsilon^2 x_2(\tau) + \dots \tag{2.21}$$

It is important to highlight that the results obtained by this method are expected only to be valid for small values of ϵ. Substituting Eq.(2.21) into Eq.(2.20) and gathering terms of the same order:

$$\begin{aligned}
&\frac{d^2x_0}{d\tau^2} + x_0 = 0 \\
&\frac{d^2x_1}{d\tau^2} + x_1 = -2k_1\frac{d^2x_0}{d\tau^2} - \alpha x_0^3 \\
&\frac{d^2x_2}{d\tau^2} + x_2 = -2k_1\frac{d^2x_1}{d\tau^2} - (2k_2 + k_1^2)\frac{d^2x_0}{d\tau^2} - 3\alpha x_0^2 x_1
\end{aligned} \tag{2.22}$$

The first equation of system (2.22) has the solution:

$$x_0(\tau) = A\cos\tau \tag{2.23}$$

Here A is the amplitude of the motion and an arbitrary phase is chosen thanks to the autonomous nature of Eq.(2.18), i.e. the absence of explicit dependency on the variable t. After substituting the solution for x_0 into the second equation of Sys.(2.22), we get:

$$\frac{d^2x_1}{d\tau^2} + x_1 = 2Ak_1\cos\tau - A^3\alpha\cos^3\tau \tag{2.24}$$

The trigonometric term $\cos^3\tau$ can be rewritten so that we obtain:

$$\frac{d^2x_1}{d\tau^2} + x_1 = \left(2Ak_1 - \frac{3A^3\alpha}{4}\right)\cos\tau - \frac{A^3\alpha}{4}\cos 3\tau \tag{2.25}$$

In order to have a periodic solution, we require the secular terms to vanish. The coefficient of $\cos\tau$ is forced to zero:

$$2Ak_1 - \frac{3A^3\alpha}{4} = 0 \tag{2.26}$$

Which provides the value of k_1:

$$k_1 = \frac{3}{8}\alpha A^2 \tag{2.27}$$

Substituting this result into the ansatz (2.19) we obtain the approximate frequency-amplitude relation:

$$\omega = 1 + k_1\epsilon + O(\epsilon^2) = 1 + \frac{3}{8}\alpha A^2\epsilon + O(\epsilon^2) \tag{2.28}$$

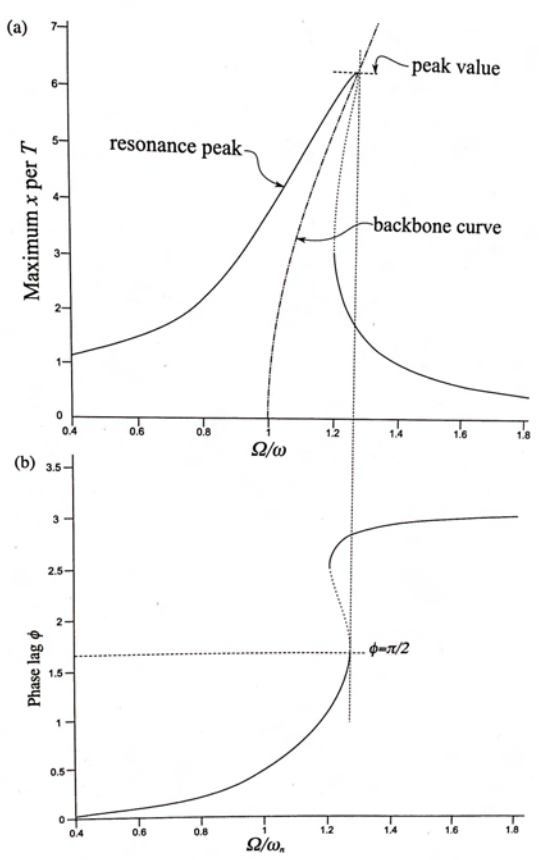

Figure 2.7: Backbone curve and forced response of the Duffing oscillator. Image from [WN15].

The solution for x_1 becomes:

$$x_1(\tau) = \frac{A^3\alpha}{32}(\cos 3\tau - \cos \tau) \tag{2.29}$$

The process may be continued indefinitely to obtain higher order approximations.

Eq.(2.28) represents the relationship between the natural frequency and the amplitude of the motion for the Duffing oscillator and is called backbone curve. The dependency of the natural frequency on the amplitude of the motion, and then on the energy of the system, is a main characteristic of nonlinear systems as well as a fundamental difference with linear systems. In Fig.2.7, the backbone curve is plotted along with the forced response for the

Duffing oscillator in the case of a hardening stiffness ($\alpha > 0$). Furthermore, we should notice that the property of having a phase $\phi = \pi/2$ at the peak value is preserved. This is an important feature that can be used in the experimental analysis of nonlinear systems.

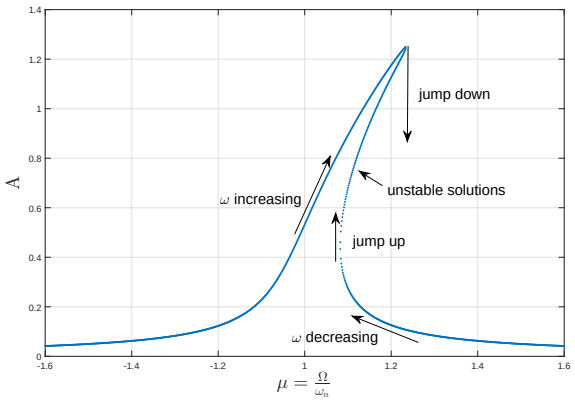

Figure 2.8: Response of the driven Duffing oscillator.

By looking more in detail at the driven response of the Duffing oscillator as reported in Fig.2.8, we can notice that there is a range of frequencies where more than one possible solution coexist. Actually Fig.2.8 can be interpreted as a bifurcation diagram for the Duffing oscillator whereas the forcing frequency is the varying parameter.

When the forcing frequency increases and the peak value is reached, the response jumps down to a stable lower amplitude state. In the same way when the forcing frequency decreases and the system reaches an unstable point, the response suddenly jumps up to a stable higher amplitude state. The jump resonance phenomenon is also an important essential characteristic nonlinear systems may exhibit.

2.1.3 Poincaré section and Chaos

The Duffing equation is an example of a dynamical system that exhibits a chaotic behavior for appropriate values of parameters. A useful way of analyzing chaotic motion is to look at what is called the Poincaré section. Rather than considering the phase space trajectory for all times, which gives a continuous curve, the Poincaré section is just the discrete set of phase space points of the particle at every period of the driving force, i.e. at $t = 2\pi/\omega, 4\pi/\omega, 6\pi/\omega$ etc. Clearly for a periodic orbit the Poincareé section

is a single point, when the period has doubled it consists of two points, and so on. When the system exhibits a chaotic behavior the Poincareé section shows what it is called a chaotic attractor [Mil85].

For the Duffing oscillator the Poincaré section Σ can be defined as:

$$\Sigma = \{(x, \dot{x}, t) \in \Re \times \Re \times S | t = 2\pi/\omega, 4\pi/\omega, 6\pi/\omega, \dots\} = \Re \times \Re \qquad (2.30)$$

Where $S = [0, 2\pi + 2k\pi]$, $k = 0, 1, \dots$

The Poincaré map converts the original three-dimensional flow $(x, \dot{x}, t)$ into a two-dimensional discrete mapping. The Poincaré section is coordinated by the displacement x and the velocity $\dot{x}$:

$$P : \Sigma \to \Sigma \quad i.e. \quad (x_0, \dot{x}_0) \to (x, \dot{x}) \qquad (2.31)$$

It means that the P moves the point (x_0, y_0) in Σ into another point in Σ via the governing equation and the impact rule. When the orbit is periodic, then P transforms the point x_0, y_0 into the same point.

The diagram in Fig.2.9 is the chaotic attractor of the Duffing oscillator. It is the limiting set of points to which the trajectory tends (after the initial transient) every period of the driving force. Further information on chaos in the Duffing oscillator can be found in [Hol79, MH79]. As a more complex exemple of chaotic system, a study on the transition to chaos for plates harmonically forced is presented in [TTA11].

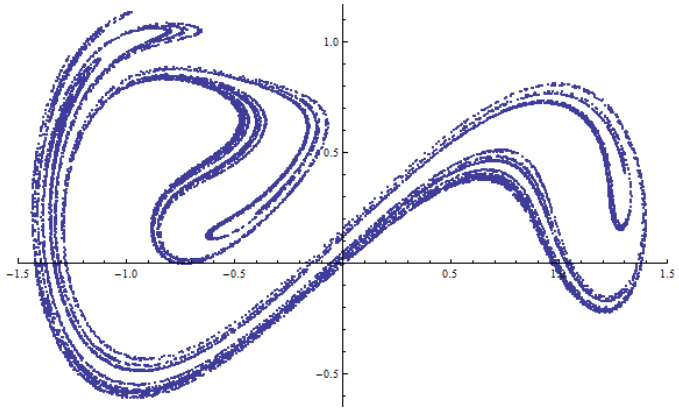

Figure 2.9: Chaotic attractor of the Duffing's equation.

2.2 Nonlinear Normal Modes

We believe it is important to introduce the concept of Nonlinear Normal Modes (NNMs) because closely related to the concept of Targeted Energy Transfer. A system composed of a linear primary system and a nonlinear attachment (NES) can be seen as a whole system which presents one (or more) nonlinearity in it. In this perspective the activation of the NES can be considered as a localized NNM. In this section we introduce the concept of NNM and some important properties (like the localization) which are tightly correlated to the TET.

The concept of normal mode is traditionally associated with linear vibration theory and related to the principle of linear superposition. Indeed, a classical result of linear vibration theory is that the normal modes of vibration of a multi-degree-of-freedom (MDOF) discrete system can be employed to decouple the equations of motion through an appropriate coordinate (modal) transformation, and to express its free or forced oscillations as superpositions of modal responses. Another result of classical linear theory is that the number of normal modes of vibration cannot exceed the number of degrees of freedom of a discrete system, and that any forced resonance of the system under external harmonic excitation always occurs in neighborhoods of frequencies of normal modes. Although in nonlinear systems the principle of linear superposition does not (generally) hold, nevertheless the concept of the normal mode can still be employed. Furthermore, it has been shown [TTC04] that using a single NNM can in certain cases lead to a better prediction of the behavior of a nonlinear structure (hardening/softening) than what a superposition of several linear normal modes can do.

2.2.1 Rosenberg's and Shaw and Pierre's definitions

Rosenberg [Ros66] defined a nonlinear normal mode (NNM) of an undamped discrete MDOF system as a synchronous periodic oscillation where all material points of the system reach their extreme values or pass through zero simultaneously; hence, the NNM oscillation is represented by either a straight modal line (similar NNM) or a modal curve (non-similar NNM) in the configuration space of the system. Like for the linear normal modes, all displacements can be expressed in terms of a single reference coordinate. NNMs are generically non-similar as similar modes can only be realized if special symmetries conditions exist [VMM$^+$96]. We should remind that in the linear case, normal modes are always similar.

The extension of the concept of NNM to non-conservative systems with

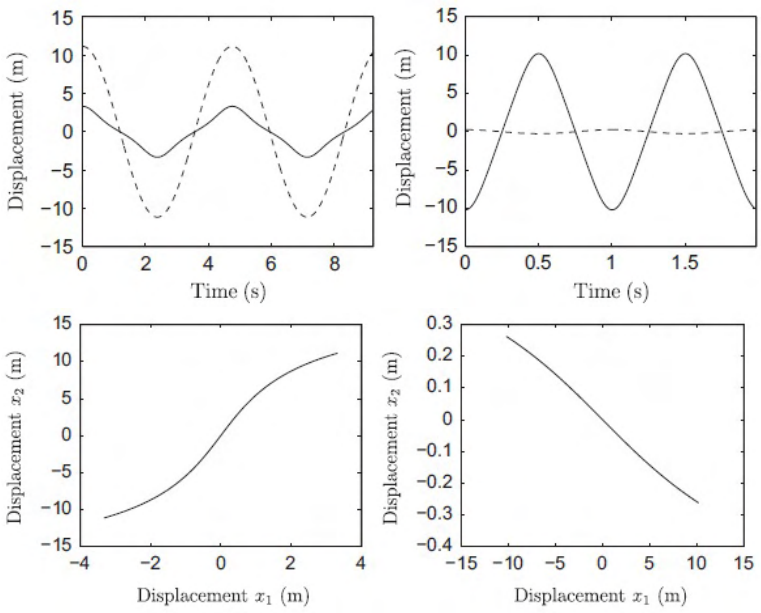

Figure 2.10: Nonlinear Normal Modes according to Rosenberg's definition [Ros66] synchronous periodic oscillation where all material points of the system reach their extreme values or pass through zero simultaneously.

damping was studied by Shaw and Pierre [SP91, SP93], who introduced the concept (based on ideas developed in [Fen71]) of damped NNM invariant manifold to account for the fact that the free oscillation of a damped nonlinear system is a non-synchronous decaying motion. This formulation computes damped NNM invariant manifolds of the damped dynamical flow by parameterizing the damped NNM response in terms of a reference displacement and a reference velocity. For sufficiently weak damping, the damped NNM invariant manifold can be viewed as a perturbation of the NNM of the corresponding undamped Hamiltonian system. When a motion is initiated on a damped NNM invariant manifold of a MDOF system, the response remains on the manifold: the system behaves as a single-DOF system on the manifold.

2.2.2 Dependence of the Nonlinear Normal Modes on the energy of the oscillations

Similar NNMs are analogous to linear normal modes, in the sense that their modal lines do not depend on the energy of the free oscillation and space-

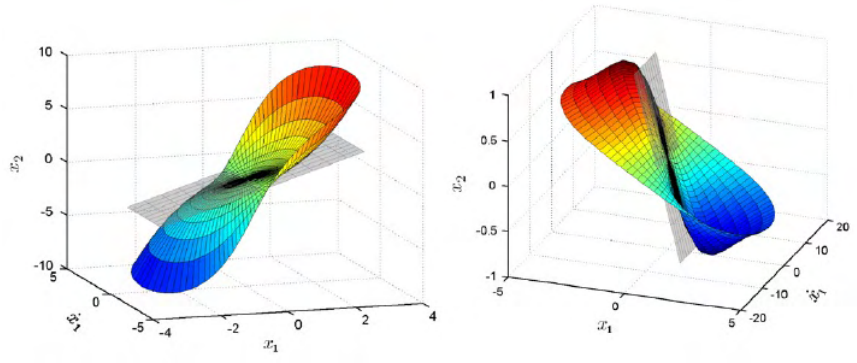

Figure 2.11: Invariant Manifolds of Nonlinear Normal Modes as defined by Shaw and Pierre [SP91, SP93].

time separation of the governing equations of motion can still be performed. However, this type of NNMs is realized only when special symmetries occur, and are not typical in nonlinear systems. More generic are non-similar NNMs, whose modal curves do depend on energy; this energy dependence prevents the direct separation of space and time in the governing equations of motion by means of non-similar NNMs, which complicates their analytical computation [Man72, Vak96].

We consider the apparently simple 2-DOF described by Eq.(2.32):

$$\begin{aligned} \ddot{x_1} + (0.02\dot{x_1} - 0.01\dot{x_2}) + (2x_1 - x_2) + 0.5x_1^3 = F\cos(\omega t) \\ \ddot{x_2} + (0.02\dot{x_2} - 0.01\dot{x_1}) + (2x_2 - x_1) = 0 \end{aligned} \tag{2.32}$$

The FRFs of the two coordinates of the system show a strong energy dependence that is illustrated in Fig.2.12. It is important to observe that the system behaves as its linear counterpart for low levels of energy. The evolution of the normal modes is shown Fig.2.13.

2.2.3 Localization of Nonlinear Normal Modes

We consider another example of 2-DOF system [KPGV09] consisting of a nonlinear oscillator linearly coupled to a linear one [KMK+08] whose equations of motion are Sys.(2.33). The system is illustrated in Fig.2.14.

$$\begin{aligned} \ddot{x_1} + (2x_1 - x_2) + 0.5x_1^3 = 0 \\ \ddot{x_2} + (2x_2 - x_1) = 0 \end{aligned} \tag{2.33}$$

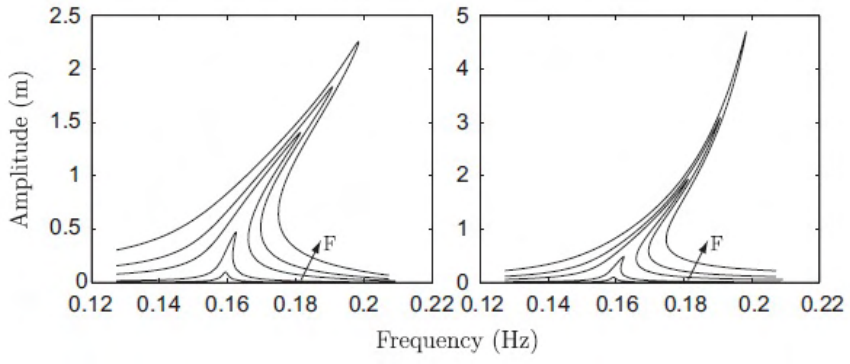

Figure 2.12: Dependence of the FRFs of Sys.(2.32) on the energy level.

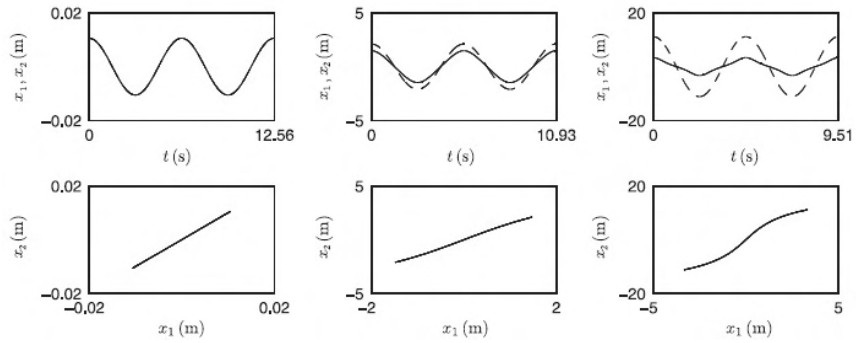

Figure 2.13: Dependence of the FRFs of Sys.(2.32) on the energy level.

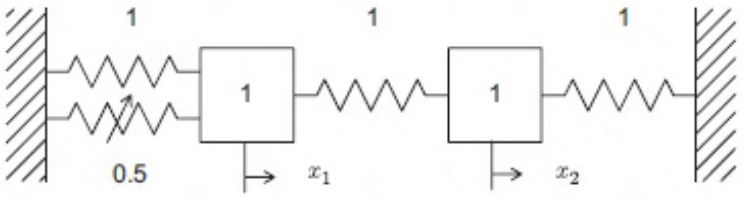

Figure 2.14: Example of 2-DOF system consisting of a nonlinear oscillator linearly coupled to a linear one [KMK$^+$08].

The Frequency-Energy Plot (FEP) of Fig.2.15 [PVR$^+$08] depicts the evolution of the NNMs as the energy of the oscillations varies. There exist two main backbone branches of NNMs, an in-phase branch, S11+, originating (for low energies) from the first linearized natural frequency and an

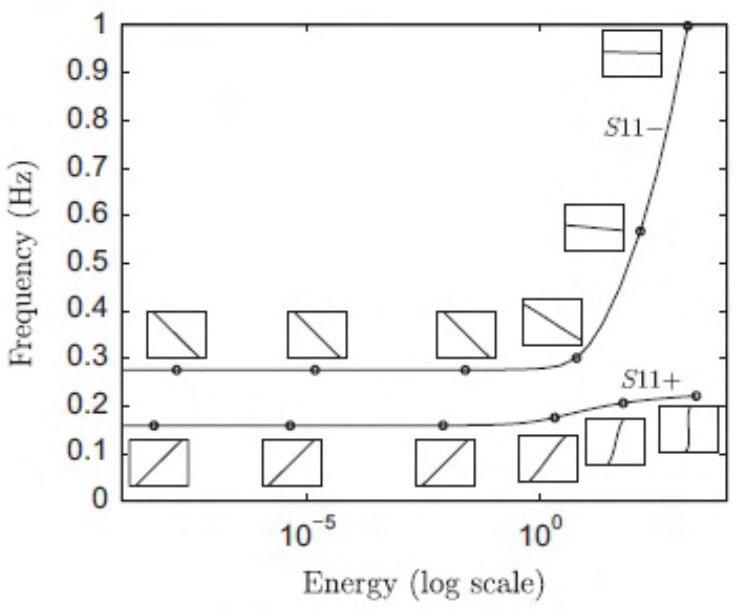

Figure 2.15: Frequency-energy of the NNMs of Sys(2.33). The corresponding modal curves in the phase plane are inset, horizontal and vertical axes in these plots depict the displacements of the nonlinear and linear oscillators respectively. Image from [KPGV09].

out-of-phase one, S11, originating from the second linearized natural frequency. The FEP of Figure 2.4 clearly shows that the nonlinear modal parameters have a strong dependence on the (conserved) energy of the oscillation. Specifically, the frequencies of the in-phase and out-of-phase NNMs increase with energy, which reveals the hardening characteristic of the system. Furthermore, the modal curves change with increasing energy, since the in-phase NNM tends to localize to the linear oscillator (i.e., its modal curve tends to become vertical in the corresponding phase plane), whereas the out-of-phase NNM tends to localize to the nonlinear oscillator (its modal curve tends to become horizontal with increasing energy). This tendency of NNMs to localize with varying energy is crucial for the realization of TET [Pil08].

2.2.4 Internal resonance

Another main feature of NNMs is that they may nonlinearly interact without their linearized natural frequencies necessarily satisfying conditions of

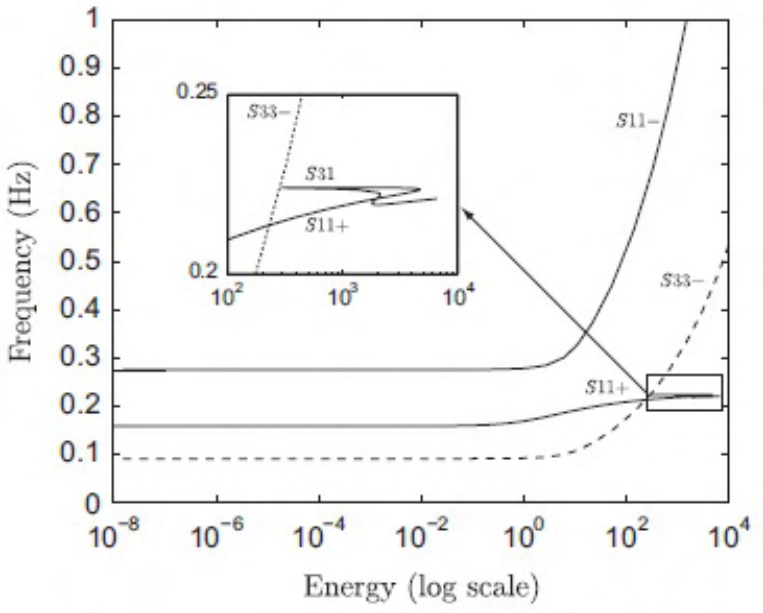

Figure 2.16: Example of internal resonance between the two NNMs of Sys(2.33). Due to the energy dependence of the frequencies, at high energy level the system goes through a 3:1 resonance although the linearized modes (low level of energy) do not have commensurate frequencies. Image from [KPGV09].

internal resonance. This purely nonlinear phenomenon appears at high level of energy and can be studied by analyzing the evolution of the NNMs on the FEP. In Fig.2.16 we can see how the frequencies of the two normal modes of Sys(2.33) evolve as the energy increases until a condition of internal resonance 3:1 occurs.

We note an additional branch of NNMs lying on a subharmonic tongue emanating from the in-phase backbone branch S11+. This tongue is denoted by S31, since it corresponds to a 3:1 internal resonance of the in-phase and out-of-phase NNMs at those energy levels.

This result clearly demonstrates that NNMs can be internally resonant without necessarily having commensurate linearised natural frequencies.

An practical example of nonlinear internal resonance in acoustic instruments can be found in [MTT15].

2.2.5 Bifurcations

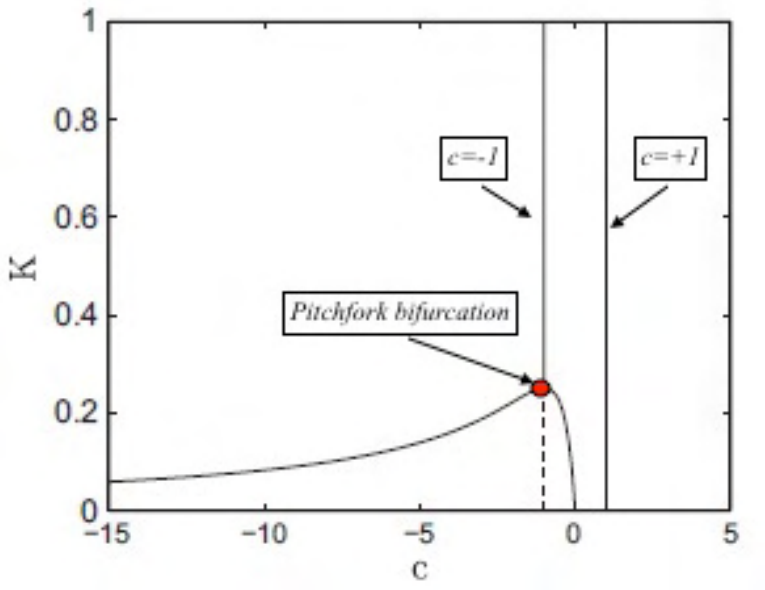

Figure 2.17: Bifurcation diagram of the NNMs of Sys(2.34). The dashed line represents the unstable solution.

We know that a linear discrete multi-degree of freedom (MDOF) structural system has as many normal modes as degrees of freedom. Reduced order models (less modes than DOF) are usually used as an approximation to describe the dynamics. However, in any case the number of normal modes cannot exceed the number of DOF.

When it comes to Nonlinear Normal Modes, the number of modes may be higher that the number of DOF and this is due to NNM bifurcations.

This feature can be illustrated by the following example [VR92a, VR92b]:

$$\begin{aligned} \ddot{x_1} + x_1 + x_1^3 + K(x_1 - x_2)^3 = 0 \\ \ddot{x_2} + x_2 + x_2^3 + K(x_2 - x_1)^3 = 0 \end{aligned} \tag{2.34}$$

Because of its symmetry, the system possesses only similar modes:

$$y_2 = f(y_1) = cy_1 \tag{2.35}$$

where c is a real constant. Substituting the similarity condition (2.35) into Sys.(2.34) we obtain an algebraic relation between the modal constant c and

the nonlinear stiffness K:

$$K(1+c)(c-1)^3 = c(1-c)^2 \tag{2.36}$$

In Fig.2.17 the real values of the modal constant c are plotted for varying coupling stiffness coefficient K, from which we infer that a pitchfork bifurcation of NNMs occurs in the system. This type of bifurcation is realized due to the symmetry of the system and is expected to break into saddle node (SN) bifurcation(s) when this symmetry is perturbed. A brief discussion about pitchfork and saddle-node bifurcations is provided in the next section.

Looking at Fig.2.17, we notice that the system has only the in-phase ($c = 1$) and out-f-phase ($c = -1$) NNMs for high values of K. These modes can be interpreted as the generalization of the linear normal modes. When $K = 0.25$ the out-of phase NNM degenerates into a pitchfork bifurcation: the NNM $c = -1$ becomes unstable and two new stable modes appear. Then for $0 < K < 0.25$ the system possesses four NNMs although it only has two degrees of freedom.

Furthermore, it can be noticed that for $K \to 0$ the two NNMs which bifurcate from the out-of phase mode localize to one of the two oscillators: $c \to -\infty$ and $c = 0$.

2.3 Saddle-node, Pitchfork and Hopf bifurcations

Here is a short description of the difference between a saddle-node, a pitchfork and a Hopf bifurcation. These are among the most common types of bifurcations encountered in nonlinear dynamics. Indeed they will be observed in the Vibro-Impact NES system presented in the next chapter.

2.3.1 Saddle-node bifurcation

In a dynamical system, a saddle-node bifurcation occurs when, as a parameter changes, the generation (or the destruction) of equilibrium points is engendered.

As a very simple example, let us take the first order system:

$$\dot{x} = r + x^2 \tag{2.37}$$

- if $r < 0$, two equilibria exist: one stable in $x = -\sqrt{-r}$ and one unstable in $x = +\sqrt{-r}$.

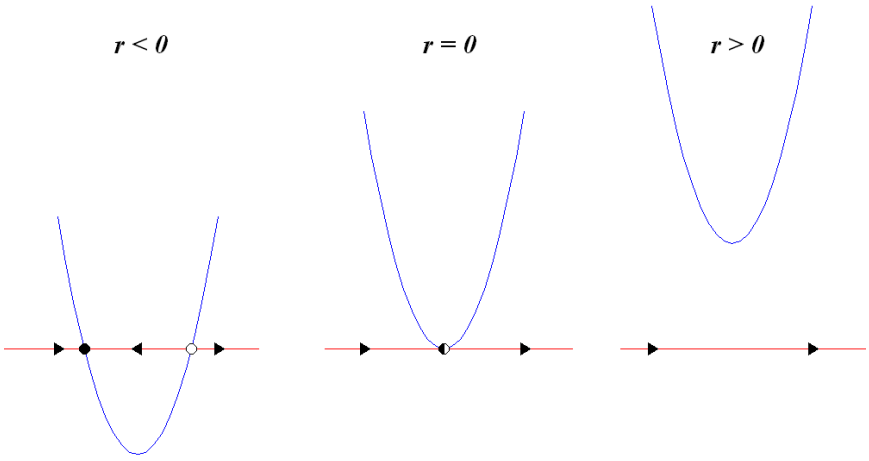

Figure 2.18: Saddle-node bifurcation as the parameter r changes

- if $r = 0$, the two equilibrium points collide in a unique point: the saddle-node point.
- if $r > 0$, no points of equilibrium exist anymore.

2.3.2 Pitchfork bifurcation

Pitchfork bifurcations are a particular type of local bifurcations. There exist two types: supercritical and subcritical.

Supercritical pitchfork bifurcation

The normal form of the supercritical pitchfork bifurcation is:

$$\dot{x} = rx - x^3 \tag{2.38}$$

- if $r < 0$, one stable equilibrium point exists in $x = 0$.
- if $r = 0$, $x = 0$ becomes a pitchfork bifurcation point.
- if $r > 0$, $x = 0$ loses its stability and two new stable equilibrium points arise in $x = \sqrt{r}$ and $x = -\sqrt{r}$.

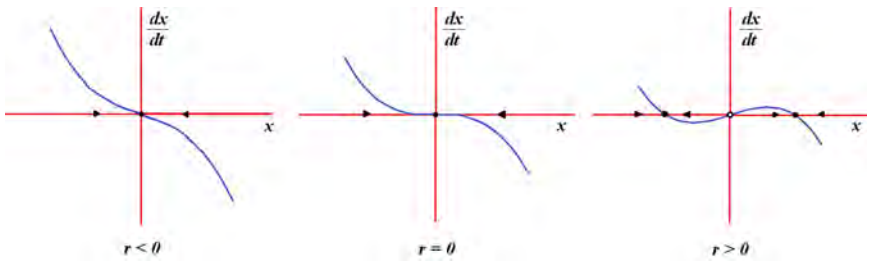

Figure 2.19: Supercritical pitchfork bifurcation as the parameter r changes

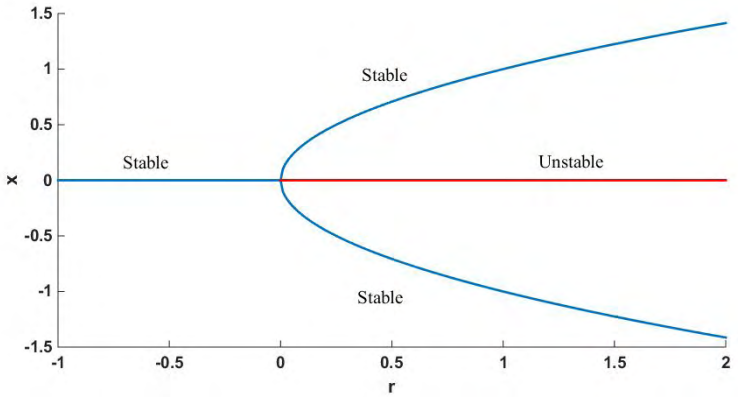

Figure 2.20: Supercritical pitchfork: bifurcation diagram

Subcritical pitchfork bifurcation

The normal form is:

$$\dot{x} = rx + x^3 \tag{2.39}$$

- if $r < 0$, three points of equilibrium exist: one stable in $x = 0$ and two unstable in $x = \pm\sqrt{r}$;
- if $r = 0$, the three points collide in $x = 0$: pitchfork bifurcation.
- if $r > 0$, only one unstable equilibrium exist.

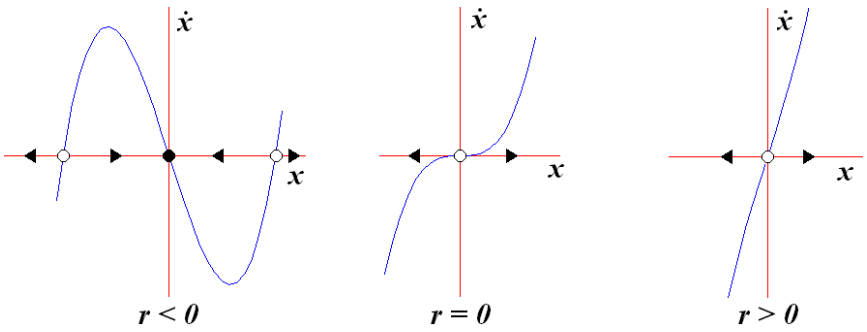

Figure 2.21: Subcritical pitchfork bifurcation as the parameter r changes

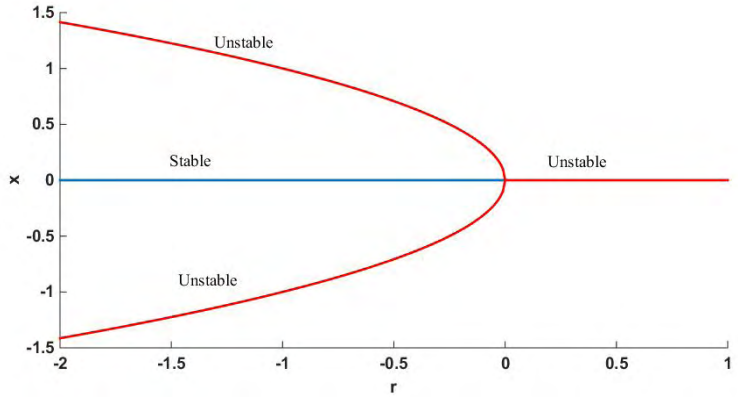

Figure 2.22: Subcritical pitchfork bifurcation as the parameter r changes

2.3.3 Hopf bifurcation

A Hopf bifurcation is a critical point where a system's stability switches and a periodic solution arises. More precisely, it is a local bifurcation in which a fixed point of a dynamical system loses stability, as a pair of complex conjugate eigenvalues (of the linearization around the fixed point) cross the complex plane imaginary axis.

The normal form of a Hopf bifurcation is:

$$\frac{dz}{dt} = z((\lambda + i) + b|z|^2) \tag{2.40}$$

Where z, b are both complex and λ is a parameter. We write $b = \alpha + i\beta$.

- if $\alpha < 0$ then there is a stable limit cycle for $\lambda > 0$: $z(t) = re^{i\omega t}$, where $r = \sqrt{-\lambda/\alpha}$ and $\omega = 1 + \beta r^2$. The bifurcation is then supercritical.

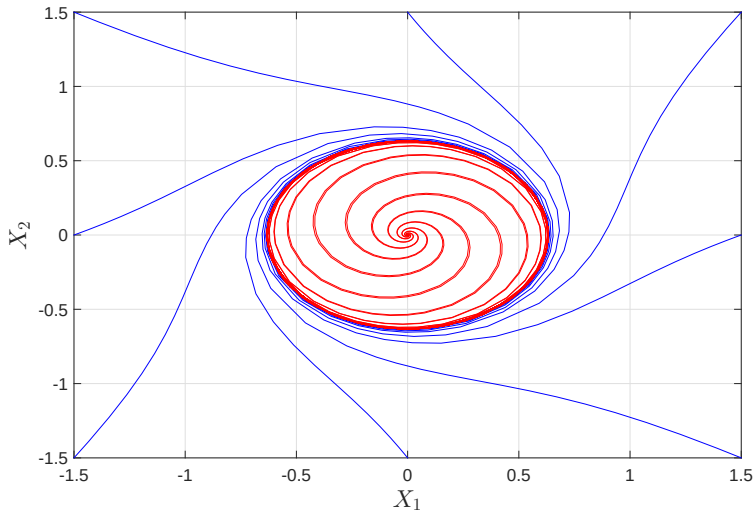

Figure 2.23: Phase plane displaying a limit cycle generated by a Hopf bifurcation.

- if $\alpha > 0$ then there is an unstable limit cycle for $\lambda < 0$. The bifurcation is then subcritical.

Chapter 3

Vibro-Impact Nonlinear Energy Sink

Abstract

In this chapter the dynamics of a Vibro-Impact Nonlinear Energy Sink (VI-NES) is experimentally investigated via a harmonically forced single-degree-of-freedom linear oscillator to which a VI-NES is attached. The mass ratio between the VI-NES and the primary system is about 1%*. Depending on external force amplitude and frequency, either a Strongly Modulated Response (SMR) or a constant amplitude response (CAR) is observed. In both cases an irreversible transfer of energy occurs from the LO towards the VI-NES: process known as passive Targeted Energy Transfer (TET). Furthermore, the problem is analytically studied by using the multiple scales method. The Slow Invariant Manifold (SIM) shows the existence of a stable and an unstable branch of solution, and of an energy threshold (a saddle-node bifurcation) for the solutions to appear. Subsequently the fixed points of the problem are calculated. When a stable fixed point exists, the system is naturally drawn to it and a CAR is reached. Otherwise a SMR state occurs and no stable point is attained. Finally a good correlation between experimental and analytical results is shown.*

3.1 Introduction

In this chapter the study of a Vibro-Impact NES coupled to a LO is carried out. In this type of system the shocks occurring between the primary mass and the NES' represent the nonlinearity through which the vibration energy is dissipated.

The main purpose of this study is to bridge the theoretical and experimental works in order to reach a comparison between the analytical results and the experimental observations. Experimentally, this system has the characteristic of being relatively simple to realize if compared to the cubic NES, where obtaining a purely cubic force between the NES and the primary system may represent a tricky task. On the other hand, the non-smooth nature of the system due to the impacts introduces an additional complication in the analytic and numerical modeling.

The study carried out in [GMSB14b] is used as an important starting point to broaden the general understanding of the VI-NES. In [GMSB14b], experimental investigations have shown how such a system may exhibit different types of response as the external forcing changes in amplitude and/or frequency. It also has been shown how an analytical study based on the multiple scales method is potentially able to describe this kind of behavior.

We decided to reformulate the analytical treatment in a different way which could take into account the forcing term since the very first steps of the multiple scales expansion. As for the experimental part, we used the same VI-NES as in [GMSB14b] but applied to a different primary system with a higher natural frequency to prove the efficacy of the absorber for different frequencies. Moreover, we avoid using a bearing slider as it turned out being a source of perturbation for the experiments.

We conducted an extensive investigation: four levels of force were tested and for each level a frequency sweep was performed. This allowed us to study the response of the VI-NES over a considerable range of cases.

Finally the analytical model is used to explain the behavior experimentally observed and a comparison is presented. In addition, the influence of the design parameters on the VI-NES behavior is discussed and explained thanks to some analytical examples.

3.2 Preliminary investigations

Before starting with the test of the VI-NES applied to the primary system, we want to investigate the impact kinematics of the NES itself.

The system is composed of the primary mass on which the VI-NES is assembled. The VI-NES is a steel cylinder inside of which a steel ball is free to roll. The primary mass is then rigidly connected to a vibrating table whose motion is controlled in frequency and amplitude. Then controlling the shaker's motion is actually equivalent to controlling the primary mass' motion. The experimental setup and its schematic are shown in Fig.3.1.

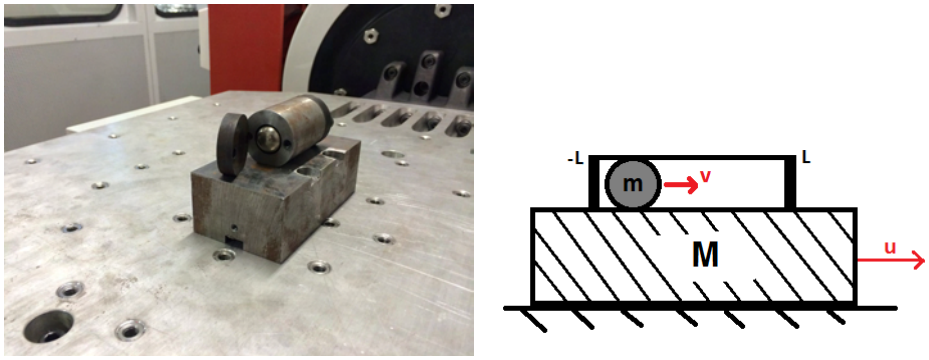

Figure 3.1: The VI-NES and its schematic.

We are interested in exploring the behavior the system may exhibit depending on the excitation it is subject to.

If the primary mass' motion is harmonic, we consider the VI-NES as "active" when two impacts per cycle of oscillation occur. This regime is particularly interesting because it potentially represents a suitable condition for energy dissipation. However, the goal of this preliminary investigation is only to analyze the kinematics of the problem since the energy transfer aspect will be introduced afterwards.

Each test is performed at a constant level of acceleration and for a slow sweeping frequency in order to identify the frequency range in which the VI-NES is active. In Tab.3.1 the results are displayed.

The VI-NES is active since the lowest frequency and it holds the 2 impact regime up to an upper limit after which no impacts occur anymore. The upper limit grows almost linearly with the acceleration. It is important to highlight that if the VI-NES is active, it does not necessarily mean it will be efficient in terms of energy dissipation. Nevertheless this preliminary investigation gives some interesting information for the experimental study that follows.

Acc [g]	Activation range [Hz]
1	7.48
2	12.42
2.5	14.26
3	15.2
3.5	17
4	18.3

Table 3.1: Activation range: experimental results

3.3 Numerical model

A numerical model of the VI-NES is developed in Matlab to predict the response that might be observed during experiments. A schematic of the model is displayed in Fig.3.2.

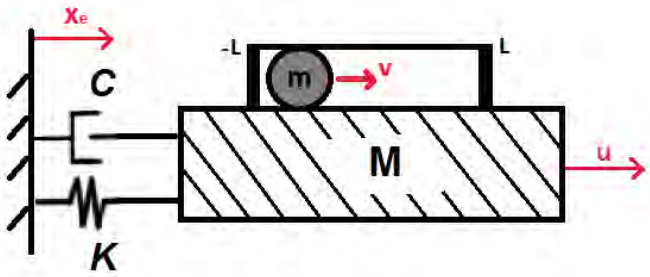

Figure 3.2: Schematic of the model.

Between two impacts, the equations of motion of the system are:

$$\begin{aligned} M\ddot{u} + C\dot{u} + Ku &= Kx_e + C\dot{x}_e \\ m\ddot{v} &= 0 \\ \forall |u - v| &< L \end{aligned} \tag{3.1}$$

When an impact occurs, i.e. when $|u - v| = L$, the velocities present a discontinuity and the relation (Newton experimental law) which provides the conditions after the impact is:

$$\dot{u}(t_j^+) - \dot{v}(t_j^+) = -r(\dot{u}(t_j^-) - \dot{v}(t_j^-)) \tag{3.2}$$

$$M\dot{u}(t_j^+) + m\dot{v}(t_j^+) = M\dot{u}(t_j^-) + m\dot{v}(t_j^-) \tag{3.3}$$

Where t_j^+ and t_j^- are the time instants after and before the j^{th} impact respectively.

Eq.(3.1) is integrated in Matlab with an *ode45* method and the impact conditions are taken into account thanks to the *event* option. This consists in defining an *event* function which in our case is the impact condition $f_{event} = |u - v| - L$. The equations are integrated up until an event is detected: the *event* function equals zero. Then the integration stops and new initial conditions are defined, i.e. the velocities after the impact calculated by Eq.3.2. Finally the integration restarts with the new initial conditions until the next impact/event.

Two cases in which Targeted Energy Transfer is observed are shown in the next section. For these simulations a primary system's natural frequency of 21.18 Hz is used. In the first case the system is unforced and an initial displacement is imposed. In the second one the system is harmonically forced and a Strongly Modulated Response responses is observed.

3.3.1 Case 1: unforced system with initial displacement ($x_e = 0$; $u(0) \neq 0$)

In this example the system is unforced and an initial displacement is imposed.

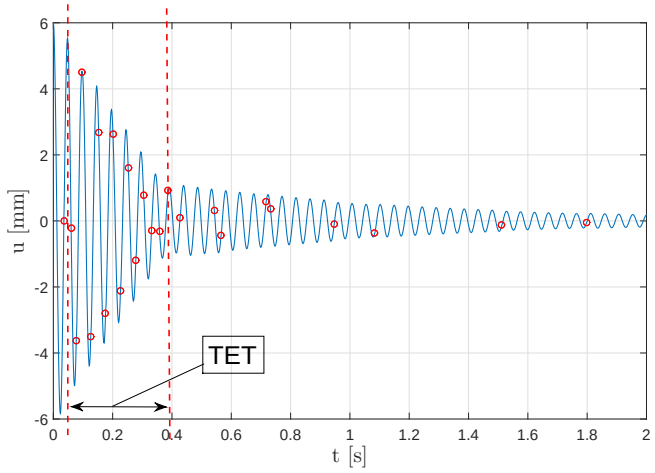

Figure 3.3: Primary mass' displacement. The red circles represent the instants when impacts occur.

In Fig.3.3 the primary system's displacement is shown. It can be observed that after a short transient the primary system and the VI-NES establish a regime with two impacts per cycle and the vibration energy is dissipated (Targeted Energy Transfer). When the primary system's displacement becomes too small ($t \approx 0.4\,s$) the TET ends and the rest of the energy is dissipated by the structural damping (the few impacts left are weak and energetically insignificant). In Fig.3.4 the energy dissipated by the impacts as a percentage of the initial potential energy of the primary system ($U = \frac{1}{2}Kx^2(0)$) is displayed.

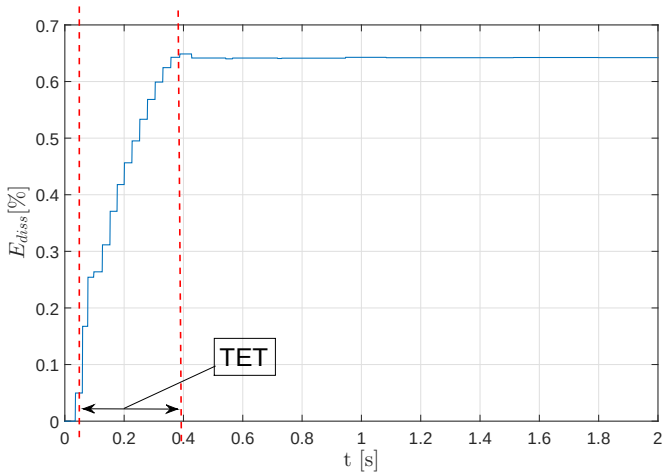

Figure 3.4: Energy dissipated by the impacts as a percentage of the initial potential energy of the primary system ($U = \frac{1}{2}Kx^2(0)$).

3.3.2 Case 2: forced system

In this example the system is harmonically forced. A base acceleration at constant amplitude and frequency is imposed.

Fig.3.5 shows the primary system's displacement for a base acceleration's amplitude and frequency of $0.4\,g$ and $21.3\,Hz$ respectively. It can be noticed that the VI-NES goes through ON-OFF cycles during which TET is cyclically observed. The amplitude of the response grows until the VI-NES turns active, the energy is dissipated, the response decreases and no more impacts occur (VI-NES inactive). Since the system is constantly forced, the whole cycle starts over.

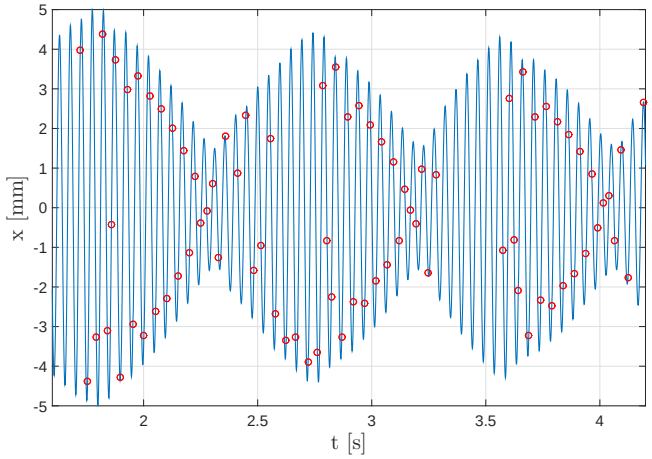

Figure 3.5: Primary system's displacement: Strongly Modulated Response.

3.4 Experimental study

The experimental study has been conducted aiming to observe the behavior of the system and to explore the different existing types of response which can arise and how they are related to the external forcing in terms of magnitude and frequency. This phase of experimental investigation will be subsequently exploited and the observations explained by the analytic study of the system.

The entire experimental setup is shown in Fig.3.6 and is constituted by a primary single-degree-of-freedom linear oscillator (LO) to which the VI-NES is attached. The LO is harmonically forced by an electrodynamic shaker coupled to a vibrating table the LO is mounted on.

Figure 3.7 displays the tested prototype and its schematic: the primary mass M is linked to its base by means of two flexible blades. The base is then screwed to the vibrating table. Upon the primary mass a cylinder is mounted and the small VI-NES mass is free to roll inside. The cylinder is pierced on the sides in order to make the air effect negligible and to visually observe the ball motion which will not be measured.

Firstly a dynamic identification of the primary system is performed. The system is forced by a swept-sine external force with constant amplitude and the displacement of the primary mass is measured by means of a Laser Doppler Vibrometer (LVD). The use of an LVD rather than an accelerom-

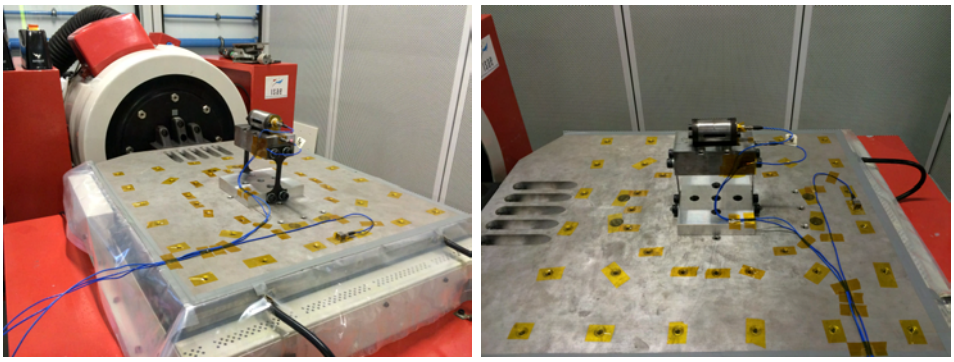

Figure 3.6: The LO coupled to the VI-NES: the experimental setup.

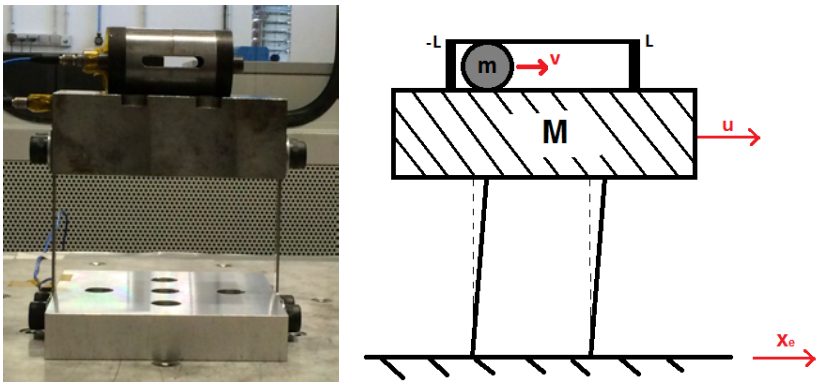

Figure 3.7: The prototype of the VI-NES applied to the LO (left) and its schematic (right).

eter has been dictated by the fact that impacts would drastically perturb measures made with an accelerometer.

The modal parameters are shown in Tab.4.1 and the masses values and their ratio in Tab.3.3. Several tests were performed on the primary structure at different levels of base acceleration between $0.2 - 0.5g$. The spectrum of the displacement is shown in Fig.3.8. The tests showed that the primary system was not perfectly linear and that a slight variation in the modal parameters, particularly the damping, occurred as the external force varied. However this was a weakly nonlinear behavior that did not affect the purpose of the tests as the quality response of the system was unaffected by it. It is important to highlight the particularly small mass ratio between the VI-NES

$F[g]$	$f_0[Hz]$	$K[N/m]$	$C[N/ms]$	ξ
0.2	21.18	67421	8.566	0.008
0.3	20.92	65776	13.325	0.013
0.4	20.85	65336	17.132	0.017
0.5	20.64	64027	20.367	0.021

Table 3.2: Modal parameters of primary system

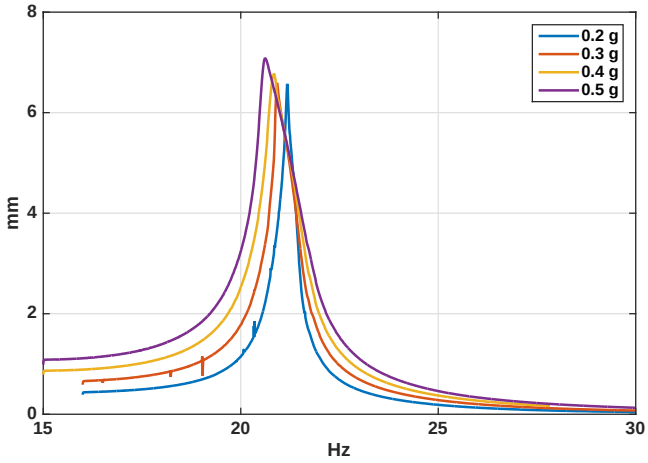

Figure 3.8: Primary system displacement spectrum for four excitation levels.

and the primary system, that is less than 1%.

Once the primary system has been identified, we arm the VI-NES by inserting the small mass into the cavity and we carry out some swept-sine tests for four different levels of base acceleration: $[0.2; 0.3; 0.4; 0.5]$g. The fact of using a heavy-mass shaker permits the shaker not to be perturbed when it goes through the natural frequency of the LO during the swept-sine. As for the tests of the primary system, the displacement is measured by the LVD and the spectra are then obtained by signal processing.

Fig.3.9 shows the displacement spectra for the system with and without VI-NES for four levels of external excitation: $[0.2; 0.3; 0.4; 0.5]$g. Fig.3.10 shows the measured displacement for two different frequencies at the same level of external excitation.

Firstly, we can observe that a threshold in the amplitude of the primary

$M[Kg]$	$m[Kg]$	$\epsilon = m/M$
3.807	0.032	0.84%

Table 3.3: Mass parameters of primary system

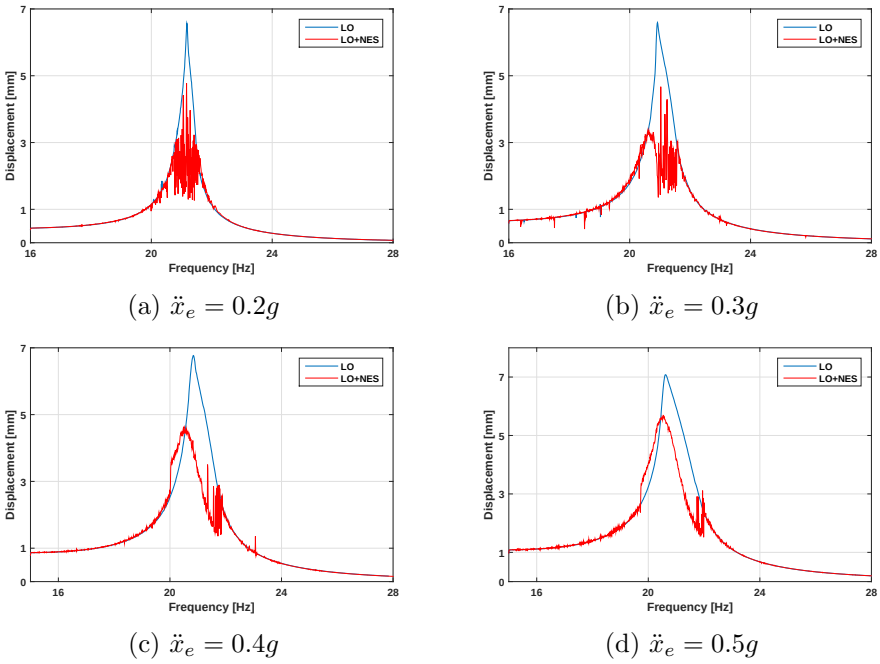

(a) $\ddot{x}_e = 0.2g$ (b) $\ddot{x}_e = 0.3g$

(c) $\ddot{x}_e = 0.4g$ (d) $\ddot{x}_e = 0.5g$

Figure 3.9: Experimental spectra of the primary mass displacement with (red) and without (blue) the VI-NES for four different levels of base acceleration.

mass oscillations exists for the VI-NES to become active: we will refer to it as activation threshold. Secondly, the system can exhibit two types of response and depending on magnitude and frequency of external forcing either one or another may appear.

The responses can be qualitatively classified as:

- Idle VI-NES: no impacts occur and the primary system's dynamics is not perturbed by the presence of the VI-NES: the LO oscillations amplitude is lower than the activation threshold.
- Constant Amplitude Response (CAR): the VI-NES is stably active and

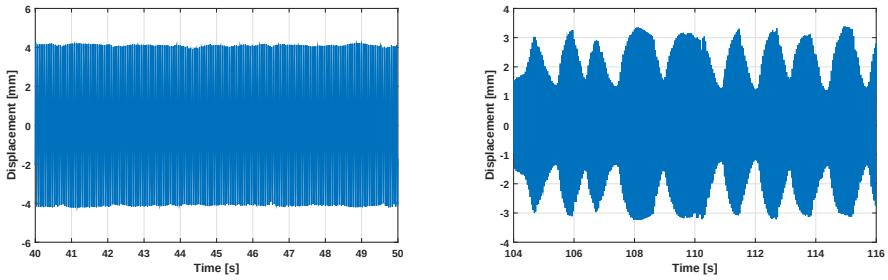

(a) Time series: constant amplitude response - $\ddot{x}_e = 0.4g - f = 20.9Hz$ (left) and strongly modulated response - $\ddot{x}_e = 0.4g - f = 21.5Hz$ (right).

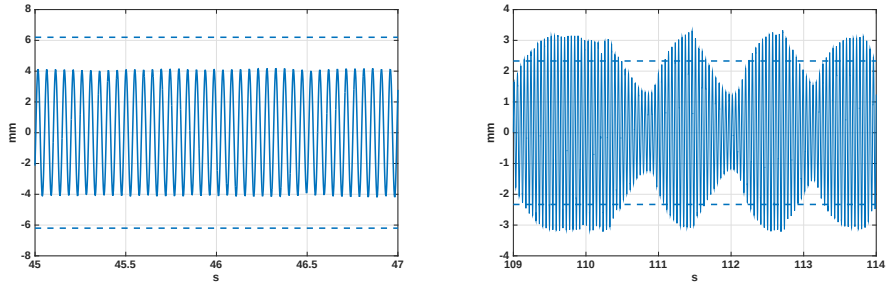

(b) Detail of the time series of above. The dashed line represents the amplitude of the LO's response at equal forcing without the VI-NES.

Figure 3.10: Recorded time series showing a constant amplitude response and a strongly modulated response.

the amplitude of primary mass displacement remains constant (fig.3.10 left).

- Strongly Modulated Response (SMR): the primary system goes through alternatively increasing and decreasing amplitude cycles and as a consequence the fast oscillations appear to be modulated. This behavior is caused by cyclical activation and deactivation of the VI-NES (fig.3.10 right).

The VI-NES seems to well accomplish its task as a vibration absorber since the response is actually reduced nearby the resonance of the primary system. This is the proof that a Targeted Energy Transfer occurs from the LO towards the VI-NES and that the energy is then dissipated by the impacts. It is important to highlight that this goal has been achieved although a proper sizing process of the VI-NES has not been carried out and with a significantly small mass ratio $\epsilon = 0.84\%$. This result proves that the VI-

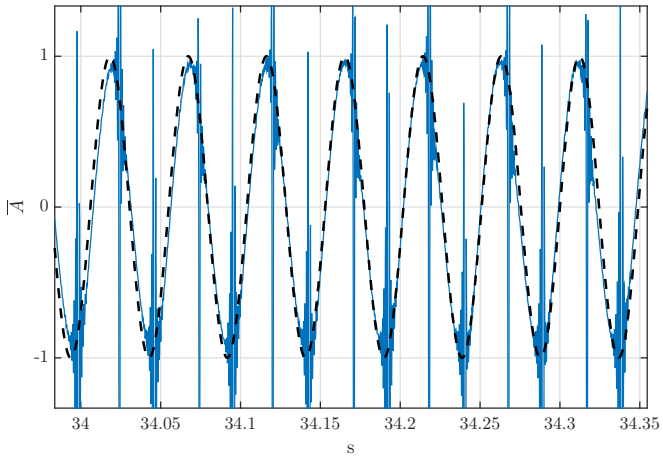

Figure 3.11: Experimental impacts detection: acceleration of the LO measured by an accelerometer placed on the VI-NES in order to capture the instants of impact. The peaks represent the shocks occurring throughout the oscillations of the LO which are highlighted by the dashed line. $\overline{A}$ denotes the normalized acceleration of the LO. It can be seen as two impacts per cycle occur, i.e. a 1:1 resonance state is established.

NES is able to automatically tune itself to the primary system. This is a relevant general feature of nonlinear absorbers due to the absence of a natural frequency for these devices. However, whereas for cubic stiffness NES the absence of a natural stiffness is a delicate aim to reach [GMSB14a], for VI-NES it appears to be as an evident outcome. Still, we remind that the primary objective of this experimental study was not to seek the optimal performance but rather to investigate the qualitative behavior of the VI-NES. Looking at the spectra of Fig.3.9 one can draw the conclusion that there exists a criterion on primary mass displacement in order to activate the VI-NES. Indeed a threshold in amplitude/energy is observed beyond which the VI-NES goes through a 1:1 resonance with respect to the LO. The terminology 1:1 resonance is used to maintain a correlation with the cubic stiffness NES, even though in this context it would mean that two impacts per oscillation cycle of the primary mass occur. This can be seen in Fig.3.11 where the signal of an accelerometer placed on the primary mass is shown. The peaks represent the shocks occurring two times per period throughout the oscillations of the LO.

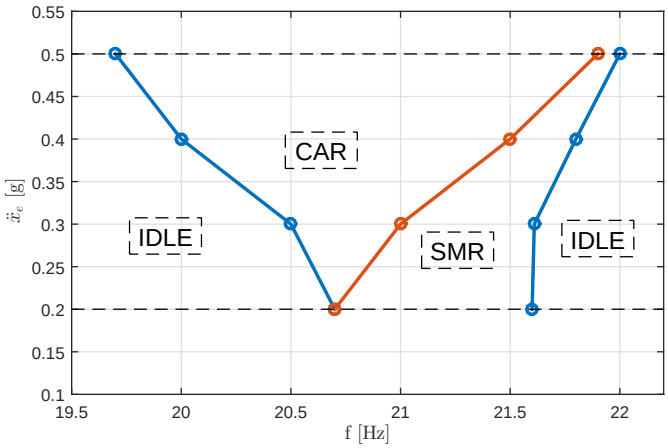

Figure 3.12: Zones of the experimental observed regimes with respect to magnitude and frequency external force.

Fig. 3.12 shows a map illustrating the types of observed responses as a function of external forcing magnitude and frequency. For low level of external forcing only the SMR is registered through the whole range of frequencies the VI-NES is active. As the external force increases, the CAR appears at the lowest frequencies of the activation range and the SMR tends to disappear. When high levels of external forcing are reached the CAR becomes the prevalent, if not the only, type of response detected. It is therefore clear that for a given VI-NES the kind of response which might arise is a function of external forcing magnitude and frequency. In the next section this behavior will be explained by an analytical analysis of the problem.

3.5 Analytic treatment

In this section the mathematical problem associated to the VI-NES is studied. An analytical treatment is presented in which the Multiple Scales method is used in order to obtain the Slow Invariant Manifold (SIM) and the fixed points of the problem. The approach followed is mainly based on the work of Gendelman [Gen12], where the analytic treatment of an unforced system with a VI-NES is presented. Here we extend the treatment to a damped and forced system such as in [GMSB14b], with the difference

that the forcing term is not hypothetically supposed to be of order 1 but considered since order 0 in the multiple scales expansion.

The schematic of the model is presented in Fig.3.7. We define the variables u, v, and x_e as the displacements of the primary mass M, of the NES mass m and of the base respectively. Before going through the study of the equations of motion, we model the impacts by using the Newton's experimental law and the momentum conservation principle. This model, although quite simple, is able to represent the physics of the impacts by means of only one parameter: the restitution coefficient r.

$$\dot{u}(t_j^+) - \dot{v}(t_j^+) = -r(\dot{u}(t_j^-) - \dot{v}(t_j^-)) \tag{3.4}$$

$$M\dot{u}(t_j^+) + m\dot{v}(t_j^+) = M\dot{u}(t_j^-) + m\dot{v}(t_j^-) \tag{3.5}$$

Where t_j^+ and t_j^- are the time instants after and before the j^{th} impact respectively. Eq.(3.4) provides a relation for the relative velocities of the two colliding masses after and before the impact by use of the restitution coefficient $0 < r < 1$. Then, in the limit cases, impacts can be characterized as perfectly elastic $r = 1$ or perfectly inelastic $r = 0$. Eq.(3.5) expresses the momentum conservation throughout an impact. Each mass experiences an instantaneous momentum variation that can be represented by a Heaviside step function. Thanks to Eqs.(3.4) and (3.5) we can write the jump in velocity for each of the two masses as a function of the relative velocity before the impact $\dot{w^-} = \dot{u^-} - \dot{v^-}$ as follows:

$$\dot{u}^+ - \dot{u}^- = -\frac{m(1+r)}{(M+m)}\dot{w}^- \tag{3.6}$$

$$\dot{v}^+ - \dot{v}^- = \frac{M(1+r)}{(M+m)}\dot{w}^- \tag{3.7}$$

The derivative of momentum with respect to time is the force acting through the impact. Then the instantaneous force caused by the impact is:

$$F = M\left.\frac{du}{dt}\right|_{t=t_j} = M(\dot{u}^+ - \dot{u}^-)\delta_j = -\frac{Mm(1+r)}{(M+m)}\dot{w}^-\delta_j \tag{3.8}$$

Where we have exploited the property of the step function according to which its derivative is the delta function $\delta(t)$.

Thus in Eq.(3.9) we express the force each mass is subjected to as a Dirac delta function since the Dirac delta function is the distributional derivative of the Heaviside step function.

Finally the equations of motion can be written as:

$$M\ddot{u} + \lambda\dot{u} + Ku + \frac{Mm(1+r)}{M+m}\sum_j \dot{w}^-\delta_j^- = Kx_e + \lambda\dot{x}_e$$
$$m\ddot{v} - \frac{Mm(1+r)}{M+m}\sum_j \dot{w}^-\delta_j^- = 0 \tag{3.9}$$

Where M, λ and K are the mass, damping and stiffness of the primary system, m is the mass of the VI-NES and r the restitution coefficient.

Or:

$$\ddot{u} + 2\omega_0\xi\dot{u} + \omega_0^2 u + \frac{m(1+r)}{M+m}\sum_j \dot{w}^-\delta_j^- = \omega_0^2 x_e + 2\omega\xi\dot{x}_e$$
$$\epsilon\ddot{v} - \frac{m(1+r)}{M+m}\sum_j \dot{w}^-\delta_j^- = 0 \tag{3.10}$$

Where $\omega_0^2 = K/M$, $2\omega_0\xi = \lambda/M$ and $\epsilon = m/M$.
Adding up the two equations of Eq.(3.10):

$$\ddot{u} + \epsilon\ddot{v} + 2\omega_0\xi\dot{u} + \omega_0^2 u = \omega_0^2 x_e + 2\omega_0\xi\dot{x}_e \tag{3.11}$$

Defining the barycentric coordinates X and w[1]

$$X := u + \epsilon v$$
$$w := u - v \tag{3.12}$$

We obtain a relation between X, u, v:

$$X + \epsilon w = u + \epsilon v + \epsilon u - \epsilon v = (1+\epsilon)u \tag{3.13}$$

And then:

$$\implies u = \frac{X + \epsilon w}{1+\epsilon} \tag{3.14}$$

Substituting Eq.(3.14) into Eq.(3.11):

$$\ddot{X} + \frac{2\omega_0\xi}{1+\epsilon}(\dot{X} + \epsilon\dot{w}) + \frac{\omega_0^2}{1+\epsilon}(X + \epsilon w) = \omega_0^2 x_e + 2\omega_0\xi\dot{x}_e \tag{3.15}$$

We now define the following new variables:

$$\tau := t\frac{\omega_0}{\sqrt{1+\epsilon}} \quad \gamma := \frac{2\xi}{\sqrt{1+\epsilon}} \tag{3.16}$$

[1]The symbol := meaning *equals by definition*

And substitute them into Eq.(3.15):

$$\frac{\omega^2}{1+\epsilon}X_{\tau\tau}+\frac{2\omega_0}{1+\epsilon}\gamma\omega_0\frac{\sqrt{1+\epsilon}}{2\sqrt{1+\epsilon}}(X_\tau+\epsilon w_\tau)+\frac{\omega_0^2}{1+\epsilon}(X+\epsilon w)=\omega_0^2 x_e+2\omega_0\gamma\sqrt{1+\epsilon}\frac{\omega_0}{2\sqrt{1+\epsilon}}x_{e_\tau}$$

After simplifications we obtain an equation for X:

$$X_{\tau\tau}+\gamma X_\tau+X+\epsilon\gamma w_\tau+\epsilon w=(1+\epsilon)x_e+\gamma(1+\epsilon)x_{e_\tau} \tag{3.17}$$

Once an equation for X is found, one for w is sought.

Subtracting the second equation of Eq.(3.9) divided by m to the first of Eq.(3.9) divided by M:

$$\ddot{u}-\ddot{v}+2\omega_0\xi\dot{u}+\omega_0^2 u+(1+r)\sum_j \dot{w}^-\delta_j^-=\omega_0^2 x_e+2\omega_0\xi\dot{x}_e$$

Which, by using Eq.(3.14), leads to an equation for w:

$$\ddot{w}+\frac{2\omega_0\xi}{1+\epsilon}(\dot{X}+\epsilon\dot{w})+\frac{\omega_0^2}{1+\epsilon}(X+\epsilon w)+(1+r)\sum_j \dot{w}^-\delta_j^-=\omega_0^2 x_e+2\omega_0\xi\dot{x}_e \tag{3.18}$$

Operating the changing of variables defined in Eq.(3.16):

$$\begin{aligned}\frac{\omega_0^2}{1+\epsilon}w_{\tau\tau}+\frac{2\omega_0}{1+\epsilon}\gamma\omega_0\frac{\sqrt{1+\epsilon}}{2\sqrt{1+\epsilon}}(X_\tau+\epsilon w_\tau)+\frac{\omega_0^2}{1+\epsilon}(X+\epsilon w)+\\ +\frac{\omega_0^2}{1+\epsilon}(1+r)\sum_j w_\tau^-\delta_j^-=\omega_0^2 x_e+2\omega_0\gamma\sqrt{1+\epsilon}\frac{\omega_0}{2\sqrt{1+\epsilon}}x_{e_\tau}\end{aligned}$$

That yields the sought equation for w:

$$w_{\tau\tau}+\epsilon\gamma w_\tau+\gamma X_\tau+\epsilon w+X+(1+r)\sum_j w_\tau^-\delta_j^-=(1+\epsilon)x_e+(1+\epsilon)\gamma x_{e_\tau} \tag{3.19}$$

At the end, here are the two equations for X and w. These are up to now exact equations since no approximation has been made.

$$\begin{aligned}X_{\tau\tau}+\gamma X_\tau+\epsilon\gamma w_\tau+X+\epsilon w&=(1+\epsilon)x_e+\gamma(1+\epsilon)x_{e_\tau}\\ w_{\tau\tau}+\epsilon\gamma w_\tau+\gamma X_\tau+\epsilon w+X+(1+r)\sum_j w_\tau^-\delta_j^-&=(1+\epsilon)x_e+(1+\epsilon)\gamma x_{e_\tau}\end{aligned} \tag{3.20}$$

3.5.1 Multiple Scales Method

Assuming that the mass of the VI-NES m is small with respect to the primary mass M, $\epsilon = m/M << 1$ can be used as a small parameter in multiple scales analysis [Nay04].

$$\begin{aligned} \tau_k = \epsilon^k \tau, k = 0, 1, \dots; \quad \frac{d}{dt} = \frac{\partial}{\partial \tau_0} + \epsilon \frac{\partial}{\partial \tau_1} + \dots; \\ X = X_0(\tau_0, \tau_1, \dots) + \epsilon X_1(\tau_0, \tau_1, \dots) + \dots; \\ w = w_0(\tau_0, \tau_1, \dots) + \epsilon w_1(\tau_0, \tau_1, \dots) + \dots; \end{aligned} \tag{3.21}$$

The Multiple Scales Method is a perturbation method which is very similar to the Lindstedt-Poincaré 's method presented in Section 2.1.2 and applied to the Duffing equation. The difference here is that instead of introducing a stretched time $\tau = t + k_1\epsilon + k_2\epsilon^2 + \dots$, we have several independent time scales. This is consistent with the physics of the problem in which fast and slow oscillations occur; i.e. the system's oscillations and their modulation.

Bearing in mind that $\epsilon << 1$, the parameter γ can be expressed as a first-order Taylor polynomial:

$$\begin{aligned} \gamma = \frac{2\xi}{\sqrt{1+\epsilon}} &= 2\xi(1+\epsilon)^{-1/2} \\ &\simeq 2\xi(1 - \frac{\epsilon}{2}) \end{aligned} \tag{3.22}$$

The same is done with the external forcing term:

$$\begin{aligned} x_e &= \overline{X} \sin(\omega t) \\ &= \overline{X} \sin\left(\frac{\omega}{\omega_0}(1+\epsilon)^{1/2}\tau\right) \\ x_e &\simeq \overline{X} \sin(\frac{\omega}{\omega_0}\tau_0) + \frac{1}{2}\frac{\omega}{\omega_0}\tau_1 \overline{X} \cos(\frac{\omega}{\omega_0}\tau_1)\epsilon \end{aligned} \tag{3.23}$$

Substituting (3.21), (3.22) and (3.23) into (3.20) and only keeping the zero-order terms:

$$\begin{aligned} \frac{\partial^2 X_0}{\partial \tau_0^2} + 2\xi\frac{\partial X_0}{\partial \tau_0} + X_0 = X_{e_0} + 2\xi\frac{\partial X_{e_0}}{\partial \tau_0} \\ \frac{\partial^2 w_0}{\partial \tau_0^2} + 2\xi\frac{\partial X_0}{\partial \tau_0} + X_0 + (1+r)\sum_j \frac{\partial w_0^-}{\partial \tau_0}\delta_j^- = X_{e_0} + 2\xi\frac{\partial X_{e_0}}{\partial \tau_0} \end{aligned} \tag{3.24}$$

Where $X_{e_0} = \overline{X}\sin(\Omega\tau_0)$ with $\Omega = \frac{\omega}{\omega_0}$.

By considering the experimental values we identified ($\xi \approx \epsilon \approx 0.8\%$) we can reasonably assume that $\xi = \frac{\lambda}{2\omega_0 M}$ has the same order as ϵ and therefore that $\xi = O(\epsilon)$. Consequently terms multiplied by ξ in Eq.(3.24) can be neglected. That yields:

$$\begin{aligned} \frac{\partial^2 X_0}{\partial \tau_0^2} + X_0 &= X_{e_0} \\ \frac{\partial^2 w_0}{\partial \tau_0^2} + X_0 + (1+r)\sum_j \frac{\partial w_0^-}{\partial \tau_0}\delta_j^- &= X_{e_0} \end{aligned} \tag{3.25}$$

Alternatively, one can say that solutions of Eq.(3.25) will be very close to solutions of Eq.(3.24) given the small influence of ξ. Then the two equations of System (3.25) can be solved for X_0 and w_0. Here we follow the ansatz given by Gendelman in [Gen12] and [GA15] with the exception that the forcing term is present even at ϵ^0 order. That leads to the following expression for X_0:

$$X_0 = C(\overline{X}, \Omega, \tau_1)\sin(\Omega\tau_0 + \psi(\tau_1)) \tag{3.26}$$

C and ψ are the amplitude and the phase of X_0. The amplitude C is a function of the external forcing X_{e_0} and terms of order-1. The phase ψ is a function of order-1 terms as it depends on damping ξ.

Substituting (3.26) in the second equation of (3.25) we obtain:

$$\frac{\partial^2 w_0}{\partial \tau_0^2} + (1+r)\sum_j \frac{\partial w_0^-}{\partial \tau_0}\delta_j^- = A\sin(\Omega\tau_0 + \theta) \tag{3.27}$$

Where $A\sin(\Omega\tau_0 + \theta)$ is the sum of X_0 and X_{e0}. These two terms are two sinus with the same frequency Ω and shifted in phase by ψ. It can be shown that the sum of those terms is a single sinus with a new amplitude A and phase θ to be determined. Proof is provided in appendix A.

A solution for w_0 in the following form is sought:

$$w_0 = -\frac{A(C, \overline{X}, \psi)}{\Omega^2}\sin(\Omega\tau_0 + \theta) + f(\tau_0, \tau_1) \tag{3.28}$$

Inserting (3.28) into (3.27):

$$\frac{\partial^2 f}{\partial \tau_0^2} + (1+k)\sum_j \left[\left.\frac{\partial f}{\partial \tau_0}\right|_{\tau_0^-} - \frac{A}{\Omega}\cos(\Omega\tau_0 + \theta)\right]\delta_j^- = 0 \tag{3.29}$$

Assuming that TET occurs in an established state of 1:1 resonance between the VI-NES and the LO and neglecting the transient process leading to 1:1 resonance, the particle will move symmetrically and at the same frequency of LO. A form of f representing the "free flights" interrupted by the impacts is:

$$f(\tau_0, \tau_1) = \frac{2\alpha}{\pi} \arcsin\left(\cos(\Omega(\tau_0 - \eta))\right) \tag{3.30}$$

Where $\eta + \pi j, j = 1, 2, \ldots$ are the unknown impact instants. A schematic representation of f is presented in Fig.3.13.

Substituting (3.30) into (3.29) and integrating over a small interval around time $\tau_0 = \eta$:

$$-\frac{4\alpha\Omega}{\pi} + (1+r)\left(\frac{2\alpha\Omega}{\pi} - \frac{A}{\Omega}\cos(\Omega\eta + \theta)\right) = 0 \tag{3.31}$$

And finally:

$$-A\cos(\Omega\eta + \theta) = \Omega^2 \frac{2(1-r)}{\pi(1+r)}\alpha = \Omega^2\sigma\alpha \tag{3.32}$$

Where $\sigma = \frac{2(1-r)}{\pi(1+r)}$. One more relation between A and α can be found by considering the expression (3.28) evaluated when an impact occurs: $\tau_0 = \eta$ and $w = \pm L$.

$$-\frac{A}{\Omega^2}\sin(\Omega\eta + \theta) + \alpha = L \tag{3.33}$$

Finally we have:

$$\begin{aligned} A_\Omega \cos(\Omega\eta + \theta) &= \sigma\alpha \\ A_\Omega \sin(\Omega\eta + \theta) &= L - \alpha \end{aligned} \tag{3.34}$$

With $A_\Omega = -A/\Omega^2$.
The two equations (3.34) allows one to analytically define the Slow Invariant Manifold of the problem:

$$\alpha = \frac{L \pm \sqrt{L^2 - (1+\sigma^2)(L^2 - A_\Omega^2)}}{1+\sigma^2}$$

Or:

$$\alpha = \frac{L \pm \sqrt{1+\sigma^2}\sqrt{A_\Omega^2 - A_{\Omega_{min}}^2}}{1+\sigma^2} \tag{3.35}$$

Where $A_{\Omega_{min}} = \frac{\sigma L}{\sqrt{1+\sigma^2}}$ is a minimum value of amplitude A/Ω^2 for TET to be established.

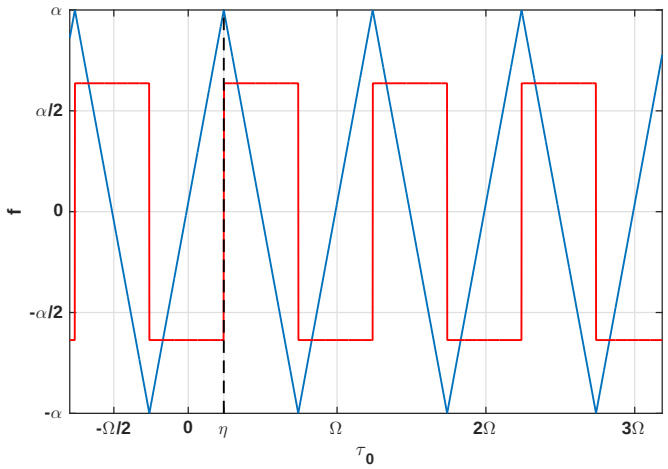

Figure 3.13: Sketch of function f according to eq.(3.30) (blue) and its derivative (red).

Eq.(3.35) defines the Slow Invariant Manifold of the system. A first important piece of information we can draw from Eq.(3.35) is that a minimum for A_Ω exists for solutions to appear. In order to have a physical meaning of the two variables of the SIM, A_Ω and α can be thought as respectively the LO's and the NES' oscillation amplitudes. Then the lower threshold is actually a minimum amount of LO's energy (oscillations amplitude) the VI-NES needs to turn active. As previously mentioned this is a typical feature of nonlinear systems [VGMM01a, VGMM01b, KLV$^+$05]. Moreover information about stability of solutions can be obtained from ϵ^0-equations. Indeed a stability analysis can be performed by means of the Poincaré Map which reveals that the SIM is composed of two branches of solutions: one stable and one unstable. We will not describe the analysis here but only suggest that the reader refer to [LRM90] for a detailed mathematical description. Indeed, to have the same formal problem as in [LRM90] we just need to rearrange the second equation in (3.25) as:

$$\begin{aligned} \frac{\partial^2 w_0}{\partial \tau_0^2} &= A\sin(\Omega\tau_0+\theta) \qquad && |w_0| < L \\ \frac{\partial w_0^+}{\partial \tau_0} &= -r\frac{\partial w_0^-}{\partial \tau_0} && |w_0| = L \end{aligned} \tag{3.36}$$

As it will be explained more in detail in the next section, from a math-

ematical point of view this threshold represents a saddle node bifurcation beyond which two branches of solutions appear, one stable and one unstable. Physically that means that a minimum amplitude of primary mass displacement has to be reached in order to engage a solution (i.e. a 1:1 resonance between the primary system and the VI-NES). This type of behavior is typical among nonlinear absorbers and has been observed and investigated for cubic stiffness NES.

The SIM strongly depends on the design parameters length L and restitution coefficient r as graphs in Fig.3.15 show. Particularly, it is interesting to highlight how in the case of $r = 1$ the value for $A_{\Omega_{min}}$ is zero and the corresponding value of α is equal to half the tube length, i.e. the distance gap between the ball and the tube before impacting. This is physically explicable as $r = 1$ means no loss of energy during the impacts, the state with two impacts per cycle could therefore be maintained without the primary mass moving, i.e. with no input of energy into the system.

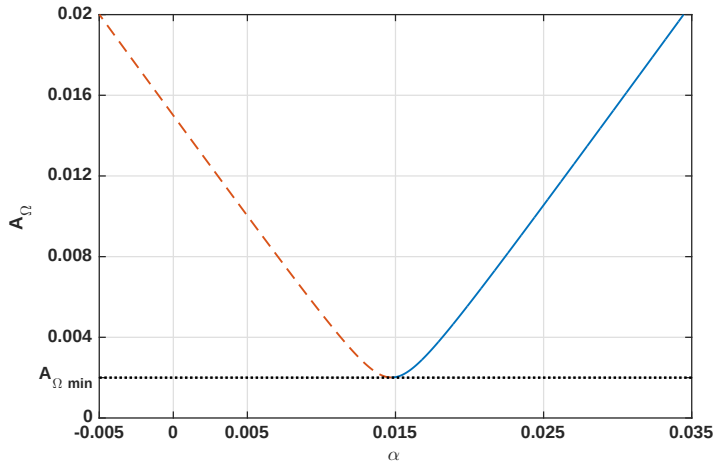

Figure 3.14: Slow Invariant Manifold - $r = 0.65$, $L = 15mm$

Once the SIM obtained, we push further our analysis and study system (3.20) at ϵ^1 scale in order to study the evolution of the system on the SIM as the amplitude and frequency of the forcing term vary.

Only keeping the ϵ^1-order terms the first equation of (3.20) becomes:

$$\frac{\partial^2 X_1}{\partial \tau_0^2} + X_1 = -2\frac{\partial^2 X_0}{\partial \tau_0 \partial \tau_1} - \gamma \frac{\partial X_0}{\partial \tau_0} - \frac{\partial^2 X_0}{\partial \tau_0^2} - w_0 + Y\cos(\Omega\tau_0 + \beta(\tau_1)) \quad (3.37)$$

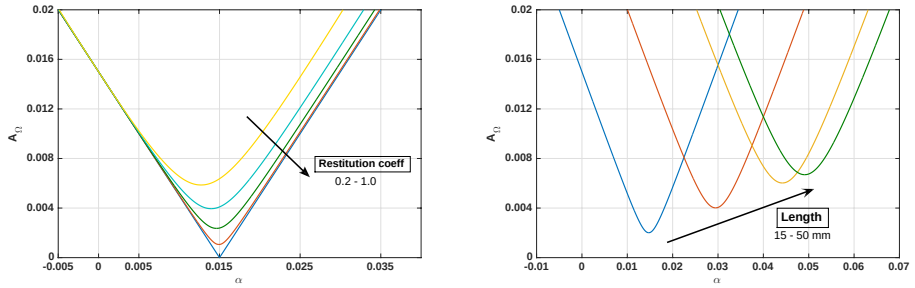

Figure 3.15: Evolution of ϵ^0-SIM for constant $L = 15mm$ as the restitution coefficient varies (left) and for constant $r = 0.65$ as the length varies (right).

Where $Y\cos(\Omega\tau_0 + \beta(\tau_1)) = \overline{X}\sin(\Omega\tau_0) + \gamma\Omega\overline{X}\cos(\Omega\tau_0)$.

After substituting (3.26) into (3.37) and eliminating secular terms we are able to find the approximate solution coming from the multiple scales method. By equaling derivatives with respect to time to zero the fixed points are obtained. These steps are not reported here for the sake of conciseness and can be found in [GMSB14b]. Finally we obtain a fourth order polynomial relating A and α:

$$a_2 A^4 + a_1 A^2 + a_0 = 0 \tag{3.38}$$

Where the coefficients a_0, a_1, a_2 are functions of α:

$$\begin{aligned} a_0 &= \frac{64}{B^2\pi^4}\left(\sigma^2+1\right)\alpha^4 - \frac{128}{B^2\pi^4}\alpha^3 + \frac{64}{B^2\pi^4}\alpha^2 \\ a_1 &= \frac{32}{B^2\pi^2}\left(\frac{\mu\sigma}{2}+\delta\right)\alpha^2 - \frac{32\delta}{B^2\pi^2}\alpha - 1 \\ a_2 &= \frac{(\mu^2+4\delta^2)}{B^2} \end{aligned} \tag{3.39}$$

Where δ is the detuning parameter defined as $\Omega = 1 + \epsilon\delta$, B is the scaled external amplitude term $B = \frac{\overline{X}}{L\epsilon}$ and μ is the scaled damping coefficient $\mu = 2\xi/\epsilon$. It can be seen that, unlike the SIM, the fixed points expression depends on the external excitation's amplitude $\overline{X}$ and frequency Ω through the variables B and δ. It is also important to notice that, as it was for the SIM, the fixed points expression is a function of the design parameters tube's length L and restitution coefficient r (through σ).

The solutions of the problem will satisfy both Eq.(3.35) and Eq.(3.38) and can graphically be identified by the intersections of these two curves

on the plane $A_\Omega - \alpha$. Alternatively, one can say that the fixed points of Eq.(3.38) have to respect the constraints given by the SIM of Eq.(3.35).

To summarize, through this section we mathematically described the physical problem, the impacts were modeled and the equations of motion obtained. The multiple scales method was applied to simplify and analytically solve the equations of motion. Under the assumption of 1:1 resonance between the LO and the VI-NES we found an expression for the Slow Invariant Manifold of the problem which provides some important information about the existence and the stability of all the possible solutions. Subsequently, by developing the equations of motion up to ϵ^1-order, the fixed points were calculated, i.e. the steady-state solutions for a given external forcing. These points should respect the conditions imposed by the SIM to be actual physical solutions.

3.6 Stability analysis

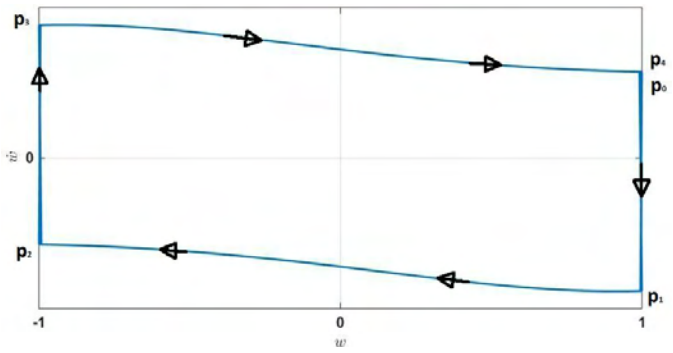

Figure 3.16: Symmetric solution: phase portrait of $w - \dot{w}$.

As a periodic solution of order n we refer to a periodic solution which has a period n times the forcing period T, with T integer. It is important to notice that if $p_0 = p_4$, then the orbit/solution is periodic. The simplest type is one in which impacts occur only once per cycle with each of the two boundaries and that takes a time nT to complete a cycle. Within these simple periodic solutions we can distinguish two different types of motion: symmetric solution in which the oscillator spends the same amount of time between any two consecutive impacts (from p_1 to p_2 and from p_3 to p_4) and asymmetric solutions in which this condition is not verified. In the stability analysis that follows, we will firstly consider the symmetric simple solutions of order 1, as that one represented in Fig.3.16.

3.6.1 Equations of motion

We rewrite the equations of motion for w_0 by splitting the continuous part and the impact rules:

$$\frac{\partial^2 w_0}{\partial \tau_0^2} = A\sin(\Omega\tau_0 + \theta) \qquad |w_0| < L \tag{3.40a}$$

$$\frac{\partial w_0^+}{\partial \tau_0} = -r\frac{\partial w_0^-}{\partial \tau_0} \qquad |w_0| = L \tag{3.40b}$$

In order to conduct the stability analysis of this system by means of the Poincaré Map, we operate the following changes of variables, which will provide a simpler form of equations.

$$x := \Omega\tau_0 + \theta \tag{3.41a}$$

$$\frac{\partial w_0}{\partial \tau_0} = \Omega\frac{\partial w_0}{\partial x} = \Omega w_0' \tag{3.41b}$$

$$\gamma := \frac{A}{L\Omega^2} \tag{3.41c}$$

After these substitutions and introducing $y := w'$, (3.40a) can be written as a first-order system:

$$w' = y \tag{3.42a}$$

$$y' = \gamma\sin(x) \qquad |w| < 1 \tag{3.42b}$$

$$y^+ = -ry^- \qquad |w| = 1 \tag{3.42c}$$

Where w has been written instead of w_0 as a simpler notation.

3.6.2 Poincaré Map

We take the Poincaré surface of section Σ:

$$\Sigma = \{(w, y, x) \in I \times \Re \times S | w = +1, y > 0\} = S \times \Re^+ \tag{3.43}$$

Where $I = [-1, +1]$ and $S = [0, 2\pi]$. The Poincaré map converts the original three-dimensional flow $(w, \dot{w}, x)$ into a two-dimensional discrete mapping. The Poincaré section is coordinated by the phase x and the velocity y:

$$P : \Sigma \to \Sigma \quad i.e. \quad (x_0, y_0) \to (x, y) \tag{3.44}$$

In the case a simple periodic orbit correspond to a stable fixed point in the Poincaré map, as the parameters γ, r change there are three ways in which this point can lose its stability. Indeed, a loss of stability occurs when at least one of the eigenvalues of the linearised Poincaré map has an absolute value ≥ 1, and the following kinds of bifurcations can take place:

- if one of the eigenvalues becomes $+1$, that corresponds to a saddle-node bifurcation;
- if one of the eigenvalues becomes -1, that corresponds to a period-doubling bifurcation;
- if a pair of complex conjugate eigenvalues has absolute value equal to unity, that corresponds to a Hopf bifurcation;

In order to determine the stability of a periodic solution starting at (x_0, y_0), we need to compute the Jacobian matrix of the Poincaré map P at (x_0, y_0).

$$DP(x_0, y_0) = \frac{\partial(x_4, y_4)}{\partial(x_0, y_0)} \tag{3.45}$$

Because of the discontinuity of the velocity, the process of differentiation is divided in four parts:

$$DP(x_0, y_0) = \frac{\partial(x_4, y_4)}{\partial(x_0, y_0)} = \frac{\partial(x_4, y_4)}{\partial(x_3, y_3)} \frac{\partial(x_3, y_3)}{\partial(x_2, y_2)} \frac{\partial(x_2, y_2)}{\partial(x_1, y_1)} \frac{\partial(x_1, y_1)}{\partial(x_0, y_0)} \tag{3.46}$$

From the impact rule we can obtain the derivatives concerning $p_0 \to p_1$ and $p_2 \to p_3$:

$$\frac{\partial(x_1, y_1)}{\partial(x_0, y_0)} = \frac{\partial(x_3, y_3)}{\partial(x_2, y_2)} = \begin{bmatrix} 1 & 0 \\ 0 & -r \end{bmatrix} \tag{3.47}$$

Solving (3.42) and evaluating in p_2:

$$-1 = c_1 + c_2(x_2 - x_1) - \gamma \sin(x_2) \equiv f(y_1, x_1, x_2) \tag{3.48a}$$

$$y_2 = c_2 - \gamma \cos(x_2) \equiv g(y_1, x_1, x_2) \tag{3.48b}$$

Where $c_1 = 1 + \gamma \sin x_1$ and $c_2 = y_1 + \gamma \cos x_1$. We can now calculate the derivatives we need by means of f and g functions:

$$\frac{\partial(x_2, y_2)}{\partial(x_1, y_1)} = \begin{bmatrix} -\frac{\partial f}{\partial x_1} \div \frac{\partial f}{\partial x_2} & -\frac{\partial f}{\partial y_1} \div \frac{\partial f}{\partial x_2} \\ \frac{\partial g}{\partial x_2}\frac{\partial x_2}{\partial x_1} + \frac{\partial g}{\partial x_1} & \frac{\partial g}{\partial x_2}\frac{\partial x_2}{\partial y1} + \frac{\partial g}{\partial y_1} \end{bmatrix} =$$

$$= \frac{1}{y_2} \begin{bmatrix} y_1 + a_1\Delta_{21} & -\Delta_{21} \\ a_1 a_2 \Delta_{21} + a_2 y_1 - a_1 y_2 & y_2 - a_2\Delta_{21} \end{bmatrix} \tag{3.49}$$

Where $a_i = \gamma \sin(x_i)$, $i = 1, 2, 3, 4$. For $p_3 \rightarrow p_4$ part, we have the same derivatives than (3.49) but with y_3 replacing y_1, y_4 replacing y_2, Δ_{43} replacing Δ_{21}, a_3 replacing a_1 and a_4 replacing a_2.

Thanks to the symmetry and the impact rule, we can express everything as a function of the conditions in p_0:

$$\begin{array}{cccc} y_1 = -ry_0; & y_2 = -y_0; & y_3 = ry_0; & y_4 = y_0 \\ a_1 = a_0; & a_2 = -a_0; & a_3 = -a_0; & a_4 = a_0 \end{array} \tag{3.50}$$

Thus, the Jacobian:

$$DP = -\frac{1}{y_0^2} \begin{bmatrix} ry_0 - a_0\Delta_{21} & r\Delta_{21} \\ a_0 y_0(1+r) - a_0^2\Delta_{21} & -r(y_0 - a_0\Delta_{21} \end{bmatrix} \times \\ \times \begin{bmatrix} -(ry_0 - a_0\Delta_{21} & r\Delta_{21} \\ a_0 y_0(1+r) - a_0^2\Delta_{21} & r(y_0 - a_0\Delta_{21}] \end{bmatrix} \tag{3.51}$$

The eigenvalues of (3.51) can be found from:

$$\lambda^2 - tr\lambda + det = 0 \tag{3.52}$$

Where the trace and the determinant:

$$\begin{array}{c} tr = -2r^2 + [2r - a_1\Delta_{21}(1+r)/y_0]^2 \\ det = r^4 < 1 \end{array} \tag{3.53}$$

3.6.3 Bifurcations

The calculation of the eigenvalues from (3.52) will tell us more about the nature of instabilities that can arise:

- No Hopf bifurcations can occur: Hopf bifurcations would require $|\lambda| = 1$ for a pair of λ complex. However, since $det(DP) = |\lambda_1||\lambda_2| < 1$, that cannot happen;

- No period-doubling bifurcations can occur: it is impossible because (3.52) has no real solutions for$\lambda = -1$, i.e. no equilibrium points;

- For $\lambda = 1$, (3.52) becomes $1 - tr + det = 0$, from which we find two equilibrium points and the corresponding bifurcations critical values γ_c.

The two equilibria for $\lambda = 1$ are:

$$y_{0_1} = \left[\frac{(1-r)^2}{\Delta_{21}(1+r)} + \frac{\Delta_{21}(1+r)}{4}\right]^{-1}$$
$$y_{0_2} = \frac{4\Delta_{21}}{(1+r)(\Delta_{21}^2 - 4)} \tag{3.54}$$

And the corresponding critical values γ_c:

$$\gamma_{c_1} = \left[1 + \frac{\Delta_{21}^2(1+r)^2}{4(1-r)^2}\right]^{-1/2}$$
$$\gamma_{c_2} = \frac{2[\Delta_{21}^2(1-r)^2 + 4(1+r)^2]^{1/2}}{(1+r)(\Delta_{21}^2 - 4)} \tag{3.55}$$

The first value γ_{c_1} corresponds to a saddle-node bifurcation. Below this value no equilibrium exists, for $\gamma > \gamma_{c_1}$ two branches of solutions appear: one stable and one unstable. Let us point out that this value is the "threshold value for TET" we calculated in the previous section.

The second bifurcation point is a pitchfork bifurcation. It differs from the first one as equilibrium exists in the neighborhood of γ_{c_2}. However, above this value an eigenvalue of the problem becomes greater than unity and an unstable branch appears.

3.7 Experimental and analytical results comparison

The purpose of this section is to find an analytical description and explanation to the VI-NES behavior we observed experimentally. Particular attention is paid to the type of response the VI-NES may exhibit depending on the magnitude and frequency of the external forcing. Three levels of forcing amplitude are considered: low, medium and high. For each level the evolution of the system on the SIM as the external frequency forcing varies is analytically analyzed and compared to the experimental observations. For the analytic calculations a coefficient of restitution $r = 0.65$ is used. This is a typical value for an impact involving two metal bodies. Each case is presented as a graph on the $A_\Omega - \alpha$ plan where the curves (3.35) and (3.38) have been plotted. It is important to notice that eq.(3.38) can have real or

imaginary solutions. In the graphs that follow only the real solutions are plotted as they represent the only physical fixed points.

3.7.1 Low level forcing

For a low level of forcing ($\ddot{x}_e = 0.1g$) the activation threshold condition is not respected at any frequency and the VI-NES is never active. Experimentally the LO is not affected at all by the presence of the VI-NES. Analytically, as shown in fig.3.17, the fixed points evaluated by solving Eq.(3.38) (green curve) do not intersect the SIM curve and as a consequence no steady solution can be reached.

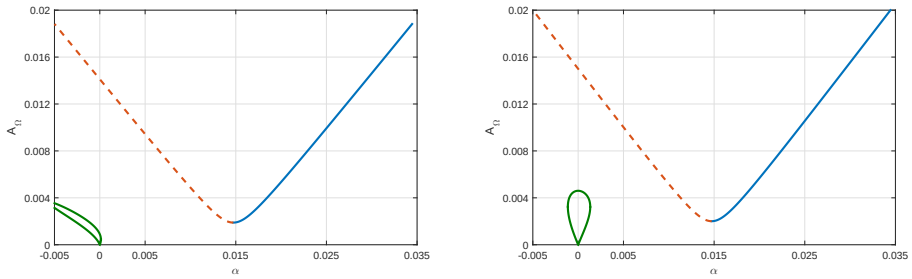

(a) $\Omega = 0.97$ (b) $\Omega = 1$

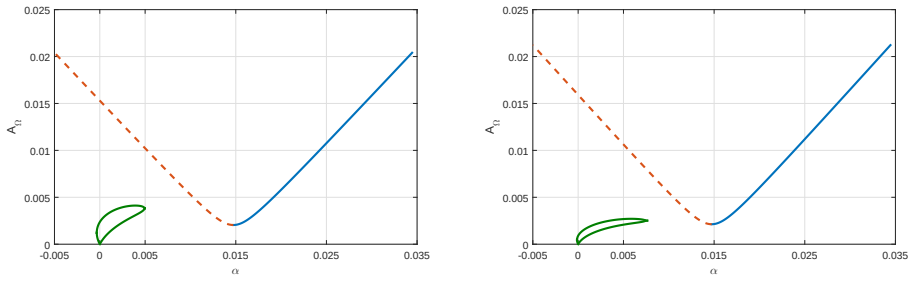

(c) $\Omega = 1.01$ (d) $\Omega = 1.03$

Figure 3.17: Evolution of the fixed points for a low level of external forcing $\ddot{x}_e = 0.1g$ and four values of Ω. The stable and unstable branches of the SIM are the blue and red-dashed lines respectively. The green curve is the solution of (3.38). No intersections are present at any frequencies: the VI-NES is never active.

3.7.2 Medium level forcing

Fig.3.18 shows the experimental spectrum of the primary mass displacement for a base acceleration $\ddot{x}_e = 0.2g$. The VI-NES is idle up until the primary system's oscillations reach the activation threshold, it is active for a range of frequency around the natural frequency of the LO and it turns idle again for higher frequencies of the forcing. However, the only type of response observed is the SMR, suggesting the VI-NES is not able to establish a stable-state solution.

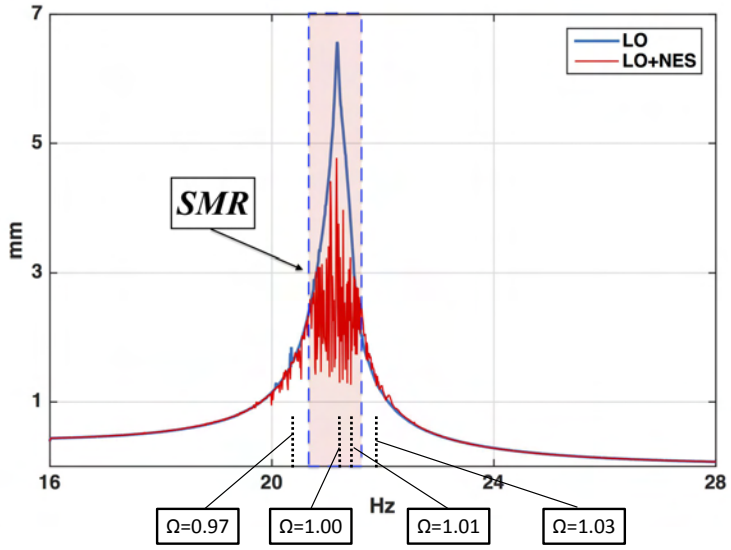

Figure 3.18: Spectra of primary mass displacement with (red) and without (blue) VI-NES. The regime of constant amplitude (CAR) and strongly modulated response (SMR) have been highlighted.

This assumption is actually confirmed by looking at the evolution of the fixed points on the SIM in fig.3.19. Four different values of forcing frequency $\Omega = 0.97; 1.00; 1.01; 1.03$ are shown. For $\Omega = 0.97$ and $\Omega = 1.03$ the isles (green curves) representing the fixed points do not intersect the SIM and the VI-NES is idle. For both $\Omega = 1.00$ and $\Omega = 1.03$ the fixed points curves have two intersection with the SIM, meaning steady solutions exist.

Nevertheless the points intersected are located on the unstable branch

of the SIM: the solutions are then unstable. This is in agreement with the experimental observations which featured a Strongly Modulated Response. Analyzing the SMR, we can assume that the phase when the VI-NES is active is an unstable solution and therefore cannot be held. Subsequently the oscillations amplitude decreases until the VI-NES is not active anymore since the activation threshold condition is not satisfied. Because of the constant external forcing the primary mass' oscillations get higher again and go beyond the activation threshold and the cycle starts over. It should be noticed that the cycles are each time different and appear to be chaotic. Recently Gendelman et al. [GA15] referred to this phenomenon as Chaotic Strongly Modulated Response (CSMR).

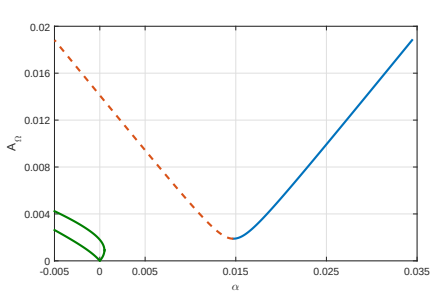

(a) $\Omega = 0.97$: Idle

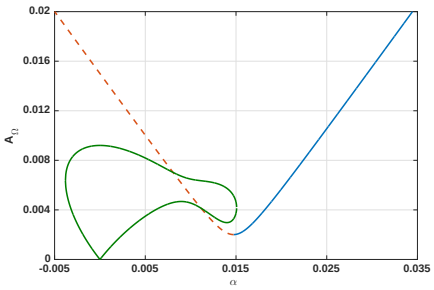

(b) $\Omega = 1.00$: SMR

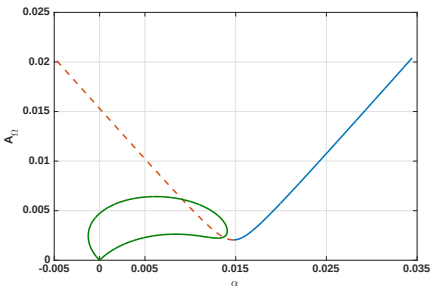

(c) $\Omega = 1.01$: SMR

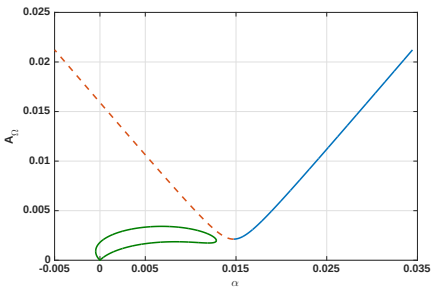

(d) $\Omega = 1.03$: Idle

Figure 3.19: Evolution of the SIMs for an external force of magnitude $F = 0.2g$ and different values of Ω. The stable and unstable branches of the ϵ^0-order SIM are the blue and red-dashed lines respectively, the ϵ-order SIM is the green curve. A SMR regime is the only type of solution that can be reached. This is in agreement with the experimental results of Fig.3.18

.

3.7.3 High level forcing

When the external base acceleration is $\ddot{x}_e = 0.4g$ the measured spectrum showed in fig.3.20 presents two zones with respectively CAR and SMR. The VI-NES exhibits a CAR for most of the frequency range of activation and a SMR for a little portion just before turning back idle. The evolution of the fixed points on the SIM is illustrated in fig.3.21. At $\Omega = 0.94$ we can see that a second fixed points-isle appears but that still there are no points of intersection with the SIM. At $\Omega = 0.97$ this second isle intersects twice the SIM on the stable and on the unstable branch. It means that at least one stable solution exists and a CAR can be established. When the frequency goes up the stable point tends to lose its stability and eventually becomes unstable ($\Omega = 1.04$) as the isle of fixed points gets smaller. At $\Omega = 1.06$ there are not intersections anymore and the VI-NES is idle again.

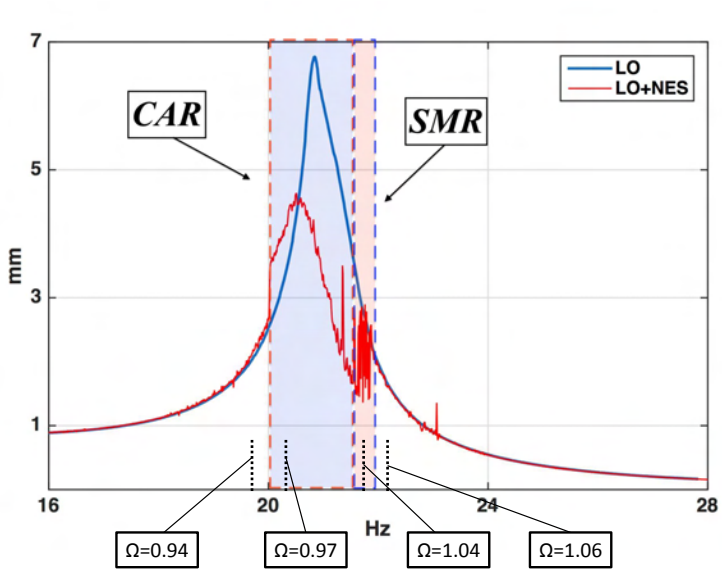

Figure 3.20: Spectra of primary mass displacement with (red) and without (blue) VI-NES for $\ddot{x}_e = 0.4g$ (right). The regimes of constant amplitude response (CAR) and strongly modulated response (SMR) have been highlighted.

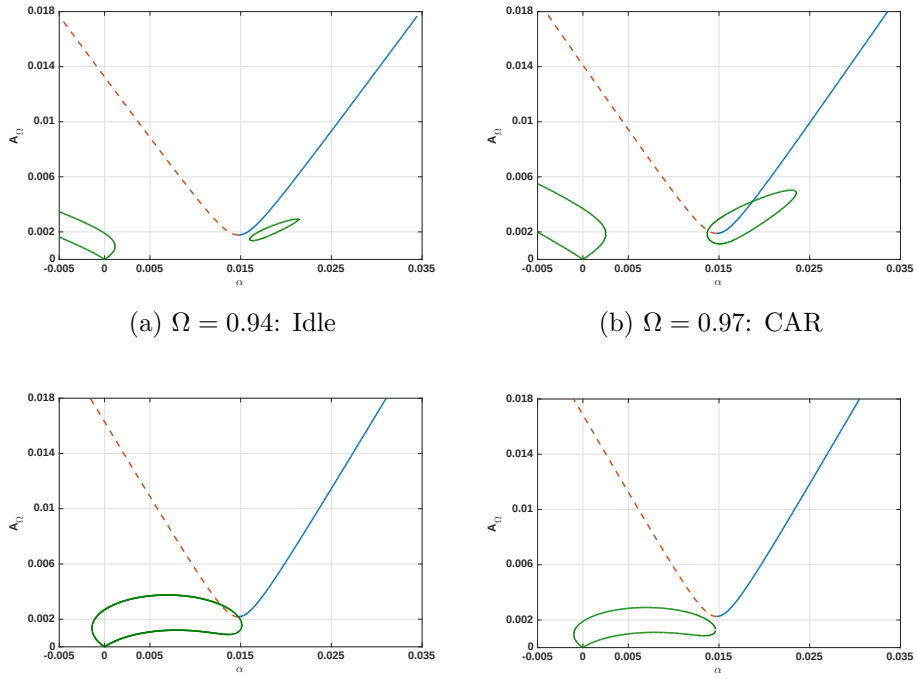

(a) $\Omega = 0.94$: Idle

(b) $\Omega = 0.97$: CAR

(c) $\Omega = 1.04$: SMR

(d) $\Omega = 1.06$: Idle

Figure 3.21: Evolution of the SIMs for an external force of magnitude $F = 0.4g$ and different values of Ω. The stable and unstable branches of the ϵ^0-order SIM are the blue and red-dashed lines respectively, the ϵ-order SIM is the green curve. The system can have either stable ($\Omega = 0.97$) or unstable ($\Omega = 1.04$) fixed point intersections. CAR and SMR can both be observed.

3.8 Influence of the tube's length and the mass ratio on the VI-NES response

In this section the influence of the mass ratio $\varepsilon = m/M$ and the tube length L on the response of the VI-NES is studied. The case of low level forcing presented in the previous section is used to show how a variation in the parameters m and L can lead to a change in the VI-NES response. This is done by means of the analytic model and by calculating the SIM and the fixed points of the problem.

In Sec.3.7.1 we saw how for a low level of forcing ($\ddot{x}_e = 0.1g$) the activation threshold condition is not respected at any frequency and the VI-NES is never active. A way to have solutions for this level of forcing would be reduc-

ing the tube length. If this happens the SIM would move left on the $A_\Omega - \alpha$ plan and the fixed points could intersect it. This example is illustrated in Fig.3.22 where the tube length has been halved ($L = L_0/2 = 7.5mm$).

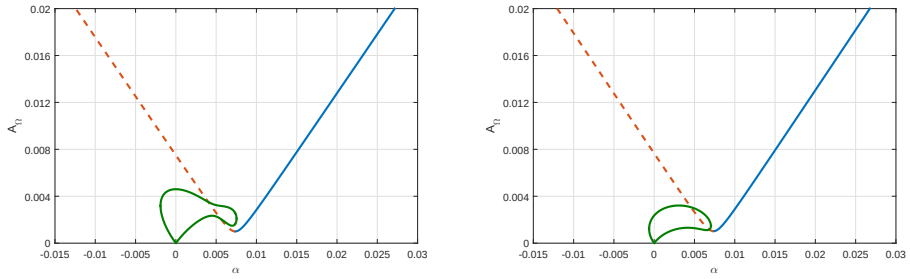

(a) $\Omega = 1.002$ (b) $\Omega = 1.010$

Figure 3.22: Same case as in Fig.3.17 of low level forcing but for a tube length divided by two ($L = L_0/2 = 7.5mm$). It can be seen that in this case a SMR regime is possible.

The VI-NES is now capable to reach a Strongly Modulated Response state. If we go further in this analysis and keep reducing the length, there will be a point when the system gets to a Constant Amplitude Response. This example is shown in Fig.3.23 where the length has been divided by three ($L = L_0/3 = 5mm$)

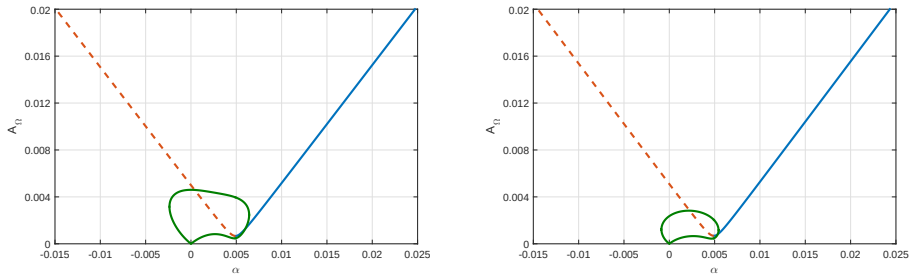

(a) $\Omega = 1.002$ (b) $\Omega = 1.010$

Figure 3.23: Same case as in Fig.3.17 of low level forcing but for a tube length divided by three ($L = L_0/3 = 5mm$). It can be seen that in this case a CAR regime is possible.

We can assume that the smaller the tube length is the easier it is to reach a stable solution (CAR), i.e. even with a low level of external excita-

tion. However, it is highly important to point out that this is a discussion about the qualitative responses the VI-NES may exhibit and not about the efficiency of the VI-NES as an absorber. The problem is viewed here from a kinematic point and not from an energetic one. It means that reducing the length and reaching a stable fixed point may potentially make the VI-NES less efficient as an absorber. This point can be better understood by studying the effect of a mass ratio variation.

A similar analysis is conducted in the case where the mass ratio $\varepsilon = m/M$ varies and the tube length is kept constant. If the VI-NES mass is decreased to $\varepsilon = 0.2\%$, a Strongly Modulated Response can be established, as shown in Fig.3.24a. When the mass ratio is further decreased ($\varepsilon = 0.15\%$) a Constant Amplitude Response state appears (see Fig.3.24b). It should be clear that the effect of reducing the mass ratio allows the VI-NES to reach a stable state but at the same time reduces the level of energy dissipated by shocks and consequently the VI-NES efficiency as an absorber. For this reason and because of the complex dependency of the problem on the parameters, an extensive energetic study will be carried out in future investigations.

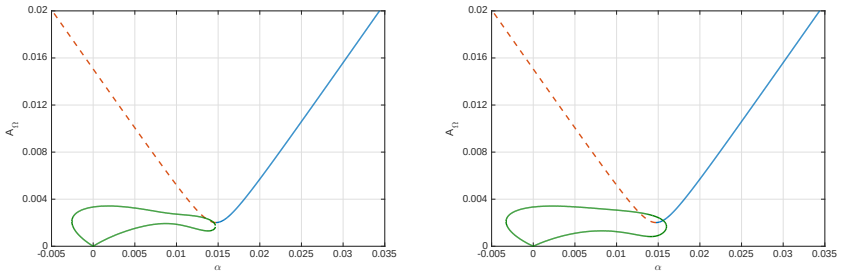

(a) $\varepsilon = 0.20\%$ - $\Omega = 1.002$ (b) $\varepsilon = 0.15\%$ - $\Omega = 1.002$

Figure 3.24: Same case as in Fig.3.17 of low level forcing but for a smaller mass ratio. It can be seen that a SMR and a CAR regime are possible.

3.9 Conclusion

In this chapter the dynamical behavior of a harmonically forced 1-dof LO coupled to a VI-NES has been explored. An experimental study has been carried out which showed the different regimes of response that may arise (constant amplitude and strongly modulated) and their dependence on the external forcing in terms of magnitude and frequency. The spectra of the primary mass displacement have shown that a Targeted Energy Transfer

occurs and that the VI-NES may actually works as dynamic vibration absorber even with a very small mass ratio ($\epsilon = 0.84\%$). Then the system has been analytically studied by using the multiple scales method and the Slow Invariant Manifolds for the fast and the slow time scale have been obtained. Finally an analytical explanation to the experimental observations has been provided. It showed that a threshold in LO amplitude for TET to take place exists. This limit mathematically represents a bifurcation point. These results will constitute the basis for further investigations which could lead to a designing process of the VI-NES as a vibration absorber.

Chapter 4

Magnetic-Strung Nonlinear Energy Sink

Abstract

This chapter illustrates the theoretical design and experimental realization of a new type of Nonlinear Energy Sink. The mass of the Magnetic-Strung NES is a magnet which is linked to the primary system by means of two strings working transversally whose pretensions are adjustable. The restoring elastic force of the strings is modulated thanks to the magnetic force applied by two magnets suitably located on the primary mass. This way, depending on the distance of the additional magnets, either a purely cubic force or a more complex shaped force may be reached. NES efficiency as an absorber is studied on a harmonically forced 1 degree-of- freedom primary system. The Target Energy Transfer (TET) from the primary system towards the NES is experimentally observed as well as different response regimes like the Strongly Modulated Response. Moreover, the energy harvesting from the vibrating energy of the NES is investigated: the NES mass, made up of a magnet, oscillates into a coil and subsequently creates an electric current. Thus, the vibrating energy of the primary mass is in this way absorbed by the NES and finally converted into electric energy.

4.1 Introduction

In this chapter the two research fields of nonlinear vibration absorbers and energy harvesting are combined. The study of a new concept of cubic NES coupled to an electromagnetic harvester is presented. A review of the energy harvesting techniques from vibrations made us lean towards a magnetic method because considered the most suitable one for the experimental realization we were looking for. The system consists in a harmonically forced single-degree-of-freedom linear oscillator to which a MS-NES is attached.

Firstly, the type of nonlinearity is illustrated: the nonlinear force between the primary system and the NES is modeled and the equations of motion are obtained. The mechanical system is then coupled to the magnetic harvester and the model of the final electro-mechanical system is defined.

Thus, the use of a magnetic force to shape the relation between the primary system and the NES is described and the cubic and the bistable configuration are presented.

Finally a numerical and an experimental investigation of three configurations of the MS-NES are carried out and the performances of the MS-NES as an energy absorber and as an energy harvester are analyzed and discussed.

4.2 The model

In Fig.4.1 the schematic of the NES is shown. The primary system is the linear oscillator (LO) composed by the mass M, spring K and damper C. The primary system is harmonically forced by the base motion X_e. The NES is composed by the little mass m which is linked to the primary system by means of two flexible strings $\overline{AB}$ and $\overline{BC}$. The strings act as elastic elements and are responsible of the force exchanged between the LO and the NES. The force acting on the mass m as a function of the displacement y can be approximated by the expression:

$$F_{strings} = \frac{T_0}{L} y + \left(\frac{EA}{2L^3} - \frac{T_0}{2L^3} \right) y^3 + \mathcal{O}(y^5) \tag{4.1}$$

Where T_0 is the pretension of the strings, i.e. for $y = 0$, E is the Young's modulus, A the section of the strings. Then the restoring force caused by the strings deflection is composed by a term linearly proportional to the displacement, a term proportional to the cube of the displacement and higher order terms which will be neglected. From eq.(4.1) we can identify a linear stiffness $K_1 = \frac{T_0}{L}$ and cubic stiffness $K_3 = \left(\frac{EA}{2L^3} - \frac{T_0}{2L^3} \right)$. Both terms

are a function of the pretension T_0 which is a parameter we can control in experiments. This is a significant advantage the use of the strings appears to have. Also one should notice that the linear term is a function of the only pretension and ideally if the pretension is zero the restoring force would be a cubic (and higher order terms) function of the displacement.

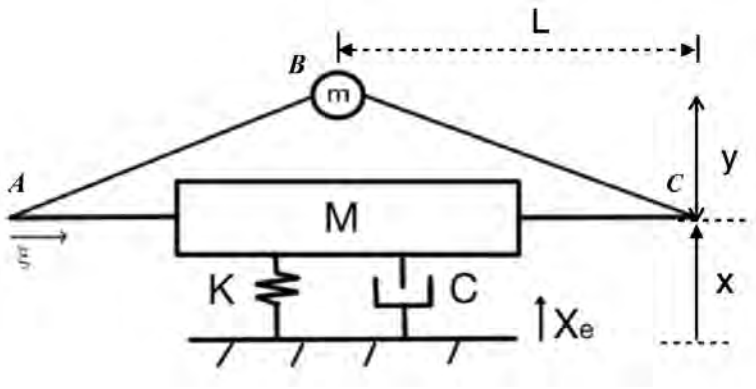

Figure 4.1: Schematic of the Strung-NES. View from the top. $\overline{AB}$ and $\overline{BC}$ are the strings which act as elastic elements.

Defining the absolute displacement of the NES mass as $z := x + y$, the equations of motion of the system can be written as:

$$\begin{gathered} M\ddot{x} + C\dot{x} + Kx + K_1(x-z) + K_3(x-z)^3 + C_1(\dot{x}-\dot{z}) = KX_e + C\dot{X}_e \\ m\ddot{z} + C_1(\dot{z}-\dot{x}) + K_1(z-x) + K_3(z-x)^3 = 0 \end{gathered} \tag{4.2}$$

An important feature an NES should have is the absence of a natural frequency. It would allow the NES to tune itself to the primary system and to be efficient as an absorber over a broad range of frequency. This characteristic could be reached by the absence of the linear stiffness. As previously mentioned the linear stiffness is zero if the pretension is zero. However, we tried to find an alternative solution in order to study the effect of the linear term and to have a better control on the shaping of the force.

4.3 The energy harvesting

The method used for the energy harvesting is electromagnetic: the NES mass is a magnet and it oscillates through an electric coil. As the Faraday's

Law says, a variation in the magnetic flux means electromotive force:

$$\varepsilon = -\frac{d\Phi_B}{dt} \tag{4.3}$$

Where ε is the electromotive force and Φ_B is the magnetic flux. The concept combining the NES and harvester is shown schematically in Fig.4.2: the vibration energy of the primary system flows to the NES and is finally converted into electric energy through the harvester.

The presence of the harvester creates an electromechanical coupling between the mechanical system and the electrical circuit, schematically presented in Fig.4.3. It contains the coil's inductance L and the internal resistance R_i along with a resistive load R_L.

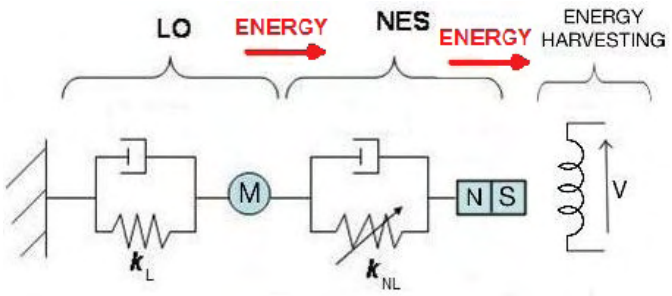

Figure 4.2: Schematic of the energy flux from the Linear Oscillator to the harvester.

The coupled electromechanical system becomes:

$$\begin{gathered} M\ddot{x} + C\dot{x} + Kx + K_1(x-z) + K_3(x-z)^3 + C_1(\dot{x}-\dot{z}) = KX_e + C\dot{X}_e \\ m\ddot{z} + C_1(\dot{z}-\dot{x}) + K_1(z-x) + K_3(z-x)^3 - \gamma I = 0 \\ L\dot{I} + (R_L + R_i)I + \gamma(\dot{z}-\dot{x}) = 0 \end{gathered} \tag{4.4}$$

We can notice that compared to the initial system (4.2), in the second equation of system (4.4) we added the coupling term γI. I is the current flowing into the circuit and γ is a transducer constant that can be derived from Faraday's Law. The third equation is the electrical equation governing the circuit in fig 4.3. Here the constant γ multiplies the relative velocity between the NES magnet and the coil and their product is a voltage.

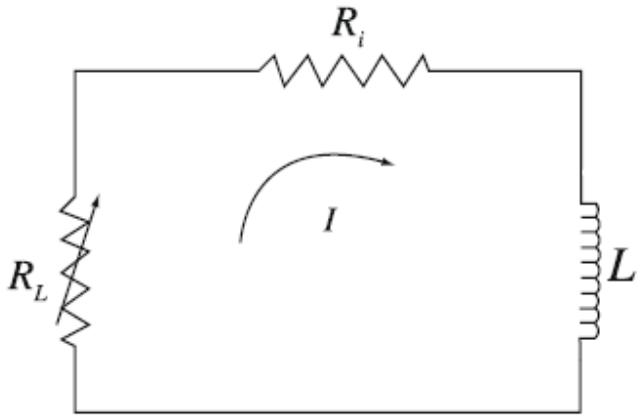

Figure 4.3: Schematic of the coupled electrical circuit.

4.4 The magnetic counterbalance

As NES mass we used a magnet because of the electromagnetic harvesting that will be explained further in the paper. This fact has been exploited as follows for a second purpose. In order to counteract the linear term and have a pure cubic force-displacement relation we put two magnets on each side of the NES magnet. The aim is to obtain a magnetic force that could counterweight the linear term of the elastic force.

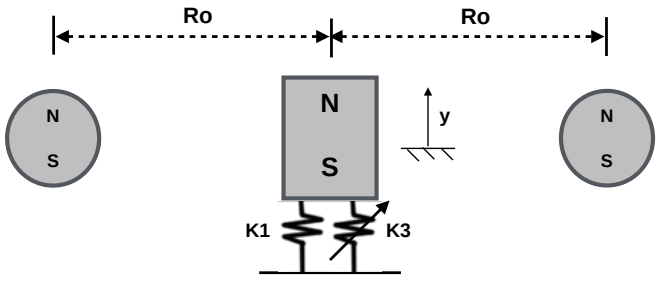

Figure 4.4: Schematic

The magnetic flux density or **B**-field at the location $\mathbf{r}_p$ due to a magnet

located at $\mathbf{r}_s$ is defined by:

$$\mathbf{B} = -\frac{\mu_0}{4\pi}\nabla\frac{\mathbf{m}_s \cdot \mathbf{r}_{p/s}}{|\mathbf{r}_{p/s}|^3} \tag{4.5}$$

Where $\mu_0 = 4\pi \times 10^{-7}$ H/m is the permeability of free space, $\mathbf{r}_{p/s}$ is the position vector to the point of interest $\mathbf{r}_p$ with respect to the source magnet position $\mathbf{r}_s$, $\mathbf{m}_s = \mathbf{M}_s v_s$ is the magnetic moment of the magnet located at $\mathbf{r}_s$, $\mathbf{M}_s$ and v_s are the magnetization and volume of the source magnet. The potential energy of the magnet at $\mathbf{r}_p$ in the field generated by the magnet at $\mathbf{r}_{p/s}$ is:

$$U = -\mathbf{m}_p \cdot \mathbf{B} \tag{4.6}$$

Then the interaction force between the two magnets can be obtained by taking the gradient of equation (4.6).

By applying equations (4.5) and (4.6) to the model shown in Fig.4.4 we obtain the following expression for the magnetic potential energy [MO10]:

$$U = -\frac{\mu_0 M_c v_c}{2\pi}\frac{M_o v_o N}{2}\left(\frac{y^2}{(y^2+R_o^2)^{5/2}} - \frac{1}{(y^2+R_o^2)^{3/2}}\right) \tag{4.7}$$

Then the restoring force is the derivative of (4.7) with respect of y:

$$F_m = -\frac{\mu_0 M_c v_c}{2\pi}\frac{M_o v_o N}{2}\left(\frac{5y}{(y^2+R_o^2)^{5/2}} - \frac{5y^3}{(y^2+R_o^2)^{7/2}}\right) \tag{4.8}$$

The expression (4.8) has a trend as shown in Fig.4.5. In the vicinity of $y = 0$ and as long as the displacement remains small compared to the distance Ro ($y/R_0 < 0.1$), the magnetic force shows a linear behavior.

Thus by taking the derivative of (4.8) in $y = 0$ we obtain a linear approximation of the magnetic force that seems to be accurate enough for $y/R_o < 0.1$:

$$a := \left.\frac{dF}{dy}\right|_{y=0} = \frac{5C}{R_o^5} \tag{4.9}$$

$$F_m \approx ay = \frac{5C}{R_o^5}y \qquad y/R_o << 1 \tag{4.10}$$

Where C is a constant: $C = -\frac{\mu_0 M_c v_c M_o v_o N}{4\pi}$ depending on the magnetic parameters.

We want the magnetic force to counterbalance the linear component of the elastic restoring force $F_{elastic} = k_1 y + k_3 y^3$. Then by equaling Eq.(4.10)

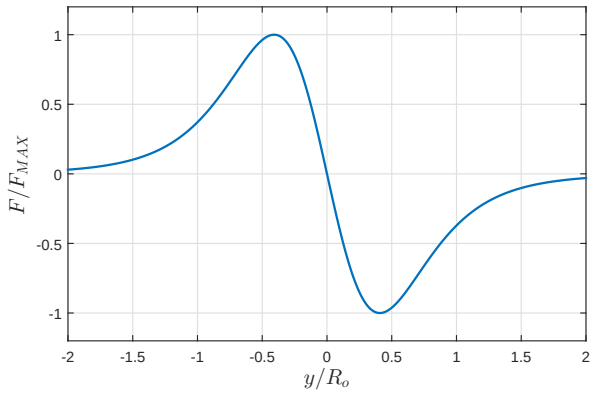

Figure 4.5: Magnetic force as a function of the normalized displacement y/R_o

to the linear component of the elastic force we can derive an expression for the distance R_o so that the linear component could be canceled out by the magnetic force.

$$R_o = \sqrt[5]{\frac{5|C|}{k_1}} \tag{4.11}$$

Fig.4.6 shows all the forces involved in a numeric example where the distance R_o has been calculated by (4.11). We can see that the linear component of the elastic force is actually counterweighted by the magnetic force and the total resultant force is purely cubic.

Finally the governing equations for the coupled electromechanical system with the magnetic counterbalance become:

$$\begin{gathered} M\ddot{x} + C\dot{x} + Kx + K_1(x-z) + K_3(x-z)^3 + C_1(\dot{x}-\dot{z}) = KX_e + C\dot{X}_e \\ m\ddot{z} + C_1(\dot{z}-\dot{x}) + K_1(z-x) + K_3(z-x)^3 + F_m(z-x) - \gamma I = 0 \\ L\dot{I} + (R_L + R_i)I + \gamma(\dot{z}-\dot{x}) = 0 \end{gathered} \tag{4.12}$$

Where the magnetic force $F_m = F_m(z-x)$ has been added to the NES equation.

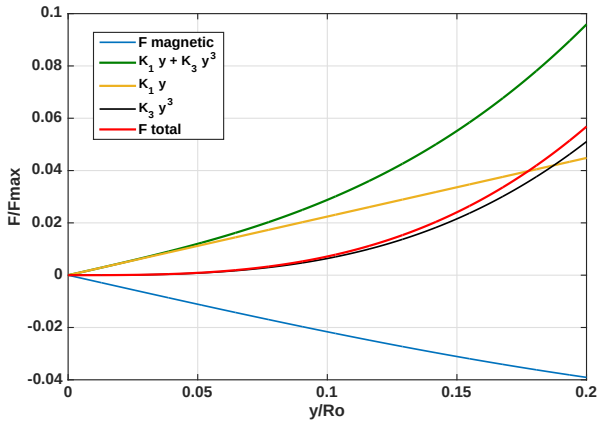

Figure 4.6: All the forces involved in the balancing: it can be seen as the magnetic force cancels out the linear elastic component and the total final force is actually cubic.

4.4.1 The bi-stable configuration

Taking a look at Eq.(4.10) it can be easily observed that the derivative of the linearized magnetic force $a = \frac{dF}{dy}\Big|_{y=0}$ increases as the distance R_o decreases. We showed that the exact distance for a to equal k_1 and then to cancel out the elastic linear term can be calculated by Eq.(4.11). Another way to describe the interaction between the elastic and the magnetic forces acting on the NES mass is by using their potential energies.

As both the elastic and the magnetic forces are conservative, they can be obtained by taking the derivative with respect to the displacement y of the correspondent potential function $U = U(y)$.

Expressing the elastic potential energy as:

$$U_{el} = U_{k_1} + U_{k_3} = \frac{1}{2}k_1 y^2 + \frac{1}{4}k_3 y^4 \tag{4.13}$$

and reminding the magnetic potential energy as expressed in Eq.(4.7):

$$U_m = -\frac{\mu_0 M_c v_c}{2\pi}\frac{M_o v_o N}{2}\left(\frac{y^2}{(y^2+R_o^2)^{5/2}} - \frac{1}{(y^2+R_o^2)^{3/2}}\right) \tag{4.14}$$

we can write the total potential energy $U_{tot}(y) = U_{el}(y) + U_m(y)$. By studying the evolution of U_{tot} as R_o varies the stability of each configuration can be analyzed.

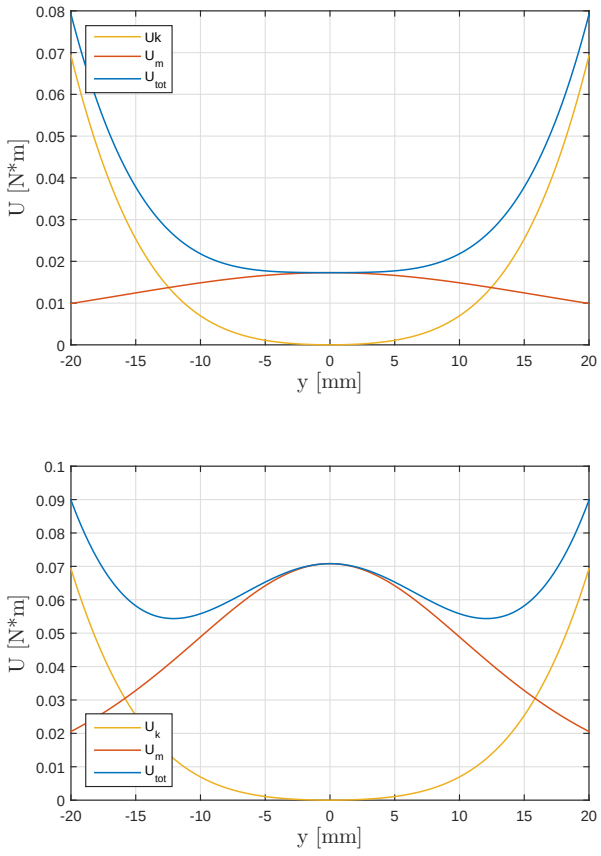

Figure 4.7: Potential energies in the case of the cubic configuration (upper) and the bistable configuration (lower).

When there are no outer magnets ($R_o = \text{inf}$) the total potential energy is composed of only the elastic energy $U_{tot} = U_{el} = U_{k1} + U_{k2}$. The point $y = 0$ is the only equilibrium point and it is stable as $\frac{dU}{dy}\Big|_{y=0} > 0$. If the outer magnets are placed at $R_o = \overline{R_o}$ so that the magnetic force cancels out the linear part of the elastic force, the equilibrium point $y = 0$ loses its stability and becomes neutrally stable as $\frac{dU}{dy}\Big|_{y=0} = 0$. This configuration, called *cubic*, is shown in Fig.4.7 (left).

When the magnets are placed at a distance $R_o < \overline{R_o}$ the point $y = 0$ becomes unstable and two new stable points appear. The potential energies

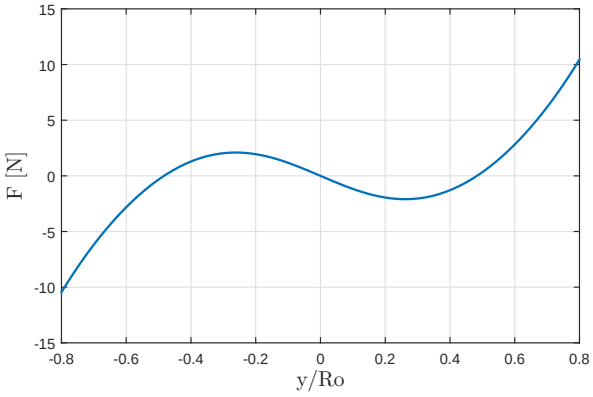

Figure 4.8: Nonlinear force between the primary system and the NES in the case of bistable configuration.

of this *bistable* configuration are illustrated in Fig.4.7 (right). Fig.4.8 shows the resultant nonlinear force between the primary system and the NES.

4.5 Frequency Power Function

In order to estimate the efficacy of the MS-NES as an absorber and as a harvester, we define the average electrical power delivered and the average viscous power dissipated:

$$\overline{P}_{el}(t_0) = \frac{1}{t_0}\int_0^{t_0} P_{el}(t) \quad \overline{P}_{vis}(t_0) = \frac{1}{t_0}\int_0^{t_0} P_{vis}(t) \tag{4.15}$$

Where $P_{el}(t) = R_L I^2(t)$ is the the electrical power delivered to the resistive load R_L and $P_{vis}(t) = C_1(\dot{y} - \dot{x})^2$ is the power dissipated by the viscous damping C_1 between the primary system and the NES.

These new quantities have a particular interest as they can be used to describe the efficacy and performance of the MS-NES when strongly nonlinear phenomena arise in the response. For example, when in a forced regime the response is not steady but periodically or even chaotic, these measurements provide an accurate estimation of the energy dissipated and converted as they reach a steady value as $t \to \infty$:

$$\overline{P}_{el_\infty} = \overline{P}_{el}(t \to \infty) \quad \overline{P}_{vis_\infty} = \overline{P}_{vis}(t \to \infty) \tag{4.16}$$

In practice a steady value is reached even after a few cycles. At each frequency and amplitude of external excitation, it is then possible to calculate a steady value $\overline{P}_{el_\infty}$ and $\overline{P}_{vis_\infty}$.

We present in Fig.4.9 the Frequency-Power plots for the no-magnets configuration and the cubic configuration of the MS-NES. The peak of energy dissipated and delivered is significantly higher in the case of cubic configuration: $60\,mW$ and $40\,mW$ respectively for the no-magnets whereas $95\,W$ and $65\,W$ for the cubic.

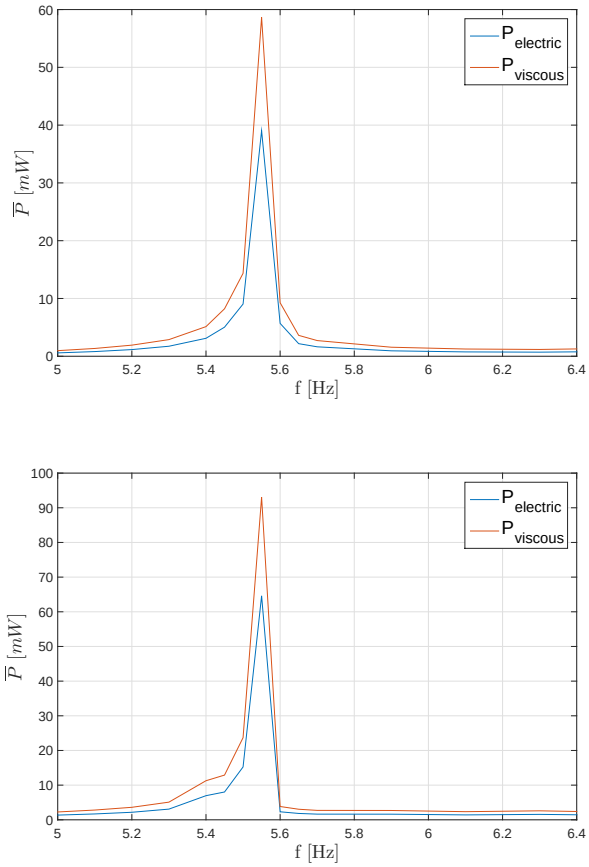

Figure 4.9: Numerical Frequency-Power Function for the no-magnet (upper) and the cubic (lower) configurations. It can be seen that the viscous power dissipated and the electrical power delivered are significantly higher in the case of cubic MS-NES.

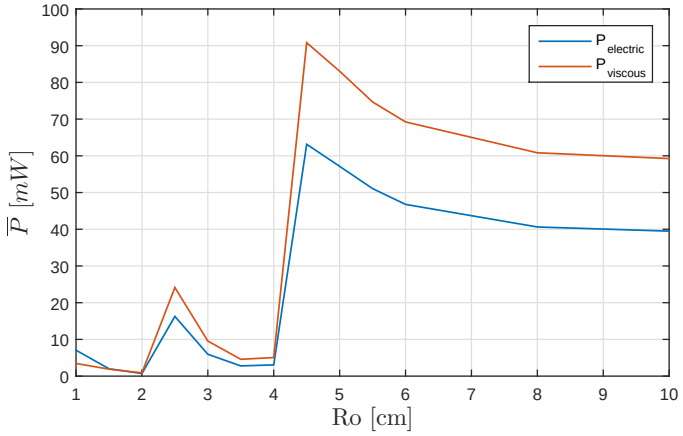

Figure 4.10: Average Power Delivered and Average Power Dissipated as a function of the outer magnets distance *Ro*. External excitation: $\ddot{x}_e = 0.6\,m/s^2$ and $f = 5.57\,Hz$.

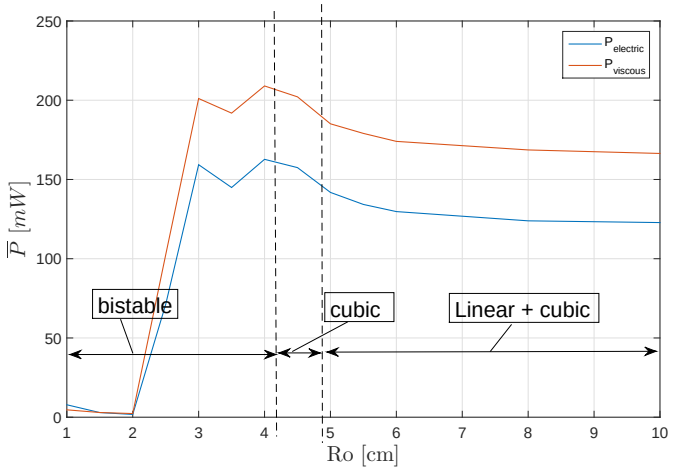

Figure 4.11: Average Power Delivered and Average Power Dissipated as a function of the outer magnets distance *Ro*. External excitation: $\ddot{x}_e = 1.8\,m/s^2$ and $f = 5.57\,Hz$.

Since we have identified the peak frequency at $f = 5.57\,Hz$, it is possible to evaluate the powers (dissipated and delivered) by keeping constant the

frequency and varying the magnets distance. Fig.4.10 shows $\overline{P}_{el_\infty}$ and $\overline{P}_{vis_\infty}$ for a level of external excitation of $\ddot{x}_e = 0.6\,m/s^2$. It can be seen that the performances get better as the distance Ro deceases down to a distance $Ro \approx 4.5\,cm$. This distance correspond to a cubic configuration. After that, the powers drastically drop down. This behavior can be explained by the fact that, since the configuration becomes bistable, the NES mass gets stuck in a potential well and does not have enough energy to escape.

If the level of external excitation is higher ($\ddot{x}_e = 1.8\,m/s^2$), the performances keep getting better even for a smaller distance Ro. Then the bistable configuration seems to be the most efficient. This scenario is displayed in Fig.4.11.

4.6 Experimental investigations

In this section the prototype is presented and the identification of the mechanical and the electrical parameters of the system is experimentally carried out. Moreover the efficacy of the magnetic counterbalance is verified by measuring the static force between the primary system and the NES.

In Fig.4.12 the prototype is shown. All the blue and the orange parts have been 3D printed at Duke University. The lower part is a cart sliding on an airtrack that minimizes the friction of the primary system. The two sides are connected by two springs respectively to the ground and to the shaker. The NES is a magnet which is placed into a hollow tube and onto a non-magnetic low-friction slider upon the primary mass. The NES is connected to the primary mass by means of two strings which work transversely when the NES oscillates. On the sides of the NES the two outer magnets can be noticed, it is important to highlight that their distance to the NES is adjustable in order to reach the suitable force shape. Finally the coil through which the NES mass oscillates is placed on the primary mass.

4.6.1 Identification of the mechanical and the electrical systems

The modal parameters of the primary system were obtained from free oscillation measurements. We know that the solution for an underdamped system subject to an initial displacement $X(t=0) = X_0$ is:

$$x(t) = X_0 e^{(-\xi\omega_n t)} \cos(\sqrt{1-\xi^2}\omega_n t) \tag{4.17}$$

Where ω_n is the natural frequency and ξ the damping ratio. Then by

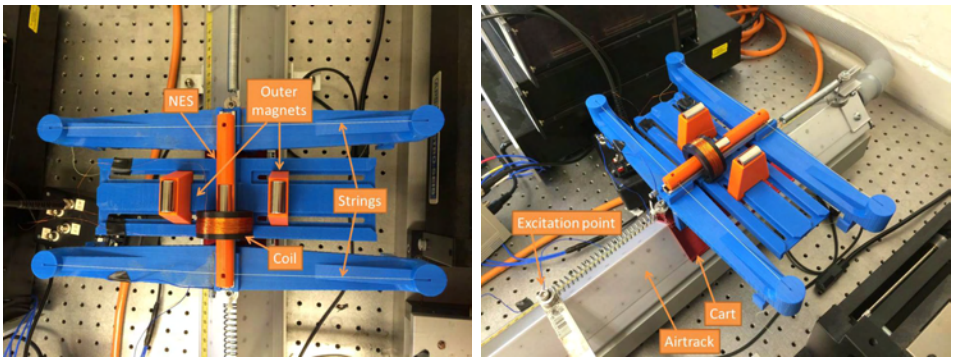

Figure 4.12: The prototype of the Magnetic-Strung NES.

calculating the envelope and the spectrum (Fig.4.13) of the measured free oscillations we are able to estimate the modal parameters of the system.

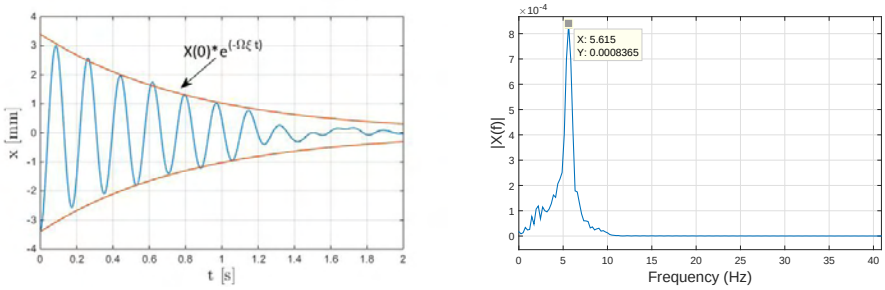

Figure 4.13: Identification of the modal parameters of the primary system: envelope (left) and spectra (right) of free oscillations are used to estimate the damping ratio and the natural frequency respectively.

In Tab.4.1 the modal parameters of the linear primary system are listed along with the mass ratio between the NES and primary system.

$f_n[Hz]$	$K[N/m]$	ξ	$\epsilon = m/M$
5.6	1223	0.036	0.04

Table 4.1: Modal parameters of primary system.

The electrical parameters have been experimentally measured and are listed in Tab.4.2.

$L[H]$	$R_L[\Omega]$	$R_i[\Omega]$	$\gamma[Vs/m]$
$100 \times 10^{-}3$	100	3500	-3.2572

Table 4.2: Electrical parameters.

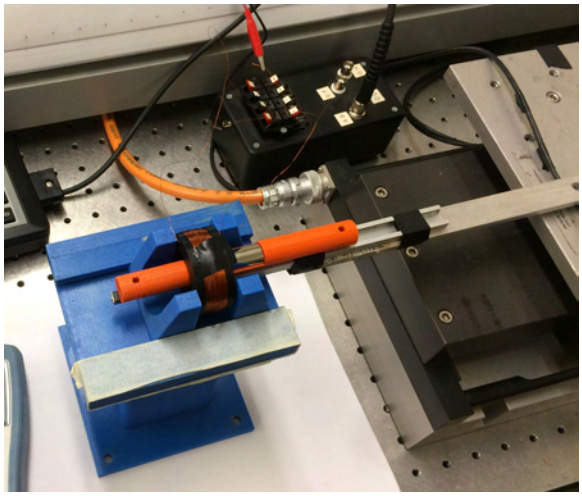

Figure 4.14: Experimental apparatus used to evaluate the transducer constant γ coupling the mechanical and the electrical system.

Where L is the coil's inductance, R_i is the coil's internal resistance, R_L is the resistive load and γ is a transducer constant that couples the mechanical and the electrical system. An extensive study on the nonlinear electromagnetic coupling between a coil and an oscillating magnet is presented in [SM10].

In this work the term γ was experimentally evaluated as follows. Taking the electrical equation of Sys.(4.4) governing the circuit shown in Fig.4.3 it can be seen that, for a steady condition, if the relative velocity $\dot{y} = \dot{z} - \dot{x}$ is known; then by measuring the current I, the only unknown is the constant γ which therefore can be evaluated.

$$L\dot{I} + (R_L + R_i)I + \gamma(\dot{z} - \dot{x}) = 0 \tag{4.18}$$

The experimental apparatus shown in Fig.4.14 was used for the purpose. The magnet was placed on the shaker and it oscillated through the coil which was at rest ($\dot{x} = 0$), i.e. $\dot{y} = \dot{z}$. As the harmonic motion of the magnet was known, by measuring the voltage across the coil the constant γ was finally

estimated as $\gamma = -3.2572\,Vs/m$.

4.6.2 Experimental verification of the cubic stiffness

The efficacy of the outer magnets was subsequently tested experimentally. Static tests were performed in order to measure the elastic force provided by the strings and to obtain a force-displacement graph.

The NES magnet and the two outer magnets were all the same and their magnetization and dimensions are listed in Tab.4.3.

$M[A/m]$	$d_o[mm]$	$d_i[mm]$	$l[mm]$
1.05×10^6	12.7	7.0	25.4

Table 4.3: Magnetization and dimensions of the NES and the outer magnets.

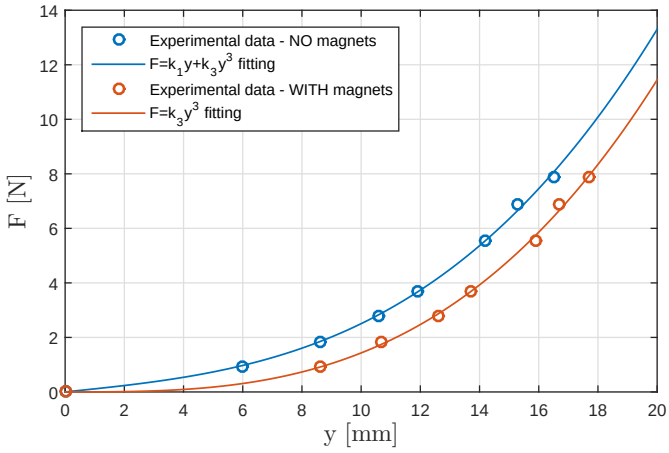

Figure 4.15: Experimental force-displacement relation without (blue) and with (red) outer magnets. The experimental points have been fitted by means of polynomial expression:

First the configuration with no outer magnets was tested. The force-displacement measurements are shown in Fig.4.15 as blue dots. These points have been polynomially interpolated using a linear and a cubic term: $F = k_1 y + k_3 y^3$, which allows us to estimate the linear and the cubic stiffness (4.4)

$k_1[N/m]$	$k_3[N/m^3]$
69.4	1.38×10^6

Table 4.4: Linear and cubic stiffness without outer magnets.

Knowing the linear stiffness k_1, the distance R_o was calculated using Eq.(4.19) in order to cancel out the linear term and to obtain an essentially cubic relation.

$$R_o = \sqrt[5]{\frac{5|C|}{k_1}} = 4\,cm \tag{4.19}$$

The measured points when the magnets were put at a distance $R_o = 4cm$ are shown in Fig.4.15 as red dots. They have been polynomially interpolated using only a cubic term: $F = k_3' y^3$, where $k_3' = 1.43 \times 10^6\, N/m^3$.

Thus, as theoretically predicted, the presence of the outer magnets allows us to cancel out the linear term of the elastic force and to obtain a purely cubic relation; this is a crucial aspect to fully take advantage of the characteristics of a nonlinear absorber.

4.7 Experimental results

The system was harmonically forced by the base motion at several amplitudes and frequencies. The aim was to observe the types of response the system could exhibit and to study its performance in terms of energy absorption and harvesting. The primary mass and the moving base were equipped with accelerometers. The NES motion was monitored by using the signal issued by the coil, indeed that signal can be considered as proportional to the magnet velocity.

The results illustrated are issued from the same case of external excitation ($0.6m/s^2$ at $6.2Hz$) and for three different configurations of the MS-NES. In the first configuration the outer magnets are not used so the relation between the absorber and the primary system is not completely nonlinear but presents the linear term. In the second configuration, called *cubic*, the outer magnets are placed at a distance which allows the magnetic force to perfectly cancel out the linear term and then the resulting force to be purely cubic. The third configuration is the so-called Bi-stable and the resulting force has a shape as illustrated in the previous section.

For each configuration a kinematic study is firstly conducted. The phase diagram as well as the Poincaré sections of the system's responses are obtained in order to evaluate their periodicity. Subsequently the capability of the MS-NES as a vibration absorber and as an energy harvester is analyzed. According to theory, this specific excitation frequency is where the Strongly Modulated Responses are expected to appear. In fact, results have shown that depending on the distance of the magnets (i.e. on the shape of the force between LO and MS-NES) the system can exhibit different types of response going from periodic to chaotic.

4.7.1 No outer magnets

In this configuration the outer magnets are not used, meaning that in Sys.(4.4) the magnetic force F_m is zero. The expression for the restoring elastic force between the MS-NES and the primary system is: $F = k_1(z-x) + k_3(z-x)^3$.

Concerning the kinematic study, in Fig.4.16 and Fig.4.17 the displacement and the velocity of the primary mass and the NES mass respectively are shown. The envelope has been highlighted. The same figures show the phase diagrams ($x - \dot{x}$ and $y - \dot{y}$) of the responses. The red dots on the phase diagrams represent the Poincaré map of the envelope.

We can observe that the solution the system reaches is steady and the response amplitude constant. The trajectories in the phase diagrams are ellipses and all the points in the Poincaré map are gathered in the same area: we can state that the global behavior is totally deterministic.

After studying the kinematics of this configuration we go further by analyzing the energetic aspects of the system. We are interested in studying the energy flow from the primary system to the NES and in evaluating the portion of energy which is dissipated by viscous friction and the amount which is converted into electrical energy.

In Fig.4.18 (upper part) the instantaneous kinetic energy during the recorded time interval of the primary system and of the NES is shown. The lower part shows the instantaneous electrical energy delivered to the resistive load $P_{el} = I^2 R_L$. As concluded after the kinematic analysis the system exhibits a steady solution: an equilibrium is reached between the vibrating energy kept into the primary system and the portion of energy transferred to the NES.

We can have a better understanding of how the energy is distributed into the system by calculating the ratio between the energy located into the NES and the total energy present in the system:

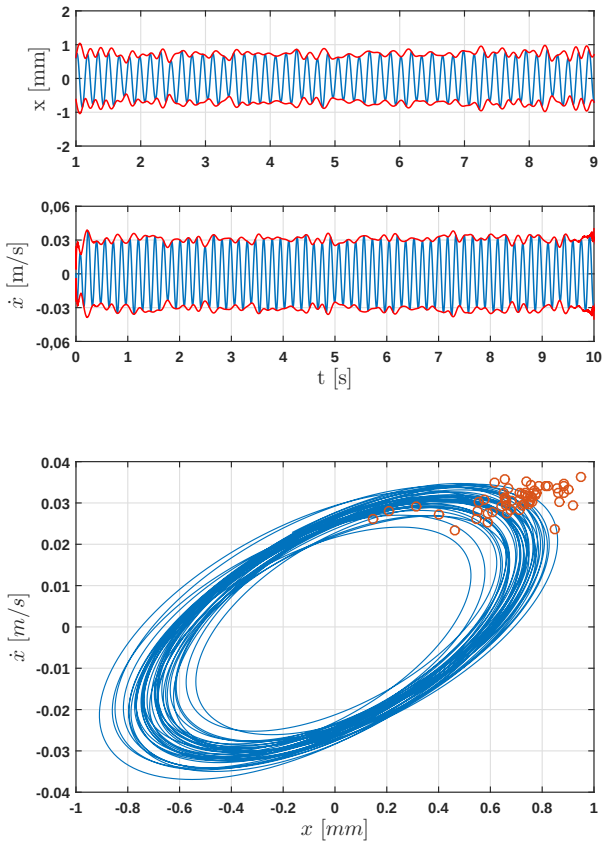

Figure 4.16: Primary system's displacement x and velocity $\dot{x}$ in the *no magnets* configuration (left) and its phase diagram (right). The envelope of the response is highlighted in red and its Poincaré Map represented by red dots in the $x - \dot{x}$ space.

$$\frac{E_{NES}}{E_{TOT}} = \frac{T_{NES} + U_{NES}}{T_{LO} + U_{LO} + T_{NES} + U_{NES}} \tag{4.20}$$

The energy ratio over the time is illustrated in Fig.4.19: about half the total energy of the system is located into the NES.

The energy transferred to the NES is then partially dissipated by the viscous damping and partially converted into electrical energy.

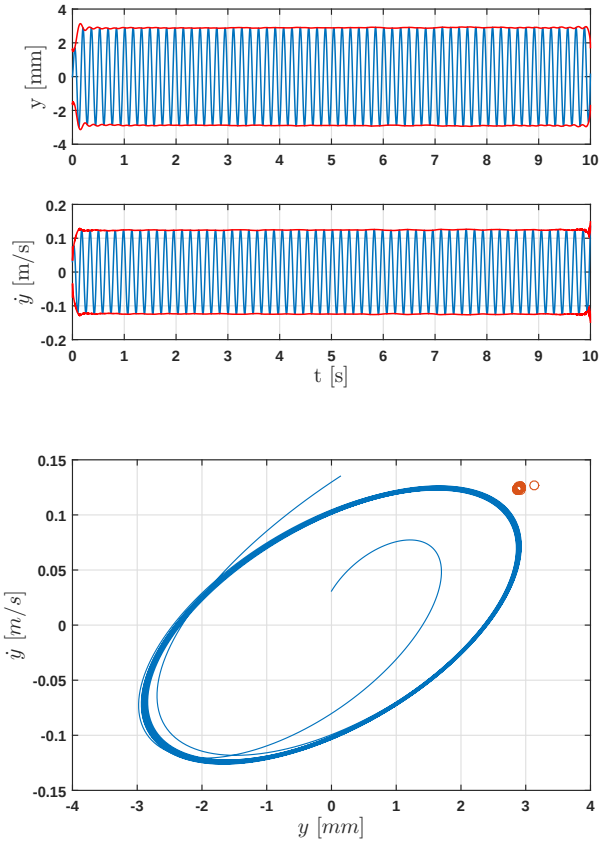

Figure 4.17: NES' displacement y and velocity $\dot{y}$ in the configuration without outer magnets (left) and its phase diagram (right). The envelope of the response is highlighted in red and its Poincaré Map represented by red dots in the $y - \dot{y}$ space. The global system behavior is totally deterministic.

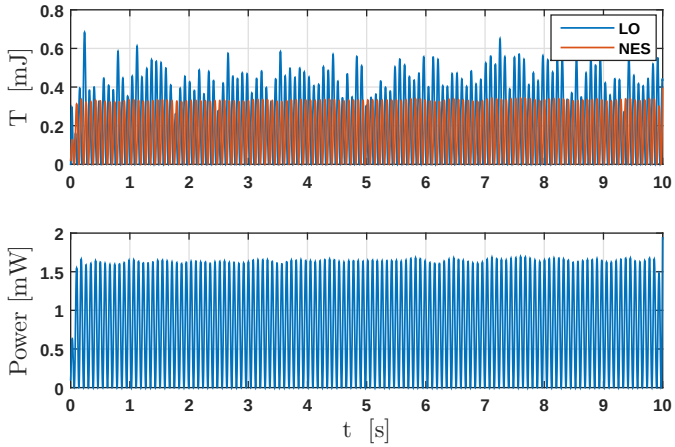

Figure 4.18: No magnets configuration: kinetic energy of the primary system (LO) and of the NES and instantaneous electrical power delivered to the resistive load.

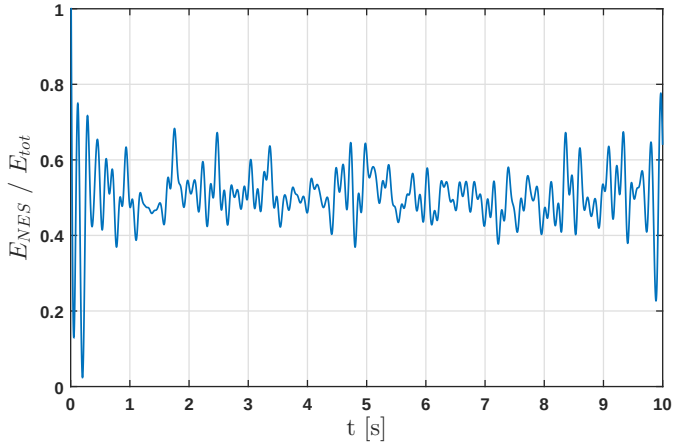

Figure 4.19: NES-LO Energy ratio defined as: $\frac{E_{NES}}{E_{TOT}} = \frac{T_{NES}+U_{NES}}{T_{LO}+U_{LO}+T_{NES}+U_{NES}}$.

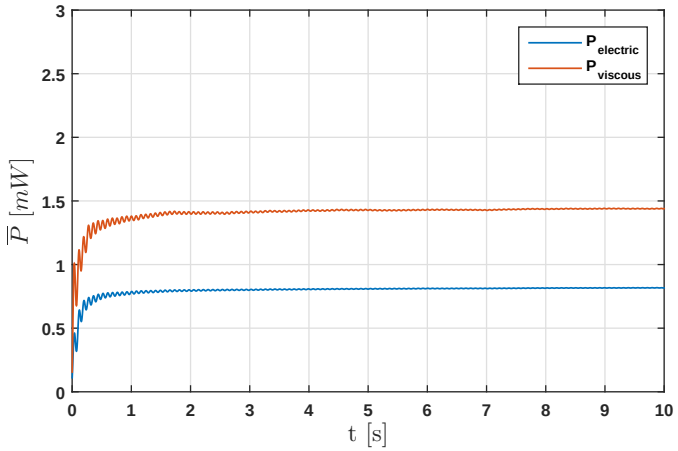

Figure 4.20: Average electrical power delivered and the average viscous power dissipated in the configuration without outer magnets.

4.7.2 Cubic

We now illustrate the results obtained from the tests performed on the *cubic* configuration. As explained in Sec.4.4, it is possible to calculate the distance of the outer magnets R_o in order to obtain a purely cubic relation between the primary system and the NES. For a linear elastic term $k_1 = 69.4\,N/m$ the distance was estimated to be $R_o = 4\,cm$.

The external forcing amplitude and frequency were the same as in the previous section: $0.6m/s^2$ at $6.2Hz$.

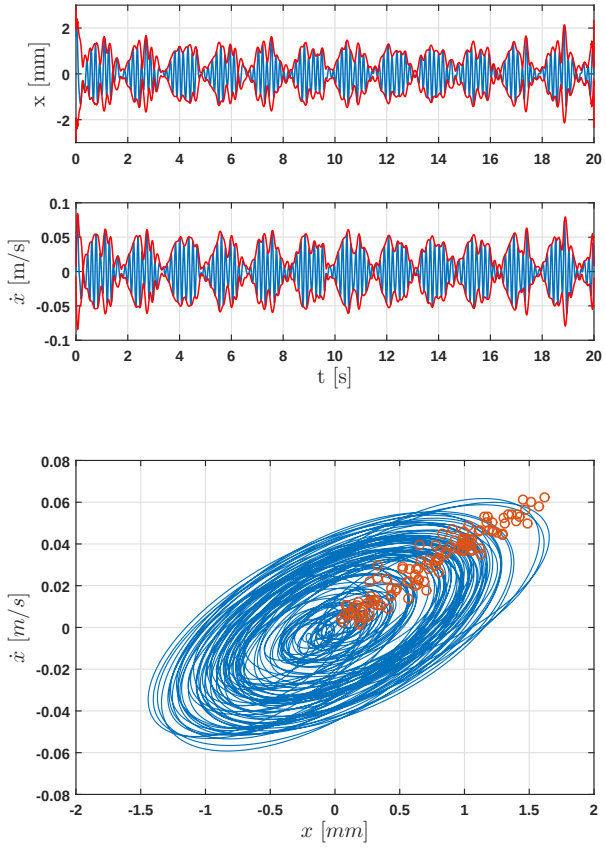

Figure 4.21: Primary system's displacement x and velocity $\dot{x}$ in the *cubic* configuration (left) and its phase diagram (right). The envelope of the response is highlighted in red and its Poincaré Map represented by red dots in the $x - \dot{x}$ space.

We will first focus on the kinematics of the response and lately discuss the energetic aspects. On the left of Fig.4.21 and 4.22 the displacement and the velocity of the primary mass and of the NES mass are shown and their envelope has been highlighted in red. On the right of the same figures the phase diagrams $x - \dot{x}$ and $y - \dot{y}$ are shown as well as the Poincaré map of the envelope (red dots).

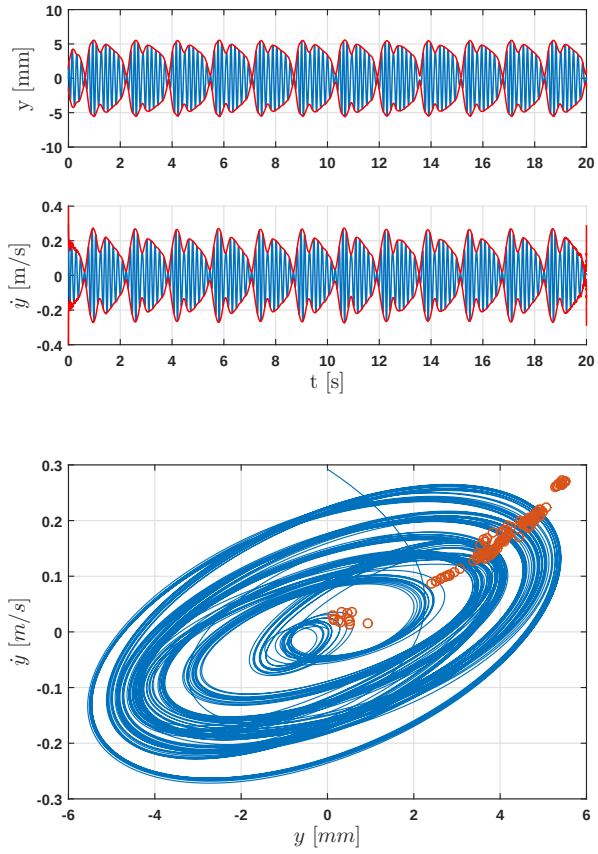

Figure 4.22: NES' displacement y and velocity $\dot{y}$ in the *cubic* configuration (left) and its phase diagram (right). The envelope of the response is highlighted in red and its Poincaré Map represented by red dots in the $y - \dot{y}$ space.

We can immediately see that the response of the system has become modulated: not steady anymore but periodic. This kind of response is

known in literature as Strongly Modulated Response (SMR) and is typically observed among nonlinear absorbers [VGMM01b].

The phase diagrams and the Poincaré map allow us to attest that, although it appears to have a complex pattern, the response is not chaotic. This can easily be deduced from the NES response in Fig.4.22. The primary mass graphs in Fig.4.21 seem to be more rough but this may also be caused by measurement noise: it is worth reminding that the primary mass acceleration was measured by an accelerometer placed on the structure whereas the velocity of the NES mass was measured through the signal coming from the coil. The NES non-intrusive method delivered a much cleaner signal than the accelerometer did.

Fig.4.23 shows the kinetic energy of the primary system and the NES (upper half) and the electrical power deliver to the resistence (lower half). It can be seen that the cycles the system goes through are periodic and repetitive. In Fig.4.24 (left) a zoom of Fig.4.23 illustrates the process of energy transfer from the primary system (LO) to the NES: the kinetic energy the primary system accumulates is transferred to the NES and subsequently partially dissipated through the viscous damping and partially converted into electrical energy.

Fig.4.24 (right) describes the energy transfer mechanism by showing the energy ratio E_{NES}/E_{TOT} as defined by Eq.(4.20): it can be seen that the total energy is cyclically entirely located into the NES.

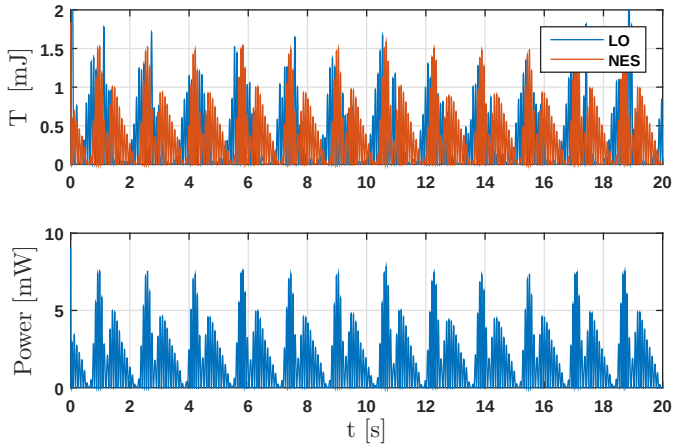

Figure 4.23: *Cubic* configuration: kinetic energy of the primary system (LO) and of the NES and instantaneous electrical power delivered to the resistive load.

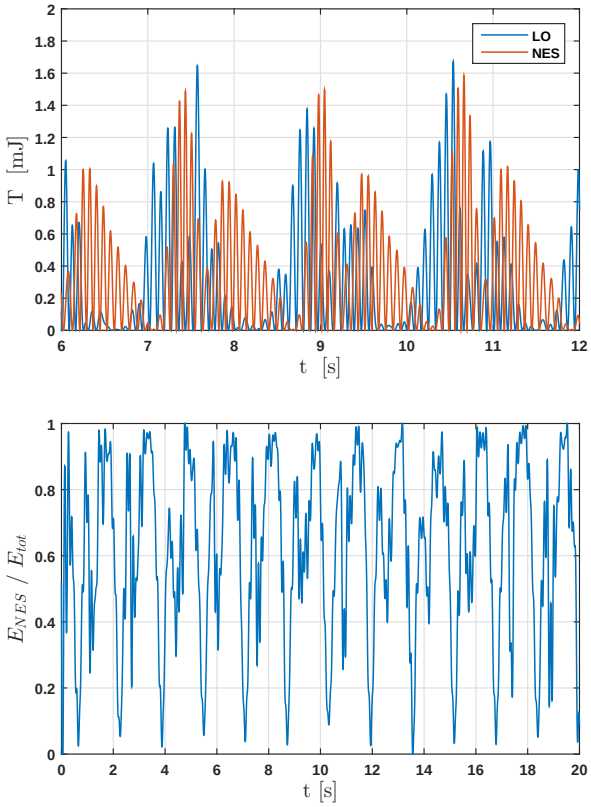

Figure 4.24: Kinetic energy transfer (left) between the primary system (blue) and the NES (red) during the strongly modulated response of the *cubic* configuration and NES-LO energy ratio (right) defined as: $\frac{E_{NES}}{E_{TOT}} = \frac{T_{NES}+U_{NES}}{T_{LO}+U_{LO}+T_{NES}+U_{NES}}$.

Comparing the electrical power delivered in the two configurations without magnets (Fig.4.18) and cubic (Fig.4.23), we can see that in the latter configuration the peaks of power reached are considerably higher than the value held constant by the first configuration ($9\,mW$ instead of $1.6\,mW$).

The average power delivered and the average power dissipated as defined by Eq.(4.15) are displayed in Fig.4.25: the asymptotic values $\overline{P}_{el_\infty}$ and $\overline{P}_{vis_\infty}$ are higher than those obtained by the previous configuration: $1.6\,mW$ and $2.1\,mW$ instead of $0.7\,mW$ and $1.4\,mW$

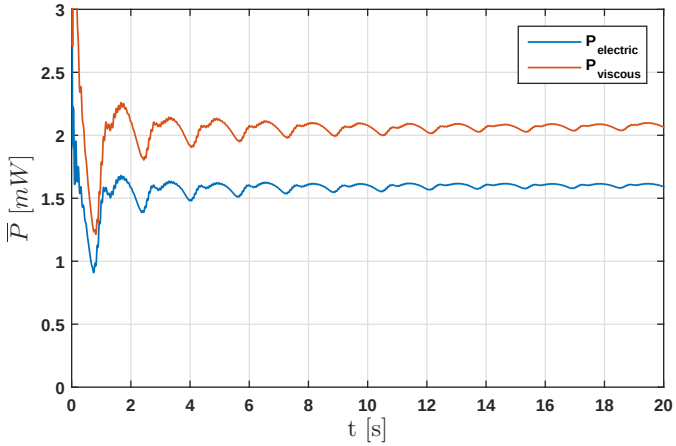

Figure 4.25: Average electrical power delivered and the average viscous power dissipated in the *cubic* configuration.

4.7.3 Bi-stable

The third configuration tested is the *bi-stable* configuration. As explained in Sec.4.4.1 it is obtained by placing the outer magnets at a distance R_o smaller than that canceling out the linear elastic term. The force-displacement relation has then a shape as shown in Fig.4.8 where three equilibria exist: one unstable ($y = 0$) and two stable ($y = \pm d$).

Examining Fig.4.26 and 4.27 it can be seen that the response is still strongly modulated but this time the cycles appears to be more chaotic as none specific periodicity can be identified.

The lack of periodicity in the system's response can also be observed by looking at the kinetic energy transfer and the electrical power delivered shown in Fig.4.28. Each cycle seems to have its own shape, different than the other ones'. As a general observation, the peaks of kinetic energy reached in this configuration are higher than those attained in the cubic one.

The average power dissipated and the average power delivered are shown in Fig.4.29. If compared to the cubic configuration, we can notice a slight improvement in the electrical power whereas the viscous power is essentially the same as previously observed.

Thus, the bi-stable configuration generates a chaotic kinematic behavior of the NES which may potentially be favorable in terms of energy absorption and energy harvesting. The response is similar to what we observed for the Vibro-Impact in the case of Chaotic Strongly Modulated Response (CSMR).

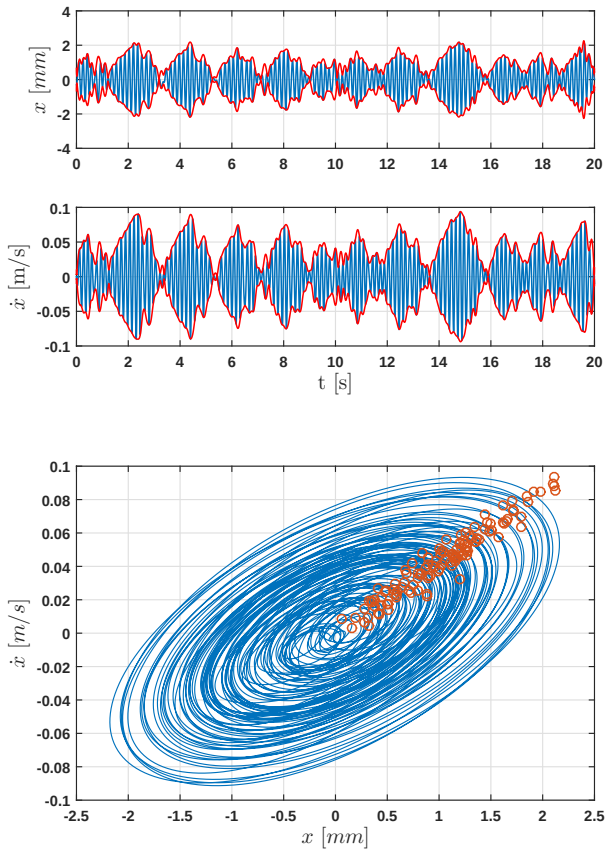

Figure 4.26: Primary system displacement x and velocity $\dot{x}$ in the *bi-stable* configuration (left) and its phase diagram (right). The envelope of the response is highlighted in red and its Poincaré Map represented by red dots in the $x - \dot{x}$ space.

Whereas for the VI-NES the chaos was introduced by the non-smooth nature of the system, for the MS-NES it is the bistability that seems to lead the system to a chaotic regime. Although the experimental results here presented do not show a significant improvement compared to those obtained with the cubic configuration, it may be worth carrying out a more extensive study on this configuration which would include an optimization process.

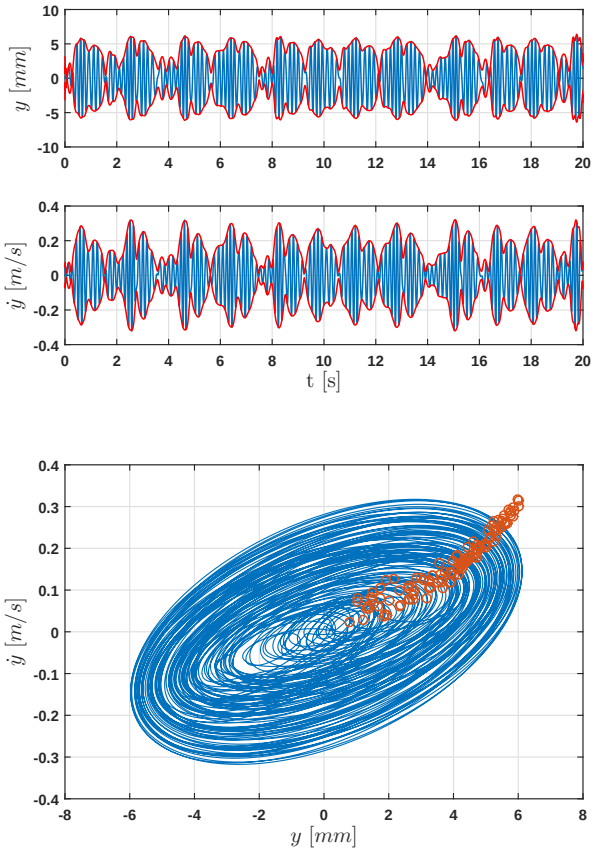

Figure 4.27: NES displacement y and velocity $\dot{y}$ in the *bi-stable* configuration (left) and its phase diagram (right). The envelope of the response is highlighted in red and its Poincaré Map represented by red dots in the $y - \dot{y}$ space.

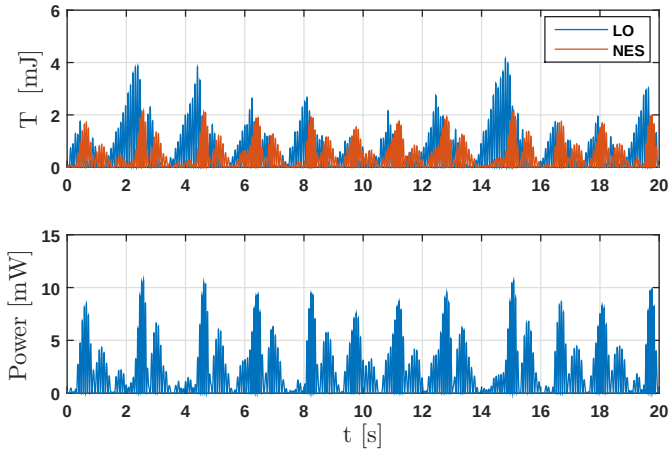

Figure 4.28: *Bi-stable* configuration: kinetic energy of the primary system (LO) and of the NES and instantaneous electrical power delivered to the resistive load.

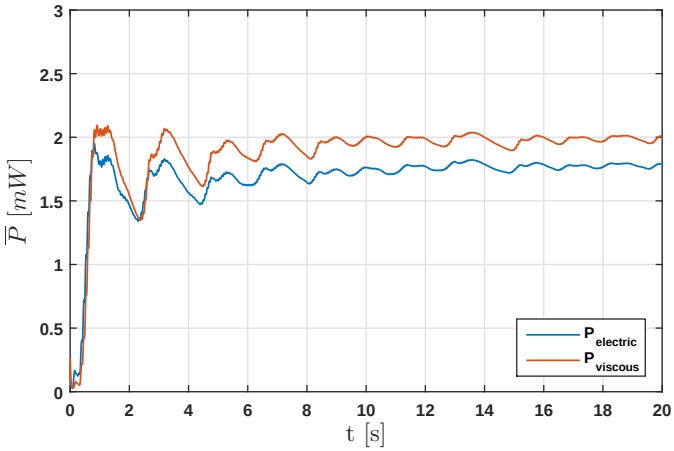

Figure 4.29: Average electrical power delivered and the average viscous power dissipated in the *bi-stable* configuration.

4.8 Bifurcation diagrams

The experimental observations showed that, for an identical external forcing, the MS-NES may exhibit several types of response depending on the distance of the outer magnets R_o. More specifically, we observed that the response goes from appearing completely steady and deterministic when the magnets are not used to being nondeterministic in the case of the bi-stable configuration.

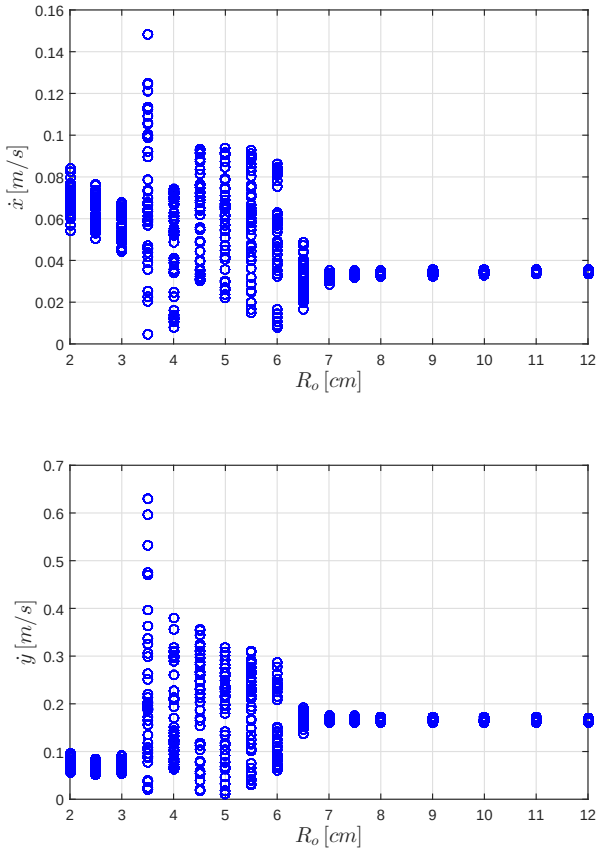

Figure 4.30: Sampled envelope's amplitude of the primary system velocity $\dot{x}$ (left) and the NES velocity $\dot{y}$ (right) are plotted as function of the distance R_o. Forcing: $0.6m/s^2$ - $6.2Hz$.

We present in this section the numerical results illustrating the transition

towards a chaotic behavior when the distance R_o gradually decreases. The simulations were performed for an amplitude and a frequency of the external forcing of $0.6m/s$ and $6.2Hz$.

In Fig.4.30 the sampled envelope's amplitude of the primary system velocity $\dot{x}$ (left) and the NES velocity $\dot{y}$ (right) are plotted as functions of the distance R_o. These plots represent two bifurcation diagrams for the system as R_o is the varying parameter. It means that where several points exist for the same distance R_o the envelope amplitude is not constant but varies during the time. We can observe that for a distance $R_o > 7cm$ the response is steady: i.e. the envelope has a constant amplitude. Between 6 and 7 cm there is the first bifurcation which brings to a periodic regime ($6cm$). When R_o decreases further the response is more and more nondeterministic until it appears to be steady again for $R_o < 3cm$. This is caused by the fact that the two stable points in the bi-stable configuration gain stability as R_o gets smaller: the system ends up oscillating steadily around one of these two points.

4.9 Conclusions

In this chapter the study of a new concept of nonlinear absorber has been introduced and its experimental realization presented. The force between the primary system and the NES is created by the combination of the elastic force delivered by the transverse motion of two strings and an additional magnetic force. The energy absorbed by the NES is converted into electrical energy by means of an electromagnetic transducer.

The results have shown that the presence of the magnetic force allows the NES to reach a purely cubic force-displacement relation and to exhibit the sought nonlinear behavior (SMR). This result confirms the importance of having a purely nonlinear force between the NES and the primary system as the presence of a linear component may radically change the global behavior. Finally the SMR seems to be more favorable in terms of energy absorbtion suggesting that the nonlinearities may be used to improve the energy harvesting.

In summary this study unifies the research fields of nonlinear vibration absorbers and energy harvesting from vibrations showing the advantages of a combined application. An optimization process is still to be done in which the performances of the NES and the harvester would be investigated.

Chapter 5

Conclusions

In this work the vibration mitigation in mechanical systems by means of a Nonlinear Energy Sink absorber was studied. The phenomenon governing the physics of this kind of device is referred to as Targeted Energy Transfer and it consists in an irreversible energy transfer from the primary system to the NES where the energy is then dissipated. This energy transfer may occur over a broad range of frequencies with no need for the NES to be tuned to a specific one.

An exhaustive literature review was presented which focused on the theoretical and experimental previous studies on the subject. The review showed that a lot of theoretical work had been done and a few interesting experimental investigations had been carried out. Thus, this work was mainly oriented towards an experimental approach based on the theoretical concepts existing in the literature.

The first type of absorber studied was the Vibro-Impact NES. This kind of absorber is characterized by a relative simplicity in the experimental realization and a considerable complexity in the analytic description because of its non-smooth nature. The main purpose of this study was to bridge the theoretical and experimental approaches in order to reach a comparison between the analytical results and the experimental observations. The system consisted in a harmonically forced single-degree-of-freedom linear oscillator to which a VI-NES was attached. Depending on external force's amplitude and frequency, either a Strongly Modulated Response (SMR) or a Constant Amplitude Response (CAR) was observed. In both cases a Targeted Energy Transfer from the LO towards the VI-NES was experimentally observed and a significant reduction of the primary system's resonance peak was obtained. The system was analytically studied by means of the Multiple

Scales method. The calculation of the Slow Invariant Manifold and of the fixed points allowed for an explanation of the experimental observations as well as for defining the dependence of the response on the design parameters (tube's length and restitution coefficient).

The second type of NES studied was the Magnetic-Strung NES. The aim of this study was to add the energy harvesting aspect to the research on nonlinear absorbers. A review of the energy harvesting techniques from vibrations made us lean towards a magnetic method because considered the most suitable one for the experimental realization we were looking for. The system consisted in a harmonically forced single-degree-of-freedom linear oscillator to which a MS-NES was attached. The type of nonlinearity used was basically cubic but with the ability to be shaped thanks of a magnetic force aptly introduced. The coupling between elastic and magnetic force permitted the NES to have several possible configurations of nonlinearity (linear+cubic, cubic, bistable). The final system was an electro-mechanical system in which the vibration energy of the primary system was absorbed by the NES and subsequently partially dissipated by the viscous damping and partially converted into electrical power. The numerical and experimental studies analyzed the performances of the MS-NES both as an energy absorber and as an energy harvester.

Perspective for future work

The results presented in this dissertation clearly show the interest in exploiting nonlinear dynamics in the field of passive vibration mitigation. However, there is still much theoretical and experimental work to be done.

Vibro-Impact NES:

- An energetic study should be done in order to identify the most favorable regimes in terms of energy dissipation. The analytical model, able to predict the response of the system as a function of the design parameters, could be used as a designing tool for an optimized version of the VI-NES.

- Considering the tube's length and the restitution coefficient as the two most relevant parameters in the VI-NES dynamics, an adaptive VI-NES can be thought where these parameters would vary in order to reach the most efficient regime. A further study should investigate whether the adaptive process would be active or completely passive.

- The energy harvesting aspect could be added. To do that, since the energy dissipation occurs through the impacts, a piezoelectric method could be implemented where the piezoelectric patches would be excited by the shocks.

- Related to the previous point, if the the impact surfaces are made up of piezoelectric patches, a process to change their mechanical properties, and then the restitution coefficient, could be investigated.

Magnetic-Strung NES:

- The energetic study should be pushed further so that an optimized MS-NES can be designed. The MS-NES performances should be analyzed both as an energy absorber and as an energy harvester and the influence of the mechanical and electric parameters should be evaluated.

- The coupling between the mechanical and the electric system should be investigated and exploited. The two systems are coupled through the electromechanic coefficient γ which relates the electrical current and the mechanical damping. Theoretically it might be possible to introduce an artificial mechanical damping thanks to the electrical properties. This aspect should be studied and might evolve in a semi-active/adaptative control method.

- The energy converted into electrical power could be stocked in a battery and not only delivered to a resistive load. Nevertheless, one should be aware that a study of this kind requires a deep knowledge in electronics and electrical circuits.

- The shaping of the force between the primary system and the NES via the magnetic force should be thoroughly analyzed. Particular attention should be put to the bistable configuration which seems to be a promising path to follow.

Appendices

Appendix A

Mathematical proofs

A.1 Sum of two sinus with the same frequency shifted in phase

Reminding Eq.(3.27) from chapter 3:

$$\frac{\partial^2 w_0}{\partial \tau_0^2} + (1+r)\sum_j \frac{\partial w_0^-}{\partial \tau_0}\delta_j^- = -C\sin(\Omega\tau_0 + \psi) + \overline{X}\sin(\Omega\tau_0) \tag{A.1}$$

The two forcing terms can be expressed as a single sinus term as follows:

$$\begin{aligned} &-C\sin(\Omega\tau_0 + \psi) + \overline{X}\sin(\Omega\tau_0) = \\ &= -C[\sin(\Omega\tau)\cos\psi + \cos(\Omega\tau)\sin\psi] + \overline{X}\sin(\Omega\tau) = \\ &= (-C\cos\psi + \overline{X})\sin(\Omega\tau) - (C\sin\psi)\cos(\Omega\tau) \end{aligned} \tag{A.2}$$

An amplitude A and a phase θ are sought so that:

$$\begin{aligned} -C\cos\psi + \overline{X} &= A\cos\theta \\ -C\sin\psi &= A\sin\theta \end{aligned} \tag{A.3}$$

It yields:

$$\begin{aligned} A^2 &= (-C\cos\psi + \overline{X})^2 + (-C\sin\psi)^2 \\ \theta &= \arcsin\left(\frac{1}{A}(-C\sin\psi)\right) \end{aligned} \tag{A.4}$$

Finally:

$$A\cos\theta\sin(\Omega\tau) + A\sin\theta\cos(\Omega\tau) = A\sin(\Omega\tau + \theta) \tag{A.5}$$

And:

$$\frac{\partial^2 w_0}{\partial \tau_0^2} + (1+r)\sum_j \frac{\partial w_0^-}{\partial \tau_0}\delta_j^- = A\sin(\Omega\tau + \theta) \tag{A.6}$$

Bibliography

[ANB02] T. Asami, O. Nishihara, and A.M. Baz. Analytical solutions to h1 and h2 optimization of dynamic vibration absorbers attached to damped linear systems. *Journal of Vibration and Acoustics*, 124:284–295, 2002.

[Arn55] F. R. Arnold. Steady-state behavior of systems provided with nonlinear dynamic vibration absorbers. *Journal of Applied Mechanics*, 22:487–492, 1955.

[BCCM12] R. Bellet, B. Cochelin, R. Cote, and P.O. Mattei. Enhancing the dynamic range of targeted energy transfer in acoustics using several nonlinear membrane absorbers. *Journal of Sound and Vibration*, 2012.

[BCHM10] R. Bellet, B. Cochelin, P. Herzog, and P.O. Mattei. Experimental study of targeted energy transfer from an acoustic system to a nonlinear membrane absorber. *Journal of Sound and Vibration*, 329(14):2768–2791, 2010.

[Bro46] J.E. Brock. A note on the damped vibration absorber. *ASME Journal of Applied Mechanics*, 13(4):A284, 1946.

[BTW06] S. P. Beeby, M. J. Tudor, and N. M. White. Energy harvesting vibration sources for micro systems applications. *Measurement Science and Technology*, 17:175–195, 2006.

[CK00] S.B. Choi and W.K. Kim. Vibration control of a semi-active suspension featuring electrorheological fluid dampers. *Journal of Sound and Vibration*, 234:537–546, 2000.

[Den92] H.H. Denman. Tautochronic bifilar pendulum torsion absorbers for reciprocating engines. *Journal of Sound and Vibration*, 159:251–277, 1992.

[DH38] J.P. Den Hartog. Tuned pendulums as torsional vibration eliminators. *S. Timoshenko 60th Anniversary Volume*, pages Macmillian, London, UK, 1938.

[DH85] J.P. Den Hartog. *Mechanical Vibrations*. Dover Books on Engineering, 4th edition, 1985.

[DSSC96] S.J. Dyke, B.F. Spencer, M.K. Sain, and J.D. Carlson. Modeling and control of magnetorheological dampers for seismic response reduction. *Smart Materials and Structures*, 5:565–575, 1996.

[FA93] Y. Fujino and M. Abe. Design formulas for tuned mass dampers based on a perturbation technique. *Earthquake Engineering and Structural Dynamics*, 22:833–854, 1993.

[Fen71] N. Fenichel. Persistence and smoothness of invariant manifolds for flows. *Indiana Univ. Math. J.*, 21:193–225, 1971.

[Fra11] H. Frahm. A device for damping vibrations of bodies, 1911.

[GA15] O. V. Gendelman and A. Alloni. Dynamics of forced system with vibro-impact energy sink. *Journal of Sound and Vibration*, 358:301–314, 2015.

[GAT+07] E. Gourdon, N. Alexander, C. Taylor, C.H. Lamarque, and S. Pernot. Nonlinear energy pumping under transient forcing with strongly nonlinear coupling: Theoretical and experimental results. *Journal of Sound and Vibration*, 300(3):522–551, 2007.

[GB10] O.V. Gendelman and T. Bar. Bifurcations of self-excitation regimes in a van der pol oscillator with a nonlinear energy sink. *Physica D*, 239(3):220–229, 2010.

[GDK+16] E. Gourc, L. Dell'Elce, G. Kerschen, G. Michon, G. Aridon, and A. Hot. Performance comparison between a nonlinear energy sink and a linear tuned vibration absorber for broadband control. *Proceedings of the 34th IMAC, A Conference and Exposition on Structural Dynamics*, 2016.

[Gen01] O.V. Gendelman. Transition of energy to a nonlinear localized mode in a highly asymmetric system of two oscillators. *Nonlinear Dynamics*, 25:237–253, 2001.

[Gen04] O.V. Gendelman. Bifurcations of nonlinear normal modes of linear oscillator with strongly nonlinear damped attachment. *Nonlinear Dynamics*, 37:115–128, 2004.

[Gen08] O. Gendelman. Targeted energy transfer in systems with non-polynomial nonlinearity. *Journal of Sound and Vibration*, 315:732–745, 2008.

[Gen12] O.V. Gendelman. Analytic treatment of a system with a vibro-impact nonlinear energy sink. *Journal of Sound and Vibration*, 331:4599–4608, 2012.

[GGL06] O.V. Gendelman, E. Gourdon, and C.H. Lamarque. Quasiperiodic energy pumping in coupled oscillators under periodic forcing. *Journal of Sound and Vibration*, 294(4-5):651–662, 2006.

[GJTBW04] P. Glynne-Jones, M. J. Tudor, S. P. Beeby, and N. M. White. Anelectromagnetic, vibration-powered generator for intelligent sensor systems. *Sensors and actuators*, A 110:344–349, 2004.

[GL05a] O.V. Gendelman and C.H. Lamarque. Dynamics of linear oscillator coupled to strongly nonlinear attachment with multiple states of equilibrium. *Chaos, Solitons and Fractals*, 24:501–509, 2005.

[GL05b] E. Gourdon and C.H. Lamarque. Energy pumping with various nonlinear structures: numerical evidences. *Nonlinear Dynamics*, 40:281–307, 2005.

[GL06] E. Gourdon and C.H. Lamarque. Nonlinear energy sinks with uncertain parameters. *Journal of Computational and Nonlinear Dynamics*, 1:187–195, 2006.

[GLP07] E. Gourdon, C.H. Lamarque, and S. Pernot. Contribution to efficiency of irreversible passive energy pumping with a strong nonlinear attachment. *Nonlinear Dynamics*, 50:793–808, 2007.

[GMSB14a] E. Gourc, G. Michon, S. Seguy, and A. Berlioz. Experimental investigation and design optimization of targeted energy transfer under periodic forcing. *Journal of Vibration and Acoustics*, 136:021021, 2014.

[GMSB14b] E. Gourc, G. Michon, S. Seguy, and A. Berlioz. Theoretical and experimental study of an harmonically forced vibro-impact nonlinear energy sink. *Journal of Vibration and Acoustic*, 137:031008, 2014.

[GMVB03] O.V. Gendelman, L.I. Manevitch, A.F. Vakakis, and L.A. Bergman. A degenerate bifurcation structure in the dynamics of coupled oscillators with essential stiffness nonlinearities. *Nonlinear Dynamics*, 33:1–10, 2003.

[Gou13] E. Gourc. *Etude du contrôle passif par pompage energetique sous sollicitation harmonique.* phdthesis, Université de Toulouse, 2013.

[GS07] O.V. Gendelman and Y. Starosvetsky. Quasi-periodic response regimes of linear oscillator coupled to nonlinear energy sink under periodic forcing. *Journal of Applied Mechanics*, 74(2):325–331, 2007.

[GSF08] O.V. Gendelman, Y. Starosvetsky, and M. Feldman. Attractors of harmonically forced linear oscillator with attached nonlinear energy sink i : Description of response regimes. *Nonlinear Dynamics*, 51:31–46, 2008.

[GV07] F. Georgiades and A.F. Vakakis. Dynamics of a linear beam with an attached local nonlinear energy sink. *Communications in Nonlinear Science and Numerical Simulation*, 12(5):643–651, 2007.

[GV09] F. Georgiades and A.F. Vakakis. Passive targeted energy transfers and strong modal interactions in the dynamics of a thin plate with strongly nonlinear attachments. *International Journal of Solids and Structures*, 46(11):2330–2353, 2009.

[GVBM10] O. Gendelman, A. Vakakis, L. Bergman, and D. McFarland. Asymptotic analysis of passive nonlinear suppression of aeroelastic instabilities of a rigid wing in subsonic flow. *SIAM Journal on Applied Mathematics .*, 70(5):1655–1677, 2010.

[GVK07] F. Georgiades, A.F. Vakakis, and G. Kerschen. Broadband passive targeted energy pumping from a linear dispersive rod

to a lightweight essentially non-linear end attachment. *International Journal of Non-Linear Mechanics*, 42(5):773–788, 2007.

[GVMB05a] F. Georgiadis, A. F. Vakakis, D. M. McFarland, and L. A. Bergman. Shock isolation through passive energy pumping caused by non-smooth nonlinearities. *International Journal of Bifurcations and Chaos*, 15:1–13, 2005.

[GVMB05b] F. Georgiadis, A.F. Vakakis, D.M. McFarland, and L. Bergman. Shock isolation through passive energy pumping caused by nonsmooth nonlinearities. *International Journal of Bifurcation and Chaos*, 15(06):1989–2001, 2005.

[HMBV10] S.A. Hubbard, D.M. McFarland, L.A. Bergman, and A.F. Vakakis. Targeted energy transfer between a model flexible wing and nonlinear energy sink. *Journal of Aircraft*, 47(6):1918–1931, 2010.

[HN82] J.B. Hunt and J.C. Nissen. The broadband dynamic vibration absorber. *Journal of Sound and Vibration*, 83:573–578, 1982.

[Hol79] P. Holmes. A nonlinear oscillator with a strange attractor. *Philosophical Transactions of the Royal Society A*, 292:419–448, 1979.

[JC88] I.N. Jordanov and B.I. Cheshankov. Optimal design of linear and nonlinear dynamical vibration absorbers. *Journal of Sound and Vibration*, 123:157–170, 1988.

[JC89] I.N. Jordanov and B.I. Cheshankov. Optimal design of linear and nonlinear dynamical vibration absorbers, reply. *Journal of Sound and Vibration*, 132:157–159, 1989.

[JMBV03] X. Jiang, D.M. McFarland, L.A. Bergman, and A.F. Vakakis. Steady state passive nonlinear energy pumping in coupled oscillators : Theoretical and experimental results. *Nonlinear Dynamics*, 33:87–102, 2003.

[KKM+07] G. Kerschen, J. Kowtko, D. McFarland, L. Bergman, and A.F. Vakakis. Theoretical and experimental study of multimodal targeted energy transfer in a system of coupled oscillators. *Nonlinear Dynamics*, 47(1):285–309, 2007.

[KLV+05] G. Kerschen, Y. S. Lee, A. F. Vakakis, D. M. McFarland, and L. A. Bergman. Irreversible passive energy transfer in coupled oscillators with essential nonlinearity. *SIAM Journal on Applied Mathematics*, 66(2):648–679, 2005.

[KMK+07] G. Kerschen, D.M. McFarland, J.J. Kowtko, Y.S. Lee, L.A. Bergman, and A.F. Vakakis. Experimental demonstration of transient resonance capture in a system of two coupled oscillators with essential stiffness nonlinearity. *Journal of Sound and Vibration*, 299(4-5):822–838, 2007.

[KMK+08] G. Kerschen, D. M. McFarland, J. J. Kowtko, Y. S. Lee, L. Bergman, and A. Vakakis. Impulsive periodic and quasi-periodic orbits of coupled oscillators with essential stiffness nonlinearity. *Communication in Nonlinear Science and Numerical Simulation*, 13:959–978, 2008.

[KPGV09] G. Kerschen, M. Peeters, J.C. Golinval, and A.F. Vakakis. Nonlinear normal modes, part i: A useful framework for the structural dynamicist. *Mech. Syst. Sign. Proc.*, 23(1):170194, 2009.

[KVG08] I. Karayannis, A. F. Vakakis, and F. Georgiadis. Vibro-impact attachments as shock absorbers. *Proceedings IMechE, Journal of Mechanical Engineering Science*, 222(222):1899–1908, 2008.

[KVM+05] G. Kerschen, Y.S. Vakakis, A.F.and Lee, D.M. McFarland, J.J. Kowtko, and L.A. Bergman. Energy transfers in a system of two coupled oscillators with essential nonlinearity: 1:1 resonance manifold and transient bridging orbits. *Nonlinear Dynamics*, 42:289–303, 2005.

[LGSE11] C.H. Lamarque, O.V. Gendelman, A. Savadkoohi, and E. Etcheverria. Targeted energy transfer in mechanical systems by means of non-smooth nonlinear energy sink. *Acta Mechanicca*, 221:175–200, 2011.

[LKM+07] Y. S. Lee, G. Kerschen, D. McFarland, W. J. Hill, C. Nichkawde, T. Strganac, L. Bergman, and A. F. Vakakis. Suppressing aeroelastic instability using broadband passive targeted energy transfers, part 2: Experiments. *AIAA Journal*, 45(10):2391–2400, 2007.

[LKV+05] Y. S. Lee, G. Kerschen, A. F. Vakakis, N. Panagopoulos, L. A. Bergman, and D. M. McFarland. Complicated dynamics of a linear oscillator with a light, essentially nonlinear attachment. *Physica D*, 204:41–69, 2005.

[LNV+09] Y. S. Lee, F. Nucera, A. F. Vakakis, D. M. McFarland, and L. A. Bergman. Periodic orbits, damped transitions and targeted energy transfers in oscillators with vibro-impact attachments. *Physica D*, 238:1868–1896, 2009.

[LRM90] G. X. Li, R. H. Rand, and F. C. Moon. Bifurcations and chaos in a forced zero-stiffness impact oscillator. *Journal of Nonlinear Mechanics*, 25(4):417–432, 1990.

[LVB+07] Y. S. Lee, A. F. Vakakis, L. Bergman, D. McFarland, and G. Kerschen. Suppressing aeroelastic instability using broadband passive targeted energy transfers, part 1: Theory. *AIAA Journal*, 45(3):693–711, 2007.

[LVB+08] Y. S. Lee, A. Vakakis, L. Bergman, D. McFarland, and G. Kerschen. Enhancing the robustness of aeroelastic instability suppression using multi-degree-of-freedom nonlinear energy sinks. *AIAA Journal*, 46(6):1371–1394, 2008.

[LW06] E. S. Leland and P. K. Wright. Resonance tuning of piezoelectric vibration energy scavenging generators using compressive axial load. *Smart Material and Structures*, 15:1413–1420, 2006.

[Mad80] J. Madden. Constant frequency bifilar vibration absorber, 1980.

[Man72] Mikhlin Yu.V. Manevitch, L.I. On periodic solutions close to rectilinear normal vibration modes. *J. Appl. Math. Mech.*, 36(6):1051–1058, 1972.

[Man01] L. I. Manevitch. The description of localized normal modes in a chain of nonlinear coupled oscillators using complex variables. *Nonlinear Dynamics*, 25:95–109, 2001.

[MBC+11] R. Mariani, S. Bellizzi, B. Cochelin, P. Herzog, and P.O. Mattei. Toward an adjustable nonlinear low frequency acoustic absorber. *Journal of Sound and Vibration*, 330(22):5245–5258, 2011.

[MBV05] D. McFarland, L. Bergman, and A.F. Vakakis. Experimental study of non-linear energy pumping occurring at a single fast frequencyexperimental study of non-linear energy pumping occurring at a single fast frequency. *International Journal of Non-Linear Mechanics*, 40(6):891–899, 2005.

[MH79] F. C. Moon and P. Holmes. A magnetoelastic strange attractor. *Journal of Sound and Vibration*, 65:275–296, 1979.

[Mil85] J. Milnor. On the concept of attractor. *Comm. Math. Phys*, 99:177195, 1985.

[MKK+05] D. M. McFarland, G. Kerschen, J. J. Kowtko, Y. S. Lee, L. A. Bergman, and A. F. Vakakis. Experimental investigation of targeted energy transfers in strongly and nonlinearly coupled oscillators. *Journal Acoustical Society of America*, 118(2)):791–799, 2005.

[MN07] P. Malatkar and A.H. Nayfeh. Steady-state dynamics of a linear structure weakly coupled to an essentially nonlinear oscillator. *Nonlinear Dynamics*, 47:167–179, 2007.

[MO10] B. P. Mann and B. A. Owens. Investigations of a nonlinear energy harvester with a bistable potential well. *Journal of Sound and Vibration*, 329:12151226, 2010.

[MR05] Y.V. Mikhlin and S.N. Reshetnikova. Dynamical interaction of an elastic system and essentially nonlinear absorber. *Journal of Sound and Vibration*, 283:91–120, 2005.

[MS09] B. P. Mann and N. D. Sims. Energy harvesting from the nonlinear oscillations of magnetic levitation. *Journal of Sound and Vibration*, 319:515530, 2009.

[MTT15] M. Monteil, O. Thomas, and C. Touze. Identification of mode couplings in nonlinear vibrations of the steelpan. *Applied Acoustics*, 89:1–15, 2015.

[Nak98] B.C. Nakra. Vibration control in machines and structures using viscoelastic damping. *Journal of Sound and Vibration*, 211:449–465, 1998.

[Nay04] A. H. Nayfeh. *Perturbation methods*. WileyVCH Verlag, 2004.

[NLIM+08] F. Nucera, F. Lo Iacono, D. M. McFarland, L. A. Bergman, and A. F. Vakakis. Application of broadband nonlinear targeted energy transfers for seismic mitigation of a shear frame: Part ii. experimental results. *Journal of Sound and Vibration*, 313:57–76, 2008.

[NM97] O. Nishihara and H. Matsuhisa. Design and tuning of vibration control devices via stability criterion. *Japanese Society of Mechanical Engineering*, 97-10-1:165–168, 1997.

[ODH28] J. Ormondroyd and J.P. Den Hartog. The theory of the dynamical vibration absorber. *ASME Journal of Applied Mechanics*, 50(7):9–22, 1928.

[Pen98] E. Pennestri. An application of chebyshevs min-max criterion to the optimal design of a damped dynamic vibration absorber. *Journal of Sound and Vibration*, 217:757–765, 1998.

[PGT+07] P. Panagopoulos, F. Georgiades, S. Tsakirtzis, A.F. Vakakis, and L.A. Bergman. Multi-scaled analysis of the damped dynamics of an elastic rod with an essentially nonlinear end attachment. *International journal of solids and structures*, 44(18):6256–6278, 2007.

[Pil08] V.N. Pilipchuk. ransient mode localization in coupled strongly nonlinear exactly solvable oscillators. *Nonlinear Dynamics*, 51:245–258, 2008.

[Pip53] L. A. Pipes. Analysis of a nonlinear dynamic vibration absorber. *Journal of Applied Mechanics*, 20:515–518, 1953.

[PLP11] T.T. Pham, C.H. Lamarque, and S. Pernot. Passive control of one degree of freedom nonlinear quadratic oscillator under combination resonance. *Nonlinear Science and Numerical Simulation*, 16(5):2279–2288, 2011.

[PVR+08] M. Peeters, Viguie, Serandour R., Kerschen G., and J.C. G., Golinval. Nonlinear normal modes, partii: Practical computation using numerical continuation techniques. *Mech. Syst. Signal Proc.*, 2008.

[Rob52] R.E. Roberson. Synthesis of a nonlinear dynamic vibration absorber. *Journal of the Franklin Institute*, 254:205–220, 1952.

[Ros66] R.M. Rosenberg. On nonlinear vibrations of systems with many degrees of freedom. *Advance Applied Mechanics*, 9:155–242, 1966.

[RWR03] S. Roundy, P. K. Wright, and J. M. Rabaey. *Energy Scavenging for Wireless Sensor Networks*. Springer NewYork, 2003.

[SBK08] I. Sari, T. Balkan, and H. Kulah. An electromagnetic micro power generator for wideband environmental vibrations. *Sensors and Actuators A*, 145-146:405–413, 2008.

[SG08a] Y. Starosvetsky and O.V. Gendelman. Strongly modulated response in forced 2dof oscillatory system with essential mass and potential asymmetry. *Physica D*, 237(13):1719–1733, 2008.

[SG08b] Y. Starosvetsky and O.V. Gendelman. trongly modulated response in forced 2dof oscillatory system with essential mass and potential asymmetry. *Physica D : Nonlinear Phenomena*, 237(13):1719–1733, 2008.

[SG10a] Y. Starosvetsky and O.V. Gendelman. Bifurcations of attractors in forced system with nonlinear energy sink : the effect of mass asymmetry. *Nonlinear Dynamics*, 59:711–731, 2010.

[SG10b] Y. Starosvetsky and O.V. Gendelman. Response regimes in forced system with non-linear energy sink : quasi-periodic and random forcing. *Nonlinear Dynamics*, 64:177195, 2010.

[SLD12] A.T. Savadkoohi, C.H. Lamarque, and Z. Dimitrijevic. Vibratory energy exchange between a linear and a nonsmooth system in the presence of the gravity. *Nonlinear Dynamics*, 70(2):1473–1483, 2012.

[SM10] A. J. Sneller and B. P. Mann. On the nonlinear electromagnetic coupling between a coil and an oscillating magnet. *J. Phys. D: Appl. Phys*, 43, 2010.

[SMM09] S. Stanton, C. McGehee, and B. P. Mann. Reversible hysteresis for broadband magnetopiezoelastic energy harvesting. *Appl. Phys. Lett.*, 95 (174103), 2009.

[SMM10] S. Stanton, C. McGehee, and B. P. Mann. Nonlinear dynamics for broadband energy harvesting: Investigation of a bistable piezoelectric inertial generator. *Physica D*, 239:640–653, 2010.

[SP91] S.W. Shaw and C. Pierre. Nonlinear normal modes and invariant manifolds. *Journal of Sound and Vibration*, 150:170–173, 1991.

[SP93] S.W. Shaw and C. Pierre. Normal modes of vibration for nonlinear vibratory systems. *Journal of Sound and Vibration*, 164:85–124, 1993.

[SSH06] S.W. Shaw, P.M. Schmitz, and A.G. Haddow. Dynamics of tautochronic pendulum vibration absorbers: Theory and experiment. *Journal of Computational and Nonlinear Dynamics*, 1:283–293, 2006.

[Tho80] A. Thompson. Auxiliary mass throw in a tuned and damped vibration absorber. *Journal of Sound and Vibration*, 70:481–486, 1980.

[Tho81] A.G. Thompson. Optimum tuning and damping of a dynamic vibration absorber applied to a force excited and damped primary system. *Journal of Sound and Vibration*, 77(3), 1981.

[TPK+07] S. Tsakirtzis, P.N. Panagopoulos, G. Kerschen, O. Gendelman, A.F. Vakakis, and L.A. Bergman. Complex dynamics and targeted energy transfer in linear oscillators coupled to multi-degree-of-freedom essentially nonlinear attachments. *Nonlinear Dynamics*, 48(3):285–318, 2007.

[TTA11] C. Touze, O. Thomas, and M. Amabili. Transition to chaotic vibrations for harmonically forced perfect and imperfect circular plates. *International Journal of Non-Linear Mechanics*, 46(1):234–246, 2011.

[TTC04] C. Touze, O. Thomas, and A. Chaigne. Hardening/softening behaviour in non-linear oscillations of structural systems using non-linear normal modes. *Journal of Sound and Vibration*, 273:77–101, 2004.

[Vak96] A.F. Vakakis. Nonlinear mode localization in systems governed by partial differential equations. *Appl. Mech. Rev*, 49(2):87–99, 1996.

[Vak01] A. F Vakakis. Inducing passive nonlinear energy sinks in vibrating systems. *Journal of Vibration and Acoustics*, 123:324–332, 2001.

[Vak04] R.H. Vakakis, A. F.and Rand. Nonlinear dynamics of a system of coupled oscillators with essential stiffness nonlinearities. *International Journal of Non-Linear Mechanics*, 39:1079–1091, 2004.

[VG10] K.V. Vramov and O.V. Gendelman. On interaction of vibrating beam with essentially nonlinear absorber. *Meccanica*, 45(3):355–365, 2010.

[VGa09] A.F. Vakakis, O. Gendelman, and al. *Nonlinear Targeted Energy Transfer in Mechanical and Structural Systems*. Springer, 2009.

[VGMM01a] A. F. Vakakis, O. V. Gendelman, L. I. Manevitch, and R. McCloskey. Energy pumping in nonlinear mechanical oscillators part ii resonance capture. *Journal of Applied Mechanics Transactions of the ASME*, 68:42–48, 2001.

[VGMM01b] A.F. Vakakis, O.V. Gendelman, L.I. Manevitch, and R. McCloskey. Energy pumping in nonlinear mechanical oscillators i: dynamics of the underlying hamiltonian system. *Journal of Applied MechanicsTransactions of the ASME*, 68:34–41, 2001.

[VMGB03] A.F. Vakakis, L.I. Manevitch, O.V. Gendelman, and L.A. Bergman. Dynamics of linear discrete systems connected to local, essentially non-linear attachments. *Journal of Sound and Vibration*, 264(3):559–577, 2003.

[VML11] B. Vaurigaud, L. Manevitch, and C. Lamarque. Passive control of aeroelastic instability in a long span bridge model prone to coupled flutter using targeted energy transfer. *Journal of Sound and Vibration*, 330(11):2580–2595, 2011.

[VMM+96] A. F. Vakakis, L. I. Manevitch, Y. V. Mikhlin, V. N. Pilipchuk, and Zevin A. A. *Normal Modes and Localization in Nonlinear Systems*. Wiley, New York, 1996.

[VR92a] A.F. Vakakis and R.H. Rand. Normal modes and global dynamics of a two-degree-of-freedom nonlinear system i. low energies. *Int. J. Nonlinear Mech*, 27(5):861–874, 1992.

[VR92b] A.F. Vakakis and R.H. Rand. Normal modes and global dynamics of a two-degree-of-freedom nonlinear system ii. high energies. *Int. J. Nonlinear Mech.*, 27(5):875–888, 1992.

[WN15] D. Wagg and S. Neild. *Nonlinear Vibration with control*. Springer, 2015.

[WY95] C. B. Williams and R. B. Yates. Analysis of a micro generator for microsystems. *Proceedings of the 8th International Conference on Solid-state Sensors and Actuators*, Eurosensors IX:87–84, 1995.

[YZZ15] Z. Yang, Y. Zhu, and J. Zu. Theoretical and experimental investigation of a nonlinear compressive-mode energy harvester with high power output under weak excitations. *Smart Mater. Struct.*, 24, 2015.

[ZZ12] Y. Zhu and J. Zu. A magnetoelectric generator for energy harvesting from the vibration of magnetic levitation. *IEEE transactions on magnetics*, 48, 2012.

Publications

List of Journal Publications

1. **G .Pennisi, C. Stephan, E. Gourc, G. Michon**, Vibro-Impact NES: A Correlation Between Experimental Investigation and Analytical Description, *Nonlinear Dynamics* (accepted)

2. **G. Pennisi, B. P. Mann, N. Naclerio, C. Stephan, G. Michon**, Magnetic-Strung NES with Energy Harvesting: Theoretical and Experimental Study of a New Concept of Nonlinear Vibration Absorber, *Journal of Sound and Vibration* (In preparation)

List of Conference Proceedings

1. **G. Pennisi, B. P. Mann, C. Stephan, G. Michon**, Magnetic-Strung NES with Energy Harvesting: Theoretical and Experimental Study of a New Concept of Nonlinear Vibration Absorber, *American Society of Mechanical Engineers, IDETC/CIE 2016*, Charlotte NC USA, August 2016

2. **G. Pennisi, B. P. Mann, C. Stephan, G. Michon**, Experimental Study of a New Concept of Nonlinear Vibration Absorber with Energy Harvesting, *European Congress on Computational Methods in Applied Sciences and Engineering*, Crete Island, Greece, June 2016

3. **G. Pennisi, B. P. Mann, C. Stephan, G. Michon**, *Preliminary study of a Nonlinear Energy Sink coupled with an electromagnetic energy harvester*, Vibrations, Shocks and Noise, Le Mans France, April 2016

4. **G. Pennisi, C. Stephan, G. Michon**, Vibro-Impact NES: A Correlation Between Experimental Investigation and Analytical Description, *Sensors and Instrumentation, Volume 5, Society for Experimental Mechanics, Proceedings of the 34th IMAC*, Orlando FL USA, January 2016

5. **G. Pennisi, C. Stephan, G. Michon**, Analytical and Experimental Study of a Vibro-Impact Nonlinear Energy Sink, *American Society of Mechanical Engineers, IDETC/CIE 2015*, Boston MA USA, August 2015

THÈSE

En vue de l'obtention du

DOCTORAT DE L'UNIVERSITÉ DE TOULOUSE

Délivré par :

Institut Supérieur de l'Aéronautique et de l'Espace (ISAE)

Présentée et soutenue par :
Giuseppe PENNISI

le jeudi 17 novembre 2016

Titre :

Passive vibration control by using Nonlinear Energy Sink absorbers.
Theoretical study and experimental investigations

Contrôle passif de vibrations à l'aide d'absorbeurs.
Étude théorique et investigations expérimentales

École doctorale et discipline ou spécialité :

ED MEGeP : Génie mécanique, mécanique des matériaux

Unité de recherche :

Institut Clément Ader

Directeur(s) de Thèse :

M. Guilhem MICHON (directeur de thèse)
M. Cyrille STEPHAN (co-directeur de thèse)

Jury :

Pr. Xavier BOUTILLON, École Polytechnique - Président
Pr. Claude-Henri LAMARQUE, ENTPE - Rapporteur
Pr. Brian MANN, Duke University - Examinateur
Pr. Guilhem MICHON, ISAE - Directeur de Thèse
Dr. Cyrille STEPHAN, ONERA DADS - Co-directeur de Thèse
Pr. Olivier THOMAS, ENSAM - Rapporteur

Résumé

Les méthodes de contrôle de vibrations passives basées sur des absorbeurs linéaires ont été largement étudiées et ils ont aujourd'hui une vaste gamme d'applications. Cependant, les absorbeurs linéaires n'étant efficaces que lorsqu'ils sont accordés à la fréquence que l'on veut contrôler, ils présentent des limites considérables quand ils sont appliqués à des systèmes possédant des incertitudes sur les paramètres modaux ou ayant une fréquence propre dépendante de la force extérieure.

Dans cette thèse la réduction des vibrations dans les systèmes mécaniques à l'aide d'un absorbeur Nonlinear Energy Sink est étudiée. Le phénomène qui gouverne la physique de ce dispositif est appelé pompage énergétique (Targeted Energy Transfer) et il consiste en un transfert irréversible d'énergie du système principal vers le NES, où l'énergie est dissipée. Ce transfert d'énergie peut se produire pour une large gamme de fréquences et sans besoin que le NES ne soit accordé à une fréquence spécifique.

La dynamique d'un premier type de NES appelé Vibro-Impact Nonlinear Energy Sink (VI-NES) est investiguée expérimentalement grâce à un oscillateur linéaire (OL) à un degré de liberté forcé harmoniquement auquel le VI-NES est attaché. Le pompage énergétique du OL vers le VI-NES est observé expérimentalement, ce qui a permis d'obtenir une importante réduction du pic de résonance du système principal. Le système est étudié analytiquement à l'aide de la méthode Multi-Echelles et le comportement non-linéaire observé est expliqué théoriquement.

Le deuxième type de NES présenté est le Magnetic-Strung NES avec récupération d'énergie. Cette étude ajoute l'aspect lié à la récupération d'énergie au domaine de recherche des absorbeurs non-linéaires. Le système consiste en un OL à un degré de liberté forcé harmoniquement auquel le MS-NES est appliqué. Le force non-linéaire de rappel peut être modulée grâce à une force magnétique introduite judicieusement, ce qui permet au NES d'avoir plusieurs configurations possibles. Le système résultant est un système électromécanique où l'énergie vibratoire du système principal est absorbée par le NES et est ensuite dissipée en partie par l'amortissement visqueux et convertie en partie en puissance électrique. Les études numérique et expérimentale analysent les performances du MS-NES en tant qu'absorbeur d'énergie et en tant que récupérateur d'énergie.

Finalement, les idées et les perspectives issues de cette étude sont traitées et les directions pour les travaux futurs sont fournies.

Abstract

Passive vibration control methods using linear dampers have been largely studied and investigated, and they have nowadays a broad range of applications. However, linear dampers are efficient when tuned to the specific frequency to control but present substantial limitations when applied to primary systems with uncertainties on the modal parameters or to systems having a natural frequency that may vary with external forcing.

In this thesis the vibration mitigation in mechanical systems by means of a Nonlinear Energy Sink absorber is studied. The phenomenon governing the physics of this kind of device is referred to as Targeted Energy Transfer and it consists in an irreversible energy transfer from the primary system to the NES where the energy is then dissipated. This energy transfer may occur over a broad range of frequencies with no need for the NES to be tuned to a specific one.

The dynamics of a first type of NES called Vibro-Impact Nonlinear Energy Sink (VI-NES) is experimentally investigated via a harmonically forced single-degree-of-freedom linear oscillator to which a VI-NES is attached. A Targeted Energy Transfer from the LO towards the VI-NES is experimentally observed and a significant reduction of the primary system's resonance peak is obtained. The system is analytically studied by means of the Multiple Scales method and the nonlinear behavior experimentally observed is theoretically explained.

The second type of NES presented is the Magnetic-Strung NES with energy harvesting. This study adds the energy harvesting aspect to the research on nonlinear vibration absorbers. The system consists in a harmonically forced single-degree-of-freedom linear oscillator to which the MS-NES is applied. The type of nonlinearity used can be shaped thanks to a magnetic force aptly introduced, allowing the NES to have several possible configurations. The resulting system is an electro-mechanical system in which the vibration energy of the primary system is absorbed by the NES and subsequently partially dissipated by the viscous damping and partially converted into electrical power. The numerical and experimental studies analyze the performances of the MS-NES both as an energy absorber and as an energy harvester.

Finally, ideas and perspectives arising from this study are discussed and future work directions are provided.

Table des matières

Chapitre 1

Introduction

Ce document en langue française est une synthèse du manuscrit officiel écrit en langue anglaise qui est à considérer comme le mémoire officiel. Cette partie en français est structurée selon le même plan que la partie en anglais. Elle comporte les passages et les illustrations principales et renvoie à la partie en anglais pour les détails.

1.1 Réduction du niveau vibratoire des structures mécaniques

Le contrôle des vibrations en dynamique des structures est toujours un domaine de recherche important puisqu'il permet une amélioration de la résistance des structures, un abaissement du niveau sonore et un confort accru. Les sources de vibrations pour les structures mécanique sont nombreuses et les méthodes de contrôle peuvent être classifiées en trois catégories principales :

- les méthodes de contrôle actif ont été largement développées durant les quinze dernières années. Le principe étant de générer une excitation hors phase, le contrôle actif fournit des bonnes performances en termes de réduction des vibrations mais a l'inconvénient majeur de requérir une source d'énergie externe.

- des méthodes de contrôle semi-actif qui utilisent des fluides électro- et magnéto-rhéologiques ont été proposées en [DSSC96, CK00]. La particularité de ces fluides est de pouvoir changer leur viscosité suivant le champ électrique ou magnétique dans lequel ils se trouvent. Ces

techniques sont robustes et fiables mais leur modélisation complexe représente un fort inconvénient pour des applications industrielles.

- les méthodes de contrôle passif réduisent le niveau vibratoire en ajoutant à la structure un matériau dissipatif [Nak98] ou alors un absorbeur de vibrations dynamique [Fra11, DH85]. Cette technique est très intéressante et représente une alternative valable aux méthodes précédentes puisqu'elle ne nécessite pas d'énergie externe.

1.2 Puits d'énergie non-linéaire (Nonlinear Energy Sink)

Pour pouvoir dépasser les performances des absorbeurs de vibrations linéaires, un domaine de recherche s'est focalisé durant ces dernières années sur les absorbeurs dits non-linéaires. Les premières études portant sur l'utilisation des non-linéarités dans la réduction des vibrations datent des années 50 [Rob52, Pip53, Arn55] et en 1982 la première réalisation d'un absorbeur avec raideur assouplissante fut présentée [HN82]. La nature de la non-linéarité peut en principe être de tout type. Par exemple, des absorbeurs à pendule centrifuge furent étudiés en [DH38] et successivement améliorés en [Mad80, Den92, SSH06].

Les absorbeurs non-linéaires ont capté l'attention des chercheurs grâce à leur capacité à s'adapter au système primaire auquel ils sont attachés sans être accordés à une fréquence spécifique. Comme ils ne possèdent pas une fréquence de résonance préférentielle, ils sont capables d'interagir avec le système principal sur une large gamme de fréquences et donc d'être efficaces sur tous les modes à l'intérieur de cette gamme.

Le Targeted Energy Transfer (TET ou pompage énergétique) a été observé par Gendelman [Gen01]. Dans cet article il a étudié un système à 2 degrés de liberté composé d'un oscillateur linéaire (OL) couplé à un oscillateur avec raideur linéaire nulle. Dans [Gen12] il a été montré que quand l'énergie de l'OL est supérieure à un certain seuil, un mouvement périodique localisé se produit pendant lequel l'énergie est transférée à l'oscillateur non-linéaire et ensuite dissipée. Un absorbeur non-linéaire qui présente ce type de comportement est appelé Nonlinear Energy Sink (NES).

Des études ultérieures ont été conduites [VGMM01a, VGMM01b] et le TET a été défini comme un transfert d'énergie irréversible de la structure directement excitée vers le NES. Le mécanisme qui conduit au TET est une capture de résonance transitoire grâce à laquelle l'OL et le NES entrent

dans une résonance 1 :1. Un critère de seuil d'activation a été formulé dans [Vak01]. En fait le NES semble être efficace quand l'énergie présente dans le système principal est au-delà d'une certaine quantité.

Des travaux expérimentaux ont examiné le TET et sont présentés dans [MBV05, GAT+07, KKM+07]. Ils ont prouvé que la dynamique qui gouverne le transfert d'énergie est une résonance 1 :1 entre le système principal et le NES. Le TET sous sollicitation harmonique a été étudié théoriquement [SG08] et expérimentalement [GMSB14a] où il a été montré que, en plus du régime de réponse stationnaire, un type de réponse fortement modulée (SMR : Strongly Modulated Response) peut également se produire.

Dans la plupart des travaux cités, une nonlinéarité de type raideur cubique a été utilisé : les nonlinéarités des éléments élastiques sont utilisées pour atteindre une force de rappel proportionnelle au cube du déplacement. Cependant la nature de la nonlinéarité peut être en théorie de n'importe quel type. Des études récentes se sont penchées sur des fonctions non-polynomiales [Gen08], des états d'équilibre multiples [GL05], des fonctions non-continues [GVMB05b, LGSE11, SLD12] et des Vibro-Impacts [GVMB05a, KVG08, LNV+09, NLIM+08]. Les travaux sur les Vibro-Impacts sont généralement basés sur des simulations numériques. Une approche analytique a été proposée dans [Gen12] et [GA15]. Dans [GMSB14b] les différent régimes de réponse d'un VI-NES appliqué à un système principal forcé harmoniquement ont été observés expérimentalement.

1.2.1 Études expérimentales sur le pompage énergétique

Ici on présente plus en détail une analyse bibliographique des travaux expérimentaux concernant le pompage énergétique (TET) que l'on peut trouver en littérature. Une grande partie de ce manuscrit de thèse a une nature expérimentale et les études présentées ici ont servi de base d'inspiration.

Une réalisation expérimentale d'un NES attaché à un système principal à 1 degré-de-liberté est présenté en [MBV05]. La nonlinéarité est à raideur cubique et elle est obtenue à l'aide de câbles élastiques travaillant transversalement. Pour avoir une force purement cubique les cables ne doivent pas être pré-chargés ; en pratique ce point est difficile à être satisfait. Le prototype du NES étudié dans [MBV05] est illustré à la Fig.1.1.

Le même système mais avec un NES légèrement différent est étudié dans [KMK+07] et illustré à la Fig.1.2. Le pompage énergétique est observé expérimentalement ainsi que le seuil d'activation du NES. Le prototype utilisé dans [BCHM10] est montré à la Fig.1.3 où le NES est formé

d'une membrane flexible.

Dans [KMK+08] le pompage énergétique sur un système à 2 ddls est examiné. Le système expérimental est similaire à celui utilisé dans [MBV05] et le pompage énergétique multi-modal est observé et validé.

Dans [GLP07] un modèle de bâtiment multi-ddl excité harmoniquement est analysé. Dans [NLIM+08] un modèle similaire soumis à une excitation séismique est étudié. Un Vibro-Impact NES est utilisé dans ce cas (Fig.1.4).

Une contribution significative à l'étude d'un NES attaché à une structure forcée harmoniquement a été apportée par les travaux de thèse d'Etienne Gourc effectués à l'ISAE/INSA Toulouse [Gou13]. Une raideur cubique (Fig.1.5) et un Vibro-Impact NES (Fig.1.6) ont été étudiés analytiquement et expérimentalement.

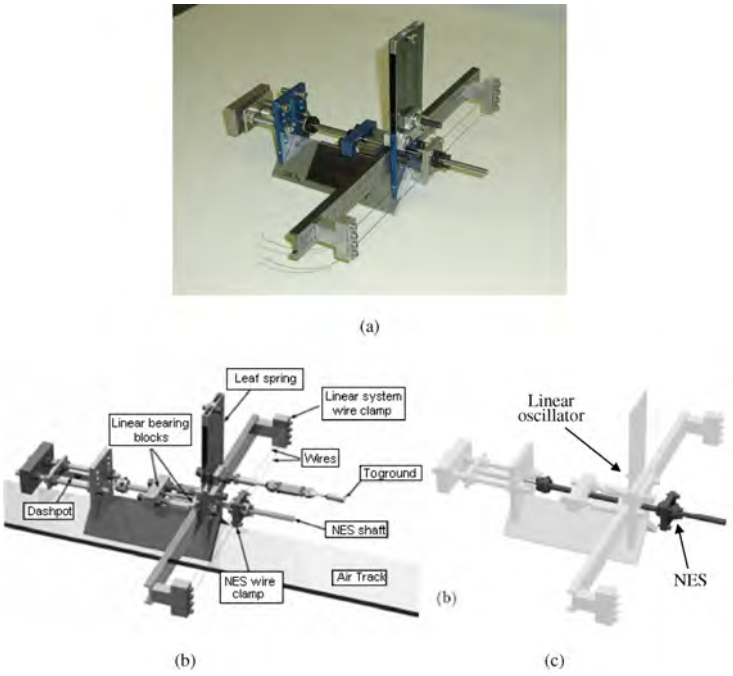

FIGURE 1.1: Réalisation expérimentale et schéma du système de NES étudié dans [MBV05].

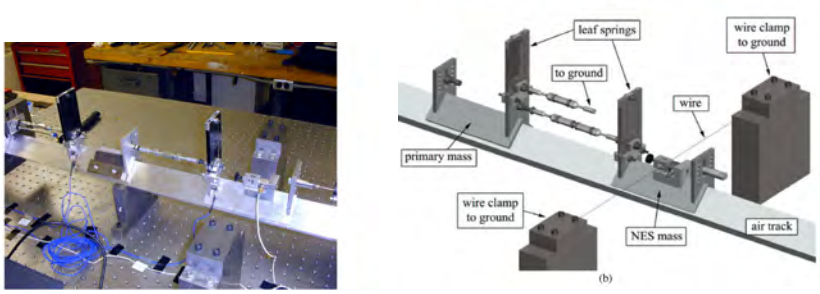

FIGURE 1.2: Réalisation expérimentale et schéma du système de NES étudié dans [KMK+07].

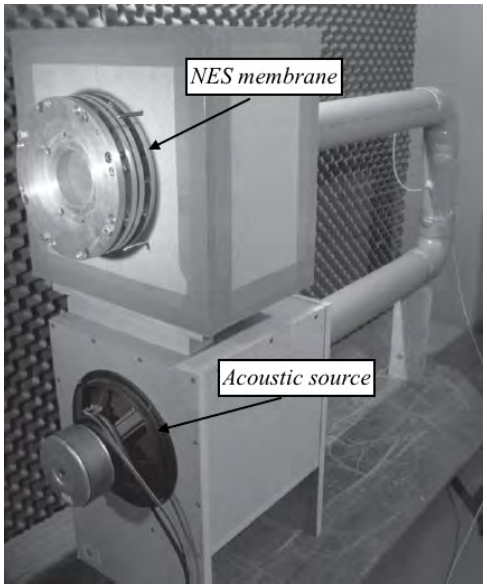

FIGURE 1.3: Réalisation expérimentale du système de NES étudié dans [BCHM10].

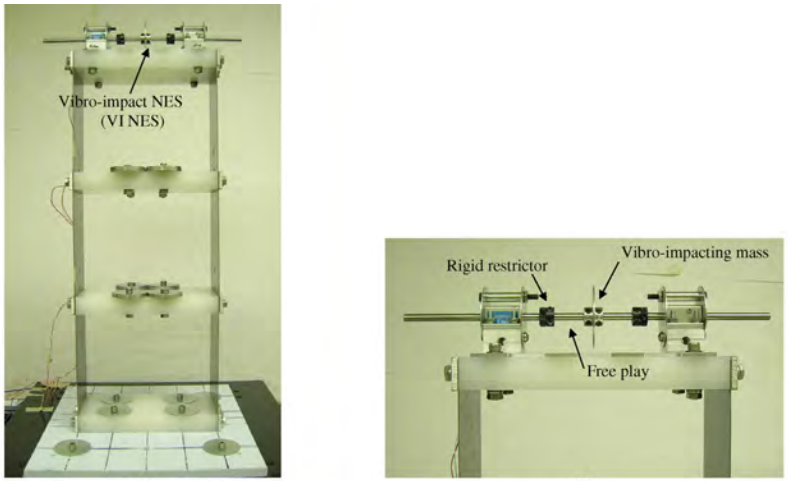

FIGURE 1.4: Réalisation expérimentale et schéma du système de Vibro-Impact NES étudié dans [NLIM+08].

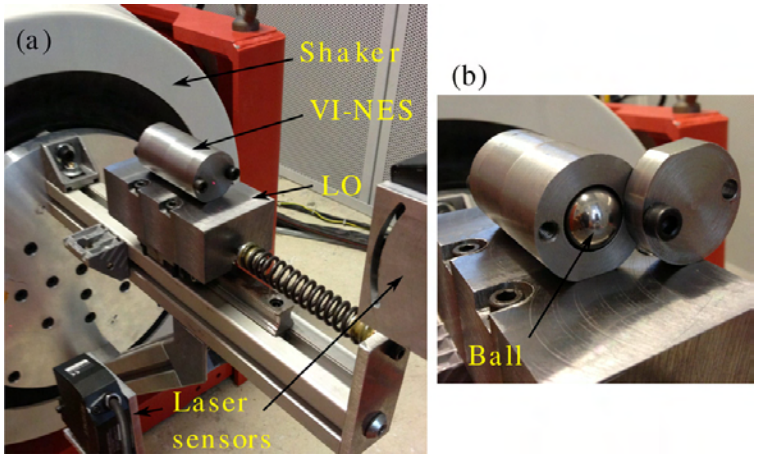

FIGURE 1.5: Réalisation expérimentale du système de Vibro-Impact NES étudié dans [GMSB14b].

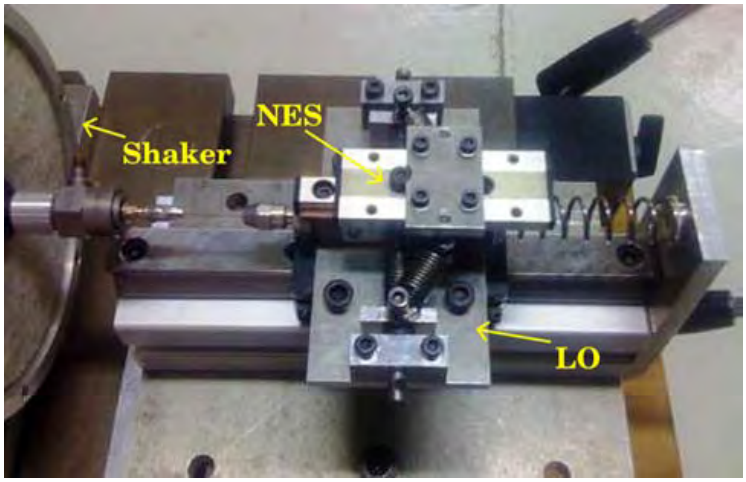

FIGURE 1.6: Réalisation expérimentale du système de NES à raideur cubique étudié dans [GMSB14a].

1.3 Récupération d'énergie vibratoire

Un des objectifs de cette thèse est d'examiner la capacité d'un absorbeur non-linéaire à non seulement dissiper de l'énergie vibratoire, mais également à la récupérer. Cet aspect est étudié dans le cadre du Magnetic-Strung NES, présenté par la suite. Une analyse bibliographique sur la récupération d'énergie vibratoire a été conduite et elle est présentée ici.

La récupération d'énergie depuis l'environnement [BTW06] a récemment connu un intérêt croissant et beaucoup de travaux ont été motivés par les avancements dans l'industrie micro-électronique, ce qui a permis une réduction de la puissance consommée par les dispositifs MEMS [GJTBW04, RWR03]. Des méthodes solaires, chimiques et thermiques ont été investiguées et ont été reconnues comme sources d'énergie potentielles. De plus, les vibrations sont une autre source d'énergie importante et la récupération d'énergie vibratoire est devenu un secteur de recherche prometteur. Les premiers travaux se sont focalisés sur des générateurs inertiels à comportement linéaire [WY95]. Une limitation des générateurs inertiels linéaires est leur efficacité concentrée sur une bande de fréquences réduite. Des méthodes ont été étudiées pour contrecarrer cet inconvénient dans [SBK08] and [LW06].

Comme pour les absorbeurs de vibrations, la dynamique non-linéaire semble offrir une alternative prometteuse pour améliorer les performances en

récupération d'énergie. Une des premières investigations expérimentales d'un récupérateur d'énergie non-linéaire a été décrit dans [MS09]. Une étude similaire basée sur une conversion piézoélectrique est présentée dans [SMM09]. Un récupérateur piézoélectrique avec des bonnes performances en termes de énergie et bande de fréquences est présenté dans [YZZ15]. Plusieurs études ont démontré l'avantage d'un oscillateur de Duffing monostable pour élargir la bande de fonctionnement. Le Duffing bistable a été aussi examiné dans [SMM10] et [MO10].

1.4 Motivation de ces travaux de thèse et plan du manuscrit

L'analyse bibliographique a montré que le pompage énergétique a été l'objet de nombreuses études théoriques et de quelques investigations expérimentales intéressantes. Cependant, pour bien exploiter ses avantages potentiels, le Nonlinear Energy Sink en tant qu'absorbeur de vibrations présente encore des points qu'il faudrait examiner et mieux comprendre. Par exemple, lorsqu'il s'agit d'atténuer une réponse vibratoire dans un contexte industriel, la complexité supplémentaire du NES est souvent décourageante. Bien sûr, l'utilisation d'un absorbeur linéaire classique peut parfois être plus avantageuse [GDK$^+$16] et en général il dépend du cas spécifique. En tout cas nous croyons que le potentiel du NES mérite des investigations ultérieures afin d'aboutir à une connaissance plus approfondie de ce dispositif et de son fonctionnement.

Avoir à faire avec la dynamique structurelle non-linéaire veut dire souvent que les principes et les concepts pris comme acquis dans la dynamique classique peuvent ne plus être valides, surtout pendant les études expérimentales, ce qui exige un effort supplémentaire pour comprendre les comportements nouveaux et inattendus qui peuvent survenir. L'étude du transfert d'énergie ciblé (TET) pose des défis techniques distincts et nécessite l'utilisation de concepts, de formulations, de méthodes d'analyse et de techniques de calcul de différents domaines des mathématiques appliquées et de l'ingénierie, tels que les systèmes dynamiques, la théorie des bifurcations, le traitement du signal et la dynamique expérimentale.

Dans le chapitre qui suit, des concepts fondamentaux en dynamique non-linéaire sont rappelés. Ces concepts seront utilisés dans la suite du manuscrit de thèse.

Le troisième chapitre est consacré à l'étude du Vibro-Impact NES. Une étude analytique et expérimentale met en évidence les différents régimes de

réponse qu'un tel système peut avoir. Les observation expérimentales sont expliquées par l'analyse théorique et les résultats comparés.

Le quatrième chapitre présente la conception théorique et la réalisation expérimentale d'un deuxième dispositif de type NES : le Magnetic-Strung NES. Cette étude a été conduite pendant une période de visite à l'université de Duke aux USA et a permis d'ajouter l'aspect lié à la récupération d'énergie à la recherche sur les absorbeurs non-linéaires.

Le manuscrit termine par une analyse des recherches conduites et une proposition de perspectives futures.

Chapitre 2

Concepts fondamentaux en dynamique non-linéaire

Dans ce chapitre l'exemple classique de l'oscillateur de Duffing est présenté pour introduire des concepts fondamentaux en dynamique non-linéaire qui seront utiles par la suite pour la compréhension des travaux présentés. Dans cette partie en français on se limite à l'introduction de l'oscillateur de Duffing et de la dépendance fréquence-amplitude. Dans le mémoire en anglais on présente aussi le concept de modes non-linéaires et leurs propriétés.

2.1 Oscillateur de Duffing

L'équation différentielle Eq.(2.4)

$$\ddot{x} + \delta\dot{x} + \beta x + \alpha x^3 = \gamma\cos(\omega t) \tag{2.1}$$

est connue comme l'équation de l'oscillateur de Duffing et représente un exemple classique de système non-linéaire manifestant des phénomènes typiquement non-linéaires.

L'oscillateur de Duffing est un modèle de système structural qui possède une force de rappel cubique. Il peut être utilisé pour une approximation du pendule simple illustré à la Fig.2.1 ; son équation de mouvement est la suivante :

$$\frac{d^2\theta}{dt^2} + \frac{g}{L}\sin\theta = 0 \tag{2.2}$$

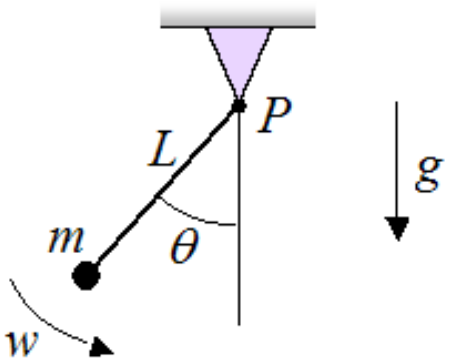

FIGURE 2.1: Pendule simple.

En écrivant $\sin\theta = \theta - \frac{\theta^3}{6} + O(\theta^5)$, on obtient un oscillateur de Duffing non-amorti et non-forcé :

$$\frac{d^2\theta}{dt^2} + \frac{g}{L}\left(\theta - \frac{\theta^3}{6}\right) = 0 \tag{2.3}$$

2.1.1 Espace des phases

Dans le cas d'un oscillateur de Duffing non-amorti et non-forcé, son équation de mouvement devient :

$$\ddot{x} + \beta x + \alpha x^3 = 0 \tag{2.4}$$

On peut reformuler le problème comme un système du premier ordre :

$$\frac{dx}{dt} = y, \quad \frac{dy}{dt} = -\beta x - \alpha x^3 \tag{2.5}$$

On peut alors décrire le mouvement du système dans le plan $x - y$, c'est-à-dire la trajectoire dans l'espace des phases. La courbe intégrale est alors :

$$\frac{dy}{dx} = \frac{\frac{dy}{dt}}{\frac{dx}{dt}} = \frac{-\beta x - \alpha x^3}{y} \tag{2.6}$$

En intégrant l'équation 2.5, cela nous amène au principe de conservation de l'énergie :

$$E(t) = \frac{y^2}{2} + \beta\frac{x^2}{2} + \alpha\frac{x^4}{4} = constant \tag{2.7}$$

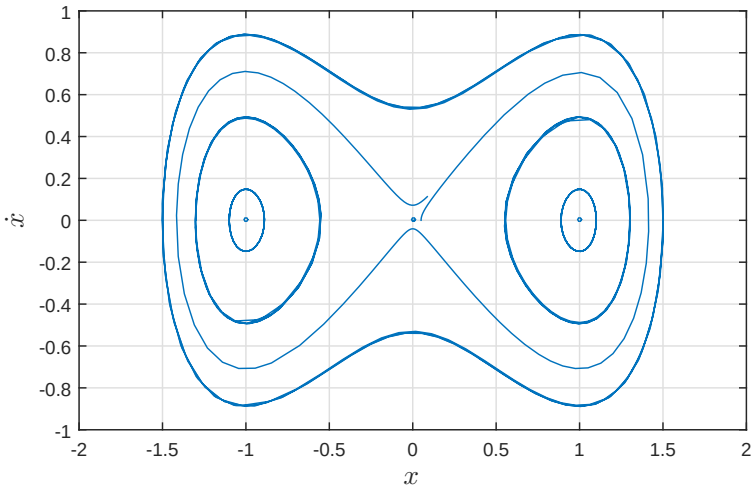

FIGURE 2.2: Espace des phases de l'oscillateur de Duffing non-amorti.

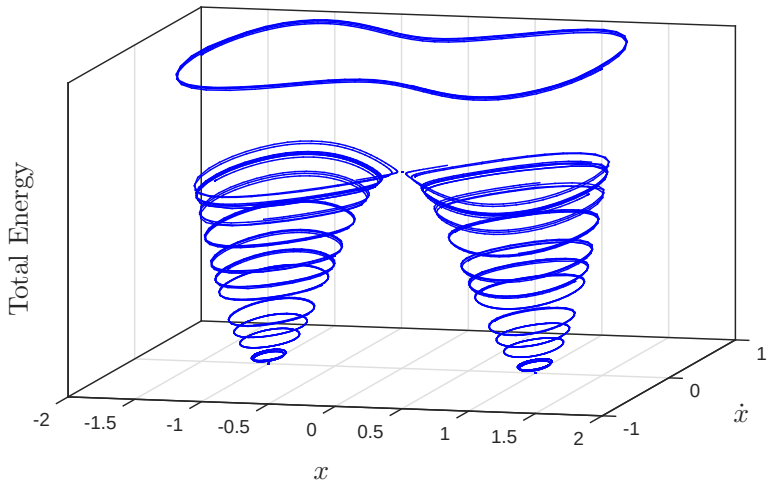

FIGURE 2.3: Orbites de l'oscillateur de Duffing non-amorti à différents niveau d'énergie.

Les figures 2.2 et 2.3 montrent l'espace des phases pour l'oscillateur de Duffing non-amorti dans le cas de $\beta < 0$ et $\alpha > 0$. On peut voir que deux solutions d'équilibre existent à basse énergie et qu'une seule solution périodique subsiste à haut niveau.

2.1.2 La backbone curve

Si on intègre l'équation de Duffing, on peut voir que la fréquence du mouvement périodique dépend de la courbe de l'espace des phases sur laquelle on se trouve et donc de l'amplitude de l'oscillation. Cet effet est typique des vibrations non-linéaires et est connu comme étant la dépendance fréquence-amplitude.

Pour le Duffing, des méthodes analytiques (méthodes de perturbation) existent pour obtenir la relation fréquence-amplitude suivante appelée Backbone curve :

$$\omega = 1 + k_1\epsilon + O(\epsilon^2) = 1 + \frac{3}{8}\alpha A^2\epsilon + O(\epsilon^2) \tag{2.8}$$

Où α est la raideur non-linéaire, ϵ est un paramètre utilisé pour le développement limité et A est l'amplitude de l'oscillation. Un exemple de réponse forcée pour l'oscillateur de Duffing est montré en Fig.2.4. On remarque que la fréquence propre augmente avec l'amplitude, ce qui dénote une nature durcissante de la non-linéarité.

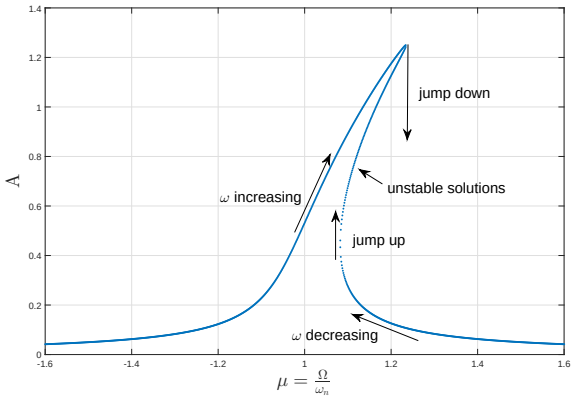

FIGURE 2.4: Réponse forcée de l'oscillateur de Duffing.

Chapitre 3

Vibro-Impact Nonlinear Energy Sink

Dans ce chapitre on présente l'étude d'un Vibro-Impact NES couplé à un oscillateur linéaire à un degré de liberté. Une analyse complète, alliant les aspects numérique, analytique et expérimental, a été conduite et est présentée en détail dans le mémoire en anglais. Ici on se limitera à la description du système et à une présentation des résultats principaux

3.1 Description du modèle

Le système se compose d'un oscillateur linéaire (OL) forcé que l'on veut contrôler à l'aide du VI-NES. Le VI-NES est une bille qui est libre de bouger dans un cylindre. Lorsque le système principal oscille, les impacts qui se produisent entre la bille et les parois du cylindre dissipe de l'énergie vibratoire de l'OL.

Un modèle numérique du VI-NES a été développé sous Matlab afin de prédire les réponses que l'on pourrait observer pendant les expériences. Un schéma du modèle est illustré à la Fig.3.1.

Hors des deux impacts, les équations de mouvement sont les suivantes :

$$\begin{aligned} M\ddot{u} + C\dot{u} + Ku &= Kx_e + C\dot{x}_e \\ m\ddot{v} &= 0 \\ \forall |u - v| &< L \end{aligned} \tag{3.1}$$

Quand un impact se produit, les vitesses deviennent discontinues et les conditions après l'impact peuvent être calculées par la relation :

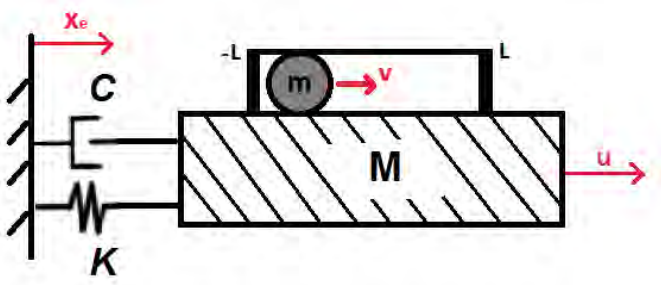

FIGURE 3.1: Schéma du modèle.

$$\dot{u}(t_j^+) - \dot{v}(t_j^+) = -r(\dot{u}(t_j^-) - \dot{v}(t_j^-)) \tag{3.2}$$

$$M\dot{u}(t_j^+) + m\dot{v}(t_j^+) = M\dot{u}(t_j^-) + m\dot{v}(t_j^-) \tag{3.3}$$

3.2 Étude expérimentale

L'étude expérimentale a été conduite avec pour but d'observer le comportement du système et d'explorer les différents types de réponse qui peuvent se manifester en fonction des conditions d'excitation extérieure.

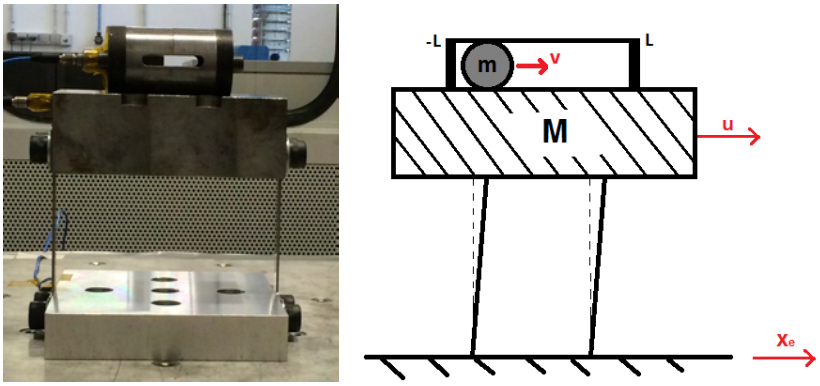

FIGURE 3.2: Le prototype (gauche) and sa représentation schématique (droite).

Le prototype est montré à la Fig.3.2 et ses paramètres de masses affichés dans le Tab.3.1.

$M[Kg]$	$m[Kg]$	$\epsilon = m/M$
3.807	0.032	0.84%

TABLE 3.1: Paramètres massiques du système principal.

Plusieurs essais ont été effectués pour différents niveaux d'accélération extérieure et pour un balayage de fréquence autour de la fréquence propre du système principal.

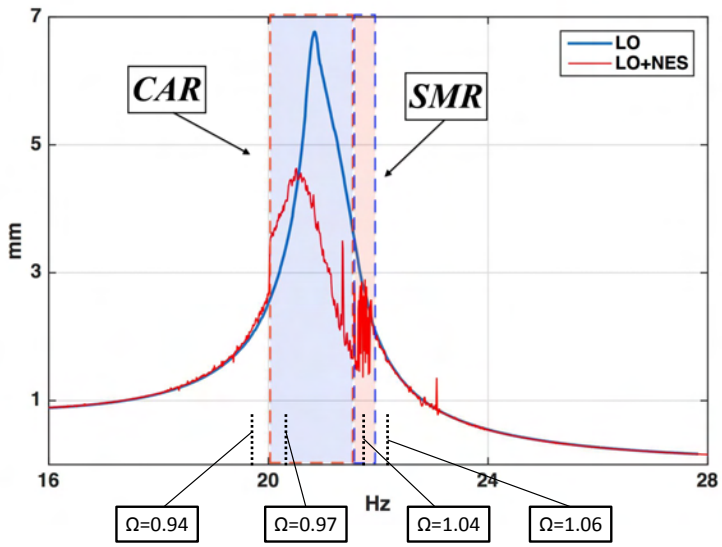

FIGURE 3.3: Spectre du deplacement du système principal sans (bleu) et avec (rouge) l'application du VI-NES. Les régime de réponse CAR et SMR ont été identifiés.

A la Fig.3.3 on montre le spectre du déplacement du système principal avec (rouge) et sans (bleu) l'utilisation du VI-NES. On remarque que le VI-NES accomplit sa fonction d'absorbeur en réduisant le pic de résonance. En plus deux zones sont identifiées car elles possèdent deux types de réponse qualitativement différente :

- Réponse à Amplitude Constante (CAR) (Fig.3.4 à gauche)

- Réponse Fortement Modulée (SMR : Strongly Modulated Response) (Fig.3.4 à droite)

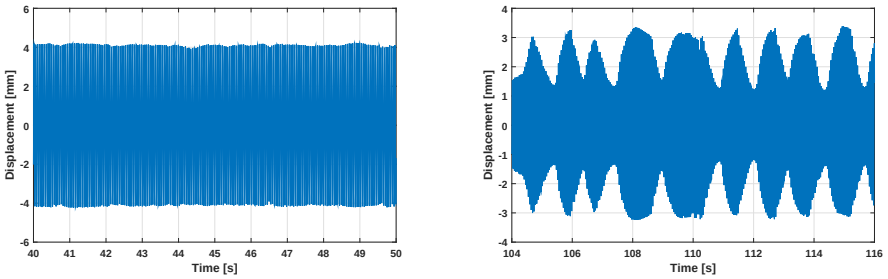

FIGURE 3.4: Réponse à Amplitude Constante (gauche) et Réponse Fortement Modulée (droite).

3.3 Étude analytique

Pour pouvoir expliquer le comportement observé expérimentalement, on a décidé de traiter le problème analytiquement. Cela a été fait en utilisant la méthode de perturbation dite Multi-Échelles, qui consiste en diviser le problème originaire en plusieurs sous-problèmes à des échelles de temps différentes.

Cela a permis l'identification de la variété invariante du problème (Slow Invariant Manifold), entité mathématique qui regroupe l'ensemble de toutes les solutions possibles du problème. Celle-ci est montrée à la Fig.3.5. Les deux coordonnées A_Ω et α sont issues du développement analytique et peuvent être interprétées comme liées respectivement aux déplacements du système principal et du NES.

Il est important de noter qu'il existe une limite inférieure $A_{\Omega min}$ à l'amplitude du déplacement du système principal pour qu'il y ait des solutions. En plus, deux branches de solution existent : une stable et une instable.

Un autre important résultat de l'étude analytique est le calcul des points fixes du problème. L'intersection des points fixes avec la variété invariante permet d'établir si le système peut aboutir à une solution stable ou si seules des solutions instables peuvent être atteintes.

A la Fig.3.6, on montre l'évolution des points fixes sur la variété invariante correspondant au cas expérimental présenté à la Fig.3.3. On peut observer que quand un point fixe stable existe, un régime à amplitude constant

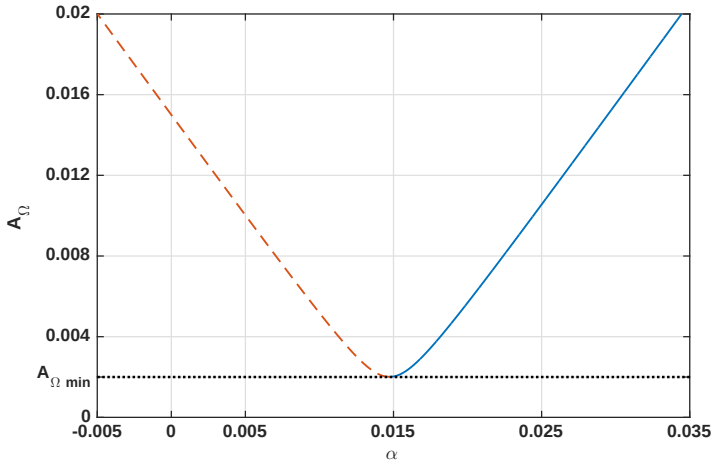

FIGURE 3.5: Variété Invariante (Slow Invariant Manifold)

s'établit, alors que lorsque les points fixes sont instables on observe un régime de réponse modulée.

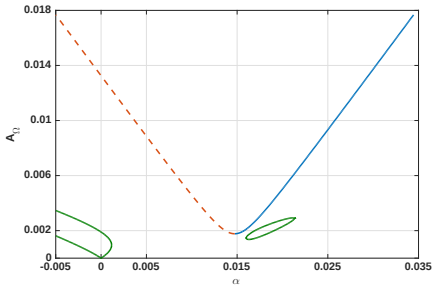

(a) $\Omega = 0.94$: Idle

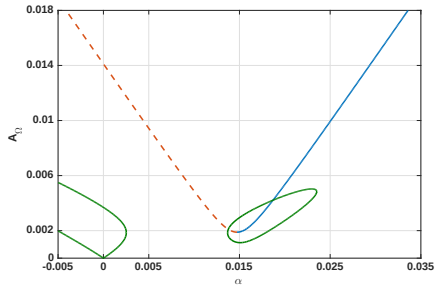

(b) $\Omega = 0.97$: CAR

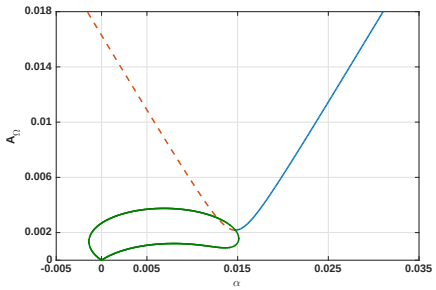

(c) $\Omega = 1.04$: SMR

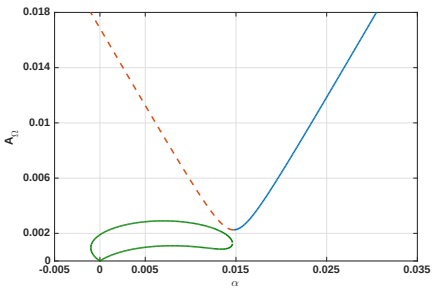

(d) $\Omega = 1.06$: Idle

FIGURE 3.6: Évolution des points fixes sur la variété invariante.

3.4 Conclusion

Dans ce chapitre on a étudié le comportement dynamique du VI-NES couplé à un oscillateur linéaire à 1 degré-de-liberté. Une étude expérimentale a permis d'observer les différent régimes de réponse existants et leur dépendance à l'excitation extérieure. Une réduction satisfaisante du niveau vibratoire du pic de résonance a été obtenu. L'étude analytique a permis d'expliquer de façon théorique les observations expérimentales et de valider l'influence des paramètres de conception du VI-NES sur sa réponse. Cela pourra être utilisé pour arriver à établir un processus de conception du VI-NES en tant qu'absorbeur de vibrations.

Chapitre 4

Magnetic-Strung Nonlinear Energy Sink

Dans ce chapitre on présente l'étude d'un nouveau concept d'absorbeur NES avec récupération d'énergie. Le système est appliqué à un oscillateur linéaire à 1 ddl forcé harmoniquement. On reporte ici les points principaux de la conception et des résultats. On renvoie au mémoire en anglais pour une description complète et détaillée.

4.1 Description du modèle

Une représentation schématique du système est fournie à la Fig.4.1. Les éléments élastiques entre le système principal et le NES sont des cordes travaillant transversalement. La force résultante comporte une composante linéaire et une composante cubique.

Afin de récupérer l'énergie vibratoire, la masse du NES est constituée d'un aimant qui translate dans une bobine. De cette façon l'énergie vibratoire du système principal est transférée au NES. Elle est ensuite dissipée en partie par l'amortissement visqueux et convertie en partie en puissance électrique. Un schéma représentant le flux énérgétique est affiché à la Fig.4.2.

Au final on se retrouve avec un système électro-mécanique décrit par les équations :

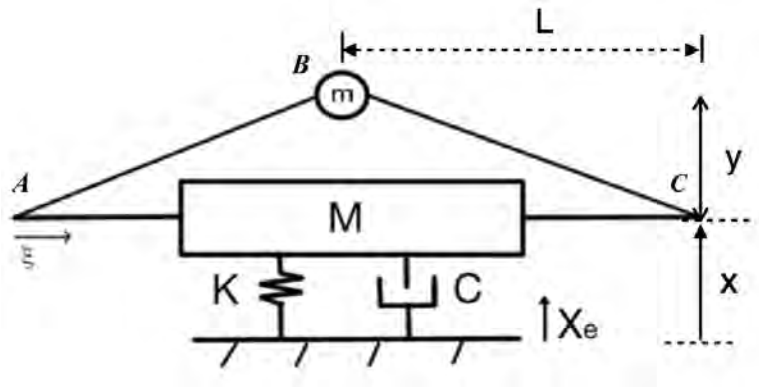

FIGURE 4.1: Schéma du MS-NES.

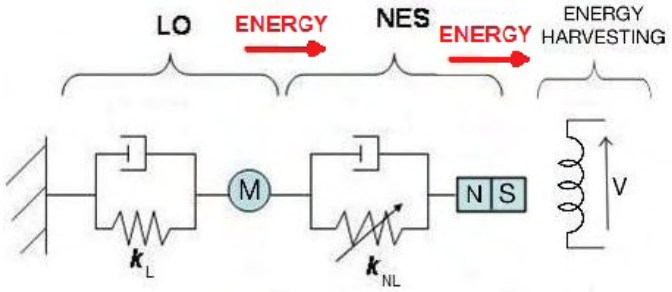

FIGURE 4.2: Flux d'énergie du système principal vers le récupérateur d'énergie.

$$\begin{gathered} M\ddot{x} + C\dot{x} + Kx + K_1(x-z) + K_3(x-z)^3 + C_1(\dot{x}-\dot{z}) = KX_e + C\dot{X}_e \\ m\ddot{z} + C_1(\dot{z}-\dot{x}) + K_1(z-x) + K_3(z-x)^3 - \gamma I = 0 \\ L\dot{I} + (R_L + R_i)I + \gamma(\dot{z}-\dot{x}) = 0 \end{gathered} \tag{4.1}$$

Où il est important de remarquer que le couplage électro-mécanique est assuré par le coefficient γ.

4.2 Modulation de la force de rappel par une force magnétique

La force de rappel entre le système principal et le NES peut être modulée grâce à la force magnétique créée par deux aimants supplémentaires et agissant sur la masse (aimant) du NES. Cette opération permet notamment de contrecarrer la composante linéaire de la force élastique due aux cordes de façon à avoir une relation purement cubique entre le système principal et le NES.

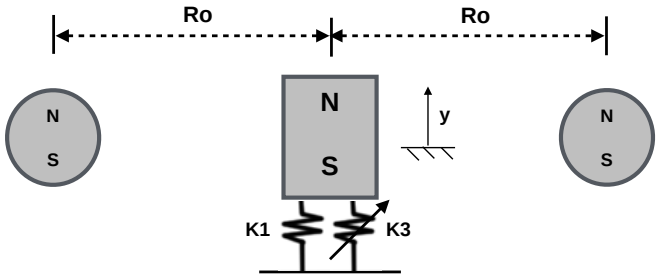

FIGURE 4.3: Les deux aimants supplémentaires placé aux cotés de la masse/aimant du NES.

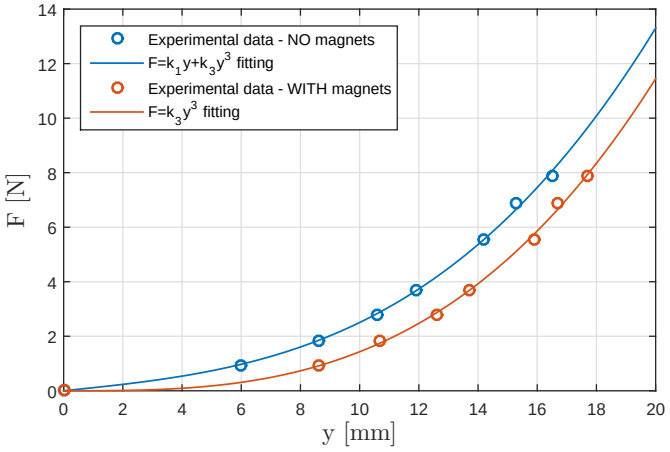

FIGURE 4.4: Relation force-déplacement : essais statiques.

A la Fig.4.4 les résultats issus des tests statiques montrent l'efficacité de cette solution.

Outre la configuration cubique, l'ajout d'une force magnétique permet également d'obtenir une configuration dite bi-stable. Dans cette configuration la force de rappel prend la forme affichée à la Fig.4.5.

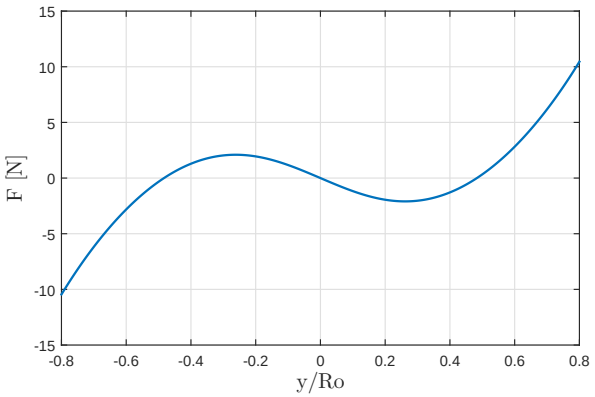

FIGURE 4.5: Force non-linéaire entre le système principal et le NES dans le cas d'une configuration bi-stable.

4.3 Prototype et résultats expérimentaux

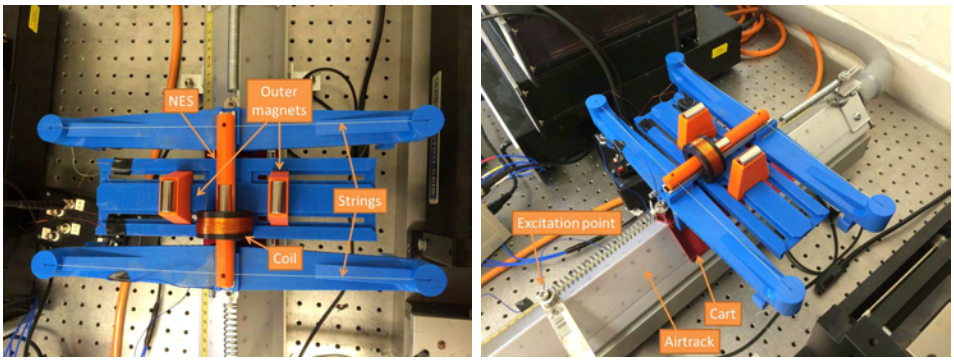

FIGURE 4.6: Le prototype du Magnetic-Strung NES.

Un prototype du MS-NES a été réalisé et il est présenté à la Fig.4.6.

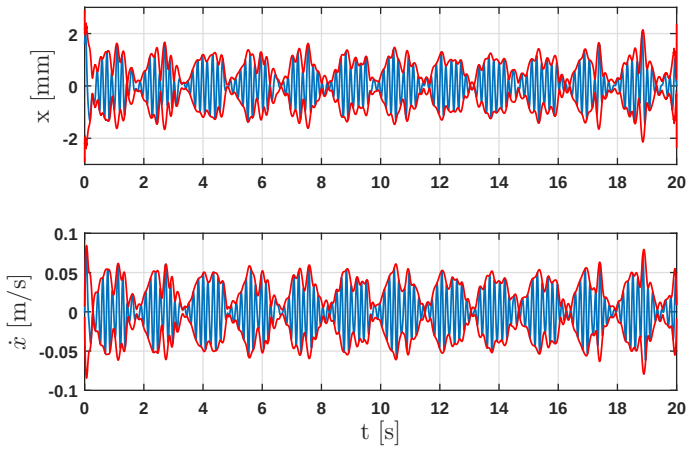

FIGURE 4.7: Observation expérimentale de la réponse fortement modulée. Déplacement x and vitesse $\dot{x}$ du système principal dans le cas d'une configuration cubique.

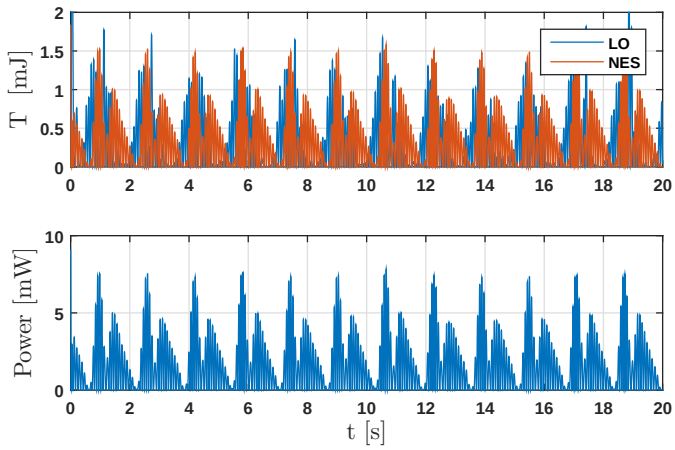

FIGURE 4.8: Énergies cinétiques instantanées du système principal et du NES (haut) et puissance électrique instantanée (bas).

La distance des aimants latéraux étant réglable, il a été possible de tester plusieurs configurations.

Pour une description et une analyse complètes des essais on renvoie au manuscrit en anglais. A titre d'exemple on reporte ici un cas d'observation

de réponse modulée pour la configuration cubique. A la Fig.4.7 on peut observer les mesures de déplacement et de vitesse de la masse principale et à la Fig.4.8 les énergies cinétiques de la masse principale et du NES ainsi que la puissance électrique instantanée délivrée.

4.4 Conclusions

Dans ce chapitre il a été présenté une étude théorique et expérimentale d'un nouveau concept de NES intégrant l'aspect de récupération d'énergie à l'aide d'une méthode électro-mécanique. Une force magnétique supplémentaire agissant sur la masse du NES a été introduite afin de moduler la force non-linéaire entre le système principal et le NES, ce qui a permis de tester différentes configurations de MS-NES. Les performances du MS-NES ont été analysées en tant qu'absorbeur d'énergie et en tant que récupérateur d'énergie.

Chapitre 5

Conclusions

Ces travaux de thèse ont permis d'étudier la réduction des vibrations dans les structures mécaniques à l'aide d'absorbeurs non-linéaires de type Nonlinear Energy Sink. Le phénomène physique à la base du fonctionnement de ces dispositifs est appelé pompage énergétique (Targeted Energy Transfer) et il consiste en un transfert irréversible d'énergie du système principal vers le NES, où l'énergie est ensuite dissipée. Ce transfert d'énergie peut se produire sur une vaste gamme de fréquences sans que le NES ne soit nécessairement accordé sur une fréquence spécifique.

Une étude bibliographique a permis d'identifier les principaux travaux menés sur le sujet tant d'un point théorique que d'un point de vue expérimental. Cette thèse a été majoritairement orientée vers une approche expérimentale en se basant sur les concepts théoriques existant dans la littérature.

Le premier type d'absorbeur étudié fut le Vibro-Imapact NES. Cet absorbeur a été appliqué à un oscillateur linéaire à 1 degré de liberté. Ce système a montré une bonne efficacité en terme de réduction du pic de résonance du système principal. Une bonne comparaison entre les résultats théoriques et les observations expérimentales a été obtenue. L'étude expérimentale a permis l'identification des régimes de réponse possibles de ce système et l'analyse analytique a permis d'en obtenir une explication théorique.

Le deuxième type de NES étudié fut le Magnetic-Strung NES. Dans cette étude l'aspect concernant la récupération d'énergie a été abordé. Le MS-NES a été conçu de façon qu'il puisse non seulement dissiper de l'énergie mais aussi la récupérer en tant que puissance électrique. En outre il a été possible de tester plusieurs configurations du MS-NES grâce à la possibilité de moduler la force non-linéaire entre le système principal et le NES. Le MS-

NES a été analysé théoriquement et expérimentalement en tant qu'absorbeur et en tant que récupérateur d'énergie.

Perspectives pour des travaux futurs

Les résultats présentés dans cette thèse ont montré l'intérêt d'utiliser la dynamique non-linéaire dans le domaine du contrôle des vibrations. Cependant, plusieurs travaux théoriques et expérimentaux restent encore à être effectués

Vibro-Impact NES :

- Une étude énergétique devrait être menée afin d'identifier les régimes les plus favorables en terme de dissipation d'énergie. Le modèle analytique pourrait être utilisé pour concevoir une version optimisée du VI-NES.
- Un VI-NES adaptatif pourrait être conçu, pour lequel les paramètres les plus influents (longueur du tube et coefficient de restitution) varieraient afin d'aboutir aux conditions optimales de fonctionnement.
- L'aspect lié à la récupération d'énergie pourrait être abordé (méthode piézoélectrique).
- L'utilisation de pièces piézoélectriques pourrait aussi être envisagée pour rendre le VI-NES adaptatif (variation du coefficient de restitution).

Magnetic-Strung NES :

- Une version optimisée du MS-NES devrait être conçue.
- Le couplage entre les système électrique et mécanique devrait être examiné et exploité. Théoriquement il est possible d'ajouter de l'amortissement mécanique fictif grâce aux propriétés électriques.
- L'énergie convertie en puissance électrique pourrait être stockée dans une batterie.
- L'analyse de la configuration bi-stable pourrait être étudiée davantage.

Bibliographie

[Arn55] F. R. Arnold. Steady-state behavior of systems provided with nonlinear dynamic vibration absorbers. *Journal of Applied Mechanics*, 22 :487–492, 1955.

[BCHM10] R. Bellet, B. Cochelin, P. Herzog, and P.O. Mattei. Experimental study of targeted energy transfer from an acoustic system to a nonlinear membrane absorber. *Journal of Sound and Vibration*, 329(14) :2768–2791, 2010.

[BTW06] S. P. Beeby, M. J. Tudor, and N. M. White. Energy harvesting vibration sources for micro systems applications. *Measurement Science and Technology*, 17 :175–195, 2006.

[CK00] S.B. Choi and W.K. Kim. Vibration control of a semi-active suspension featuring electrorheological fluid dampers. *Journal of Sound and Vibration*, 234 :537–546, 2000.

[Den92] H.H. Denman. Tautochronic bifilar pendulum torsion absorbers for reciprocating engines. *Journal of Sound and Vibration*, 159 :251–277, 1992.

[DH38] J.P. Den Hartog. Tuned pendulums as torsional vibration eliminators. *S. Timoshenko 60th Anniversary Volume*, pages Macmillian, London, UK, 1938.

[DH85] J.P. Den Hartog. *Mechanical Vibrations*. Dover Books on Engineering, 4th edition, 1985.

[DSSC96] S.J. Dyke, B.F. Spencer, M.K. Sain, and J.D. Carlson. Modeling and control of magnetorheological dampers for seismic response reduction. *Smart Materials and Structures*, 5 :565–575, 1996.

[Fra11] H. Frahm. A device for damping vibrations of bodies, 1911.

[GA15] O. V. Gendelman and A. Alloni. Dynamics of forced system with vibro-impact energy sink. *Journal of Sound and Vibration*, 358 :301–314, 2015.

[GAT+07] E. Gourdon, N. Alexander, C. Taylor, C.H. Lamarque, and S. Pernot. Nonlinear energy pumping under transient forcing with strongly nonlinear coupling : Theoretical and experimental results. *Journal of Sound and Vibration*, 300(3) :522–551, 2007.

[GDK+16] E. Gourc, L. Dell'Elce, G. Kerschen, G. Michon, G. Aridon, and A. Hot. Performance comparison between a nonlinear energy sink and a linear tuned vibration absorber for broadband control. *Proceedings of the 34th IMAC, A Conference and Exposition on Structural Dynamics*, 2016.

[Gen01] O.V. Gendelman. Transition of energy to a nonlinear localized mode in a highly asymmetric system of two oscillators. *Nonlinear Dynamics*, 25 :237–253, 2001.

[Gen08] O. Gendelman. Targeted energy transfer in systems with non-polynomial nonlinearity. *Journal of Sound and Vibration*, 315 :732–745, 2008.

[Gen12] O.V. Gendelman. Analytic treatment of a system with a vibro-impact nonlinear energy sink. *Journal of Sound and Vibration*, 331 :4599–4608, 2012.

[GJTBW04] P. Glynne-Jones, M. J. Tudor, S. P. Beeby, and N. M. White. Anelectromagnetic, vibration-powered generator for intelligent sensor systems. *Sensors and actuators*, A 110 :344–349, 2004.

[GL05] O.V. Gendelman and C.H. Lamarque. Dynamics of linear oscillator coupled to strongly nonlinear attachment with multiple states of equilibrium. *Chaos, Solitons and Fractals*, 24 :501–509, 2005.

[GLP07] E. Gourdon, C.H. Lamarque, and S. Pernot. Contribution to efficiency of irreversible passive energy pumping with a strong nonlinear attachment. *Nonlinear Dynamics*, 50 :793–808, 2007.

[GMSB14a] E. Gourc, G. Michon, S. Seguy, and A. Berlioz. Experimental investigation and design optimization of targeted energy transfer under periodic forcing. *Journal of Vibration and Acoustics*, 136 :021021, 2014.

[GMSB14b] E. Gourc, G. Michon, S. Seguy, and A. Berlioz. Theoretical and experimental study of an harmonically forced vibro-impact nonlinear energy sink. *Journal of Vibration and Acoustic*, 137 :031008, 2014.

[Gou13] E. Gourc. *Etude du contrôle passif par pompage energetique sous sollicitation harmonique*. phdthesis, Université de Toulouse, 2013.

[GVMB05a] F. Georgiadis, A. F. Vakakis, D. M. McFarland, and L. A. Bergman. Shock isolation through passive energy pumping caused by non-smooth nonlinearities. *International Journal of Bifurcations and Chaos*, 15 :1–13, 2005.

[GVMB05b] F. Georgiadis, A.F. Vakakis, D.M. McFarland, and L. Bergman. Shock isolation through passive energy pumping caused by nonsmooth nonlinearities. *International Journal of Bifurcation and Chaos*, 15(06) :1989–2001, 2005.

[HN82] J.B. Hunt and J.C. Nissen. The broadband dynamic vibration absorber. *Journal of Sound and Vibration*, 83 :573–578, 1982.

[KKM+07] G. Kerschen, J. Kowtko, D. McFarland, L. Bergman, and A.F. Vakakis. Theoretical and experimental study of multimodal targeted energy transfer in a system of coupled oscillators. *Nonlinear Dynamics*, 47(1) :285–309, 2007.

[KMK+07] G. Kerschen, D.M. McFarland, J.J. Kowtko, Y.S. Lee, L.A. Bergman, and A.F. Vakakis. Experimental demonstration of transient resonance capture in a system of two coupled oscillators with essential stiffness nonlinearity. *Journal of Sound and Vibration*, 299(4-5) :822–838, 2007.

[KMK+08] G. Kerschen, D. M. McFarland, J. J. Kowtko, Y. S. Lee, L. Bergman, and A. Vakakis. Impulsive periodic and quasi-periodic orbits of coupled oscillators with essential stiffness nonlinearity. *Communication in Nonlinear Science and Numerical Simulation*, 13 :959–978, 2008.

[KVG08] I. Karayannis, A. F. Vakakis, and F. Georgiadis. Vibro-impact attachments as shock absorbers. *Proceedings IMechE, Journal of Mechanical Engineering Science*, 222(222) :1899–1908, 2008.

[LGSE11] C.H. Lamarque, O.V. Gendelman, A. Savadkoohi, and E. Etcheverria. Targeted energy transfer in mechanical systems by means of non-smooth nonlinear energy sink. *Acta Mechanicca*, 221 :175–200, 2011.

[LNV+09] Y. S. Lee, F. Nucera, A. F. Vakakis, D. M. McFarland, and L. A. Bergman. Periodic orbits, damped transitions and targeted energy transfers in oscillators with vibro-impact attachments. *Physica D*, 238 :1868–1896, 2009.

[LW06] E. S. Leland and P. K. Wright. Resonance tuning of piezoelectric vibration energy scavenging generators using compressive axial load. *Smart Material and Structures*, 15 :1413–1420, 2006.

[Mad80] J. Madden. Constant frequency bifilar vibration absorber, 1980.

[MBV05] D. McFarland, L. Bergman, and A.F. Vakakis. Experimental study of non-linear energy pumping occurring at a single fast frequencyexperimental study of non-linear energy pumping occurring at a single fast frequency. *International Journal of Non-Linear Mechanics*, 40(6) :891–899, 2005.

[MO10] B. P. Mann and B. A. Owens. Investigations of a nonlinear energy harvester with a bistable potential well. *Journal of Sound and Vibration*, 329 :12151226, 2010.

[MS09] B. P. Mann and N. D. Sims. Energy harvesting from the nonlinear oscillations of magnetic levitation. *Journal of Sound and Vibration*, 319 :515530, 2009.

[Nak98] B.C. Nakra. Vibration control in machines and structures using viscoelastic damping. *Journal of Sound and Vibration*, 211 :449–465, 1998.

[NLIM+08] F. Nucera, F. Lo Iacono, D. M. McFarland, L. A. Bergman, and A. F. Vakakis. Application of broadband nonlinear targeted energy transfers for seismic mitigation of a shear frame :

Part ii. experimental results. *Journal of Sound and Vibration*, 313 :57–76, 2008.

[Pip53] L. A. Pipes. Analysis of a nonlinear dynamic vibration absorber. *Journal of Applied Mechanics*, 20 :515–518, 1953.

[Rob52] R.E. Roberson. Synthesis of a nonlinear dynamic vibration absorber. *Journal of the Franklin Institute*, 254 :205–220, 1952.

[RWR03] S. Roundy, P. K. Wright, and J. M. Rabaey. *Energy Scavenging for Wireless Sensor Networks*. Springer NewYork, 2003.

[SBK08] I. Sari, T. Balkan, and H. Kulah. An electromagnetic micro power generator for wideband environmental vibrations. *Sensors and Actuators A*, 145-146 :405–413, 2008.

[SG08] Y. Starosvetsky and O.V. Gendelman. Strongly modulated response in forced 2dof oscillatory system with essential mass and potential asymmetry. *Physica D*, 237(13) :1719–1733, 2008.

[SLD12] A.T. Savadkoohi, C.H. Lamarque, and Z. Dimitrijevic. Vibratory energy exchange between a linear and a nonsmooth system in the presence of the gravity. *Nonlinear Dynamics*, 70(2) :1473–1483, 2012.

[SMM09] S. Stanton, C. McGehee, and B. P. Mann. Reversible hysteresis for broadband magnetopiezoelastic energy harvesting. *Appl. Phys. Lett.*, 95 (174103), 2009.

[SMM10] S. Stanton, C. McGehee, and B. P. Mann. Nonlinear dynamics for broadband energy harvesting : Investigation of a bistable piezoelectric inertial generator. *Physica D*, 239 :640–653, 2010.

[SSH06] S.W. Shaw, P.M. Schmitz, and A.G. Haddow. Dynamics of tautochronic pendulum vibration absorbers : Theory and experiment. *Journal of Computational and Nonlinear Dynamics*, 1 :283–293, 2006.

[Vak01] A. F Vakakis. Inducing passive nonlinear energy sinks in vibrating systems. *Journal of Vibration and Acoustics*, 123 :324–332, 2001.

[VGMM01a] A. F. Vakakis, O. V. Gendelman, L. I. Manevitch, and R. McCloskey. Energy pumping in nonlinear mechanical oscillators part ii resonance capture. *Journal of Applied Mechanics Transactions of the ASME*, 68 :42–48, 2001.

[VGMM01b] A.F. Vakakis, O.V. Gendelman, L.I. Manevitch, and R. McCloskey. Energy pumping in nonlinear mechanical oscillators i : dynamics of the underlying hamiltonian system. *Journal of Applied MechanicsTransactions of the ASME*, 68 :34–41, 2001.

[WY95] C. B. Williams and R. B. Yates. Analysis of a micro generator for microsystems. *Proceedings of the 8th International Conference on Solid-state Sensors and Actuators*, Eurosensors IX :87–84, 1995.

[YZZ15] Z. Yang, Y. Zhu, and J. Zu. Theoretical and experimental investigation of a nonlinear compressive-mode energy harvester with high power output under weak excitations. *Smart Mater. Struct.*, 24, 2015.

Publications

Journaux

1. **G .Pennisi, C. Stephan, E. Gourc, G. Michon**, Vibro-Impact NES : A Correlation Between Experimental Investigation and Analytical Description, *Nonlinear Dynamics* (accepted)

2. **G. Pennisi, B. P. Mann, N. Naclerio, C. Stephan, G. Michon**, Magnetic-Strung NES with Energy Harvesting : Theoretical and Experimental Study of a New Concept of Nonlinear Vibration Absorber, *Journal of Sound and Vibration* (In preparation)

Conférences

1. **G. Pennisi, B. P. Mann, C. Stephan, G. Michon**, Magnetic-Strung NES with Energy Harvesting : Theoretical and Experimental Study of a New Concept of Nonlinear Vibration Absorber, *American Society of Mechanical Engineers, IDETC/CIE 2016*, Charlotte NC USA, August 2016

2. **G. Pennisi, B. P. Mann, C. Stephan, G. Michon**, Experimental Study of a New Concept of Nonlinear Vibration Absorber with Energy Harvesting, *European Congress on Computational Methods in Applied Sciences and Engineering*, Crete Island, Greece, June 2016

3. **G. Pennisi, B. P. Mann, C. Stephan, G. Michon**, *Preliminary study of a Nonlinear Energy Sink coupled with an electromagnetic energy harvester*, Vibrations, Shocks and Noise, Le Mans France, April 2016

4. **G. Pennisi, C. Stephan, G. Michon**, Vibro-Impact NES : A Correlation Between Experimental Investigation and Analytical Description, *Sensors and Instrumentation, Volume 5, Society for Experimental Mechanics, Proceedings of the 34th IMAC*, Orlando FL USA, January 2016

5. **G. Pennisi, C. Stephan, G. Michon**, Analytical and Experimental Study of a Vibro-Impact Nonlinear Energy Sink, *American Society of Mechanical Engineers, IDETC/CIE 2015*, Boston MA USA, August 2015